UTS UNIVERSITY OF TECHNOLOGY SYDNEY

Risk Assessment and Reliability Analysis on Long-term Settlement of Soft Soils

by Mehrnaz Alibeikloo

Thesis submitted in fulfilment of the requirements for the degree of

Doctor of Philosophy

under the supervision of Prof Hadi Khabbaz and A/Prof Behzad Fatahi

University of Technology Sydney
Faculty of Engineering and Information Technology

May 2023

Certificate of Original Authorship

I, Mehrnaz Alibeikloo declare that this thesis, is submitted in fulfilment of the requirements for the award of Doctor of Philosophy, in the School of Civil and Environmental Engineering, Faculty of Engineering and Information Technology at the University of Technology Sydney.

This thesis is wholly my own work unless otherwise referenced or acknowledged. In addition, I certify that all information sources and literature used are indicated in the thesis. This document has not been submitted for qualifications at any other academic institution.

This research is supported by the Australian Government Research Training Program.

Signature:

Production Note:
Signature removed prior to publication.

Date: 20/05/2023

Acknowledgement

My challenging and pleasant research journey would not have been completed without the supports and helps of various groups of staff, family members and friends. I would like to mention them below and appreciate them to be with me along this journey.

First of all, I would like to thank my advisor, my main supervisor, Prof. Hadi Khabbaz, who was abundantly helpful and offered me invaluable assistance. Likewise, I would like to express my sincere gratitude to my co-supervisor, A/Prof. Behzad Fatahi, for the thoughtful comments and recommendations on this dissertation. I deeply appreciate his inspiring and encouraging ideas and support and providing me the opportunity to learn more.

I am also thankful to the Graduate Research School (GRS) and Faculty of Engineering and Information Technology (FEIT) for and all its staff members for all the considerate guidance. I gratefully acknowledge the funding received from Research Training Program (RTP) funded by the Australian Government and UTS Research Excellence Scholarship which made my research possible.

Furthermore, my special thanks go to my family and friends for all the support they have provided to me through this research. My parents kind-heartedly set me off on the right road a long time ago. I really appreciate my husband, Hadi, for his unwavering support and belief in me, and also all my friends for their tremendous encouragement and support in the past few years.

Lastly, I would like to thank the Covid-19 for teaching me life is too short, unprecedented, uncertain, carrying a lot of surprises. I should treasure the moments as tick along and be well equipped for unprecedented events.

List of Publications

Journal papers:

Alibeikloo, M., Khabbaz, H., Fatahi, B. and Le, T.M., 2021, 'Reliability Assessment for Time-Dependent Behaviour of Soft Soils Considering Cross Correlation between Visco-Plastic Model Parameters', *Reliability Engineering & System Safety*, *213*, p.107680.

Alibeikloo, M., Khabbaz, H. and Fatahi, B., 2022, 'Random Field Reliability Analysis for Time-Dependent Behaviour of Soft Soils Considering Spatial Variability of Elastic Visco-Plastic Parameters', *Reliability Engineering & System Safety*, *219*, p.108254.

Conference papers:

Alibeikloo, M., Khabbaz, H. and Fatahi, B., 2022, 'Importance of Cross Correlation and Spatial Correlation Length for Reliability Assessment of Low Embankment Strategy Considering Soft Soil Creep', Australian Geomechanics Society (*AGS) Symposium on Reliability-based Design: Advances, Innovation and Experiences, Sydney.*

Alibeikloo, M. and Share Isfahani, H., 2019, 'The Effect of Impact Roller Compaction on Closed Landfill Settlements', *13th Australian New Zealand Conference on Geomechanics, Perth, Western Australia.*

Alibeikloo, M., Isfahani, H.S. and Khabbaz, H., 2020, 'Effect of Surcharge Height and Preloading Time on Long-term Settlement of Closed Landfills: a Numerical Analysis', *WIT Transactions on Ecology and the Environment*, *247*, pp.81-92.

Table of Contents

List of Tables

List of Figures

Notations

Latin letters

$B(x_1, x_2)$	Covariance function between x_1 and x_2
C_α	Secondary compression index
C_C	Primary compression index
CGSE	Australian research council centre of excellence for geotechnical science and engineering
$c_i(\vartheta)$	Random variables with specific variance
$C_{\hat{H}\hat{H}(x_1,x_2)_K}$	Covariance function developed by K-L expansion method
CI	Confidence interval
CMD	Covariance Matrix Decomposition
COV_i	Coefficient of variation of random variable i
$Cov[X, Y]$	Covariance
c_k	Permeability change index
CSRSM	Collocation-based stochastic response surface method
c_v	Consolidation coefficient
CY	Construction years
d	Number of random variables
DFT	Discrete Fourier Transform
EOLE	Expansion Optimal Linear Estimation
EOP	End of primary consolidation
e_0	Initial void ratio
EPWP	Excess pore water pressures
EVP	Elastic visco-plastic
E_x	Error in determning indicators RMSE and MAE
$F_X(x)$	cumulative density function
f_i	Basis function
$f(S_m)$	Evidence of measured settlement
$f(x)$	Prior probability density function (PDF) of model parameters
$f_X(X)$	probability density function of X for continuous random variables
$f(x\|S_m)$	Posterior probability density function (PDF) of model parameters
$f(S_m\|x)$	Likelihood function
$f(X, Y)$	Joint probability density function of random variables X and Y

FFT	Fast Fourier Transform
FORM	First Order Reliability Method
FOSM	First Order Second Moment
H	Dimension of the random field
H_0	Initial thickness of soil layer
$H(x,\theta)$	Continuous random field function in space
$\widehat{H}(x,\vartheta)$	Approximation of a continuous random field $H(x,\vartheta)$
i,j	Counter subscript
k	Coefficient of hydraulic conductivity
k_h	Hydraulic conductivity
K-L	Karhunen-Loeve
l	Number of random field variables
l_C	Scale of fluctuation or spatial correlation length
l_{Cw}	Worst case correlation length
LAS	Local average subdivision
LB	Lower bound
M	Number of truncated terms/ Margin of safety
M_{max}	Maximum number of truncated terms
M_{min}	Minimum number of truncated terms
m_v	Coefficient of volume compressibility
MA	Moving Average
MAE	Mean absolute error
MH	Metropolice-Hastings
MP	Most probable
MP	Midpoint method
n	Number of finite difference nodes in depth direction
N	Number of samples
N_d	Number of measured data
N_j	Total number of stages in TMCMC algorithm
OCR	Over consolidated ratio
OSE	Orthogonal Series Expansion
p	Number of Monte-Carlo simulations
$p(X_i)$	Probability of the value X_i for discrete random variables
PC	Polynomial Chaos
PCY	Post construction years

$P_{Eceedance}$	Probability of exceedance
PEM	Point Estimate Method
PDFs	Probability density function
PF	Probability of failure
q	uniform surcharge loading
R	Reliability
R^2	Coefficient of determination
RF	Random Field
$RMSE$	Root Mean square error
S_{all}	Allowable settlement
S_e	Settlement prediction error
S_j	Factor to compute the evidence $f(S_m)$ in TMCMC algorithm
S_m	Measured settlement
S_{max}	Maximum settlement
S_{min}	Minimum settlement
S_{M-X}	Measured settlement at depth X
S_P	Predicted settlement
S_{P-X}	Predicted settlement at depth X
S_t	Ground surface settlement at time t
SA	Spatial average
SDF	Spectral density function
SR_0	Settlement ratio at ground surface
$SR_{2.5}$	Settlement ratio at 2.5 m depth
$SR_{5.0}$	Settlement ratio at 5.0 m depth
$SR_{7.5}$	Settlement ratio at 7.5 m depth
SR_X	Settlement ratio at depth X
SRSM	Stochastic response surface method
SRV	Single random variable
SSCM	Soft soil creep model
t	Elapsed time
t_0	Yin model parameter corresponding to the choice of reference time line
t_e	Equivalent time
t_{e2}	Equivalent time at stage 2
$t_{e2'}$	Equivalent time at stage $2'$
t_{EOP}	End of primary consolidation time

t_{vp}	Creep time
TBM	Turning Band Method
TMCMC	Transitional Markov Chain Monte Carlo
u	Total water pressure
u_0	Initial equilibrium water pressure
u_e	Excess pore water pressure
UB	Upper bound
V	Specific volume
$Var[X]$	Variance
$w(x_{j,k})$	Plausibility weight
X	Random variable
x	Vector containing random variables
x_1, x_2	Spatial coordinates in space
Y_m	Measured data
Y_p	Predicted data
z	Depth
Z	Correlated random variables with zero mean and one standard deviation

Greek letters

β	Reliability index
γ_w	Water unit weight
$(\Delta e)_p$	Void ratio changes during primary consolidation
$(\Delta e)_s$	Void ratio changes during secondary compression
Δt	Time increment
Δt_2	Loading time at stage 2
Δz	Depth increment
$(\varepsilon_v)_t$	Total vertical strain
ε_z	Vertical strain
ε_{lm}^{vp}	Creep strain limit
ε_z^e	Elastic strain
ε_z^{vp}	Visco-plastic strain
ε_z^r	Elastic-plastic strain
$\varepsilon_{z_0}^e$	Elastic strain at unit stress σ'_u
$\varepsilon_{z_0}^r$	Reference strain

ε_{z2}	Strain at stage 2
θ	Dimensionless correlation length
θ_w	Worst case correlation length
ϑ	A parameter indicating a random nature
κ/V	Elastic model parameter
Λ	Eigenvalue of correlation function
λ/V	Elastic plastic model parameter
μ	Mean value
μ_{lni}	Mean value of underlying normal distribution for lognormally distributed random variables
μ_s	Mean of predicted settlement
μ_u	Mean of predicted excess pore water pressure
μ_X	Mean value of random variable X
μ_{lnX}	Mean value of underlying normal distribution for log-normally distributed random variables
$\mu_{(\lambda/V)}$	Mean of generated elastic-plastic model parameter
$\mu_{(\psi_0/V)}$	Mean of generated initial creep coefficient
$\xi_i(\vartheta)$	Vector of uncorrelated standard normal variables
υ	Poisson's ratio
ρ	Cross correlation coefficient
ρ_k	Kendall's rank cross correlation coefficient
ρ_p	Pearson cross correlation coefficient
$\rho(x_1, x_2)$	Correlation function
Σ_s	The covariance matrix of the Gaussian proposal PDF in TMCMC algorithm
ς	Prescribed scaling factor in TMCMC algorithm
$\sigma(.)$	Standard deviation operator
σ_e	Standard deviation of the error between predicted and measured settlement
σ_{lni}	Standard deviation of underlying normal distribution for lognormally distributed random variables
σ_s	Standard deviation of predicted settlement
σ_u	Standard deviation of predicted excess pore water pressure
σ_X	Standard deviation of random variable X
σ_{lnX}	Standard deviation of underlying normal distribution for log-normally distributed random variables

$\sigma_{(\lambda/V)}$	Standard deviation of generated elastic-plastic model parameter
$\sigma_{(\psi_0/V)}$	Standard deviation of generated initial creep coefficient
σ'_u	Unit stress
σ'_z	Vertical effective stress
σ'^r_z	Reference point effective stress
σ'_{z_0}	Yin model parameter (vertical effective stress corresponding to the initial ε_z^r)
σ'_{z_2}	Effective stress at stage 2
τ_k	Kendall's rank correlation coefficient
$\emptyset_z(z)$	Probability distribution of the standard normal Z
$\varphi_i(.)$	Eigenfunction of correlation function
ψ_0/V	Initial creep coefficient
ψ_{02}/V	Initial creep coefficient at stage 2
ω, ω^*	Angular frequency
Ω	Space of spatial variability

Abstract

Nowadays, there is a growing interest in applying reliability analysis in geotechnical design approaches as a method of managing and quantifying geotechnical risks with respect to uncertain geotechnical input parameters. Since creep settlement occurs in an extremely long period of time, prediction of creep settlement is a challenging task for geotechnical engineers to utilize soft grounds. Among several methods to evaluate the long-term behaviour of soft soils, the elastic visco-plastic model could be an effective model. However, the difficulties and uncertainties in determining the model parameters is one of the most important limitation of this method. As a result, the aim of this study is to investigate the influence of model parameters uncertainties on predicting the time dependent behaviour of soft soils.

In this research, an elastic visco-plastic creep model was combined with the Monte-Carlo probabilistic method to investigate the effects of uncertainties in the elastic visco-plastic model parameters on time-dependent behaviour in soft soils. By adopting monitoring data from the case study of Väsby test fill, the most appropriate cross correlation coefficient between an elastic-plastic model parameter (λ/V) and the creep coefficient (ψ_0/V) was introduced.

Moreover, the time-dependent behaviour of soft soils was analysed incorporating spatial variability of elastic visco-plastic model parameters. Standard Gaussian random fields for the adopted random variables were generated adopting Karhunen-Loeve expansion method. The probability of failure was calculated adopting random field (RF) and single random variable (SRV) analysis to determine the critical spatial correlation length, resulted in a maximum probability of failure.

In this study, Bayesian updating method of identifying the model parameters was used to update the elastic visco-plastic model parameters using field and oedometer test data by applying the transitional Markov Chain Monte Carlo (TMCMC) method for two case studies. The results confirm that adopting even 20% of total monitored data has a considerable impact in predicting more realistic post-construction settlements.

This study provides an insight into selecting the most suitable cross correlation coefficient and the critical spatial correlation length while adopting elastic visco-plastic model parameters as random variables. Therefore, the risks in predicting long-term settlement of soft soils reduces and the reliability of the design in construction increases. Moreover, adopting field monitoring data at early stages to update model parameters has significant impact in predicting more realistic long-term settlement which affects the risks associated with time and cost when adopting low embankment strategy for design of transport infrastructure.

1 Introduction

1.1 Overview

At each site the properties of soil and rock vary, depending on the lithological heterogeneity of the soil and its inherent spatial variability (Elkateb et al. 2003) in contrast to manufactured materials with controlled properties. To quantify geotechnical uncertainties, probabilistic or reliability analysis was introduced to distinguish conditions with high or low uncertainties (Duncan 2000). In recent decades, reliability analysis has been significantly recognized as a great importance in various engineering projects. Moreover, a great deal of research has adopted probabilistic analysis to manage and control the risks associated with uncertainties in soil for geotechnical problems such as bearing capacity, settlement of foundations, slope stability, piling, tunnelling, and seepage. The probabilistic methods can also be used for back analysis and updating parameters based on the existing data. Some of these methods include the maximum likelihood method and Bayesian probabilistic method incorporated for geotechnical engineering problems such as characterization of sub surface profiles, the model and parameter updating based on measured data.

Nowadays, by increasing population and developing urban areas, available space becomes scarce. As a result, development on top of or adjacent to the waterfront areas alongside lakes, rivers, maritime coasts and even closed landfills is sometimes inevitable. The prevalent soils in these areas are soft soils or in landfill areas there are different type of waste materials. Dealing with soft soils in geotechnical engineering, the long-term behaviour is a considerable challenge. Creep which is defined as a time dependent viscous behaviour of soil is an important part of soft soil settlement which can result in large and destructive deformation in long-term. Moreover, in another definition, creep is considered as destruction or adjustment of soil structures under a constant effective stress.

The reduction in soil void ratio under vertical loads causes soil settlement, which may occur in three stages, including:

- **Immediate settlement**: This settlement takes place immediately after an external load applied with zero volume change in fully saturated soils and the shape change only occurs.
- **Primary settlement:** In saturated soil with no air among the particles, the increased in vertical pressure transferred to water which is incompressible. The water seep out of the soil leading to the dissipation of excess pore water pressure and transferring the pressure to the soil skeleton which is defined as primary consolidation.
- **Secondary settlement**: this settlement is determined as a continuation of volume change following the primary deformation. Mesri (1973) explained this mechanism as individual or relative movement of particles due to normal stress or shear displacement at particle contacts as a result of exceedance of shear stresses to the bond shear resistance of the contacts. Since creep is usually defined as settlement under a constant effective stress, it should be mentioned that creep may also

occur during the dissipation of excess pore water pressure. As reported by Bjerrum (1967) and Taylor (1942), creep compression may lead to increasing the resistance of the soil structure against further compression. Creep compression also influences other soil properties such as preconsolidation pressure. As a result, creep settlement is an important contributing factor for evaluating time-dependent behaviour of soft soils.

There are two different approaches to predict time-dependent behaviour of soft soils. In the first method, which is referred to as Hypothesis A, the creep contribution is explicitly added to the settlement after complete dissipation of the excess pore water pressure (i.e. the total settlement is the sum of the primary consolidation and the secondary compression) and the void ratio of soil at the end of primary consolidation is unique irrespective of the sample size (Jamiolkowski et al. 1985; Ladd et al. 1977). The second method, known as Hypothesis B generally adopts a constitutive model in which creep and excess pore water pressure dissipation occur simultaneously and the void ratio when only negligible excess pore water pressure is remaining depends on the sample size and thus is not unique (Aboshi 1973; Barden 1965; Gibson 1961; Olszak and Perzyna 1966a; Perzyna 1963; Taylor and Merchant 1940; Yin and Graham 1989).

Of the various constitutive models that support Hypothesis B, the category of constitutive models developed by Yin and co-workers is one of the widely accepted approaches to describe the time-dependent behaviour of soft soils. Initially, Yin (1990) proposed a model based on elastic visco-plastic (EVP) behaviour that applied a linear logarithmic function for creep compression to provide an infinite creep settlement as time approaches infinity. However, it is presumed that creep settlement

will eventually cease after a very long time when there are no more accessible voids to be compressed. On this basis, Yin (1999) improved the proposed elastic visco-plastic (EVP) model by introducing a non-linear creep function with a creep strain limit, but in order to calculate the creep settlement of soft soil using the EVP model, the model parameters must be determined in advance, which limits its practicality.

1.2 Problem Statement

Elastic visco-plastic (EVP) model developed by Yin (1999) is an effective model to predict time-dependent behaviour of soft soils. Yin (1999) introduced a non-linear creep function with a strain limit presuming that creep settlement will finally stop after a long time. In order to calculate the creep settlement of soft soil using the EVP model, the model parameters must be determined in advance. Since it is not practical and cost-effective to carry out very long-term creep tests, determining visco-plastic model parameters and creep limit values is practically challenging, introducing uncertainties in design. There are several common methods based on curve fitting to the experimental data to determine the model parameters (Yin 1999; Yin and Graham 1994; Yin et al. 2002). These methods enable the creep parameters to be obtained based on the data measured in the laboratory after completing the primary consolidation stage. For multi-stage loading tests, the time required for excess pore water pressure to dissipate (i.e. end of primary consolidation) varies with the applied stress causing difficulties and uncertainties in evaluating the elastic visco-plastic parameters. This procedure may also violate the concept whereby the reference-time line may include a large viscous strain, particularly for thicker soil samples or materials with a high creep rate such as organic soils.

To overcome the limitations of these curve fitting methods, an optimisation method was proposed based on the trust-region reflective least square method in which the model parameters are obtained simultaneously based on the test data, while assuming a reference time parameter as the unit value (Le et al. 2017; Le et al. 2016). Yin et al. (2017) also adopted an enhanced genetic algorithm to determine the creep model parameters of soft soils based on an efficient optimisation method. Note that when the experimental data are limited the curve fitting and optimisation methods can lead to uncertainties in determining the visco-plastic parameters. Furthermore, the main concern with determining the parameters in the optimisation methods is finding the best fit between the predicted and observed experimental data, regardless of the statistical characteristics, the measurements, and the model uncertainties. In order to consider uncertainties in determining the model parameters, Zhou et al. (2018) adopted the Bayesian model class selection approach and the transitional Markov Chain Monte Carlo (TMCMC) method to select the model and corresponding model parameters best suited to predict the creep behaviour of soft soil using laboratory measurements. In the research conducted by Zhou et al. (2018), the uncertainties of soil parameters were quantified via the posterior probabilistic distributions that were obtained based on the Bayesian probabilistic method. In this method, similar to traditional curve fitting and optimisation methods, a limited set of experimental data was used to determine the creep parameters by introducing significant uncertainties. Since it is not either practical or cost-effective to carry out long-term creep tests to capture creep nonlinearities, the method proposed by Zhou et al. (2018) can be used to determine the optimised creep parameters. Although, this method can provide a probabilistic evaluation of model predictions based on the given data, it will not address the uncertainties of model parameters due to the lack

of sufficient long term test data. Similar to many geotechnical parameters, the elastic visco-plastic parameters are interdependent parameters in reality which are characterized by the concept of cross correlation in practice (Zhang et al. 2019). However, in reliability analysis performed by Liu et al. (2018), the cross correlation between elastic visco-plastic parameters were not considered. Thus, a more rigorous research for predicting the time-dependent settlement of soft soils, while addressing the uncertainties of elastic visco-plastic parameters, particularly the cross correlated parameters, is deemed necessary.

In addition, another source of uncertainties is due to spatial variability of soil parameters due to its inherent variability. Random field (RF) analysis captures the soil variability in different directions in space. Introduction of correlation length is essential in RF analysis. Since the in-situ experimental data are often scattered and limited, establishing a reliable spatial correlation length for a design parameter is a quite challenging task. Therefore, RF analysis and determining the critical spatial correlation length, spatial correlation length with maximum risk or probability of failure, is deemed necessary in the absence of good quality data.

1.3 Objectives

The main objective of this research is to investigate the influence of the elastic-plastic and creep parameter uncertainties and contribution of each random variable on the time-dependent deformation of soft soils. Three specific objectives of this research are as follows:

- Investigating the influence of the elastic-plastic (λ/V) and initial creep (ψ_0/V) model parameter uncertainties, contribution of each random variable,

and cross correlation coefficients between two selected random variables on the time-dependent deformation of soft soils.

- Investigating the influence of spatial variability of the elastic visco-plastic model parameters, namely the elastic-plastic parameter (λ/V) and the initial creep coefficient (ψ_0/V) affecting the time-dependent behaviour of soft soils and determining critical spatial correlation length.

- Updating the elastic-plastic parameter (λ/V) and the initial creep coefficient (ψ_0/V) by adopting Bayesian updating method and field monitoring data

1.4 Structure of the Thesis

This thesis comprises 6 chapters as described below:

Chapter 1 presents a brief introduction about the importance of probabilistic methods and reliability analysis in managing the risks of predicting long-term behaviour of soft soils.

In Chapter 2, a comprehensive literature review on various probabilistic methods is presented. This chapter also reviews several existing methods to predict time-dependent stress-strain behaviour of soft soils. Additionally, this chapter presents a literature review on several probabilistic methods and reliability analysis in geotechnical engineering, particularly for long-term settlement of soft soils.

Chapter 3 investigates the influence of the elastic-plastic and initial creep parameter uncertainties and contribution of each random variable on the time-dependent deformation of soft soils. It also presents a comprehensive study to determine how the cross correlation coefficients between two random variables generated by "Gaussian" copula function, namely the elastic-plastic (λ/V) and initial

creep (ψ_0/V) model parameters will affect the Probability Distribution Function (PDFs) that corresponds to the system response. Additionally, the predicted settlement and excess pore water pressures are compared with the field measurements to evaluate the validity of the proposed model. This chapter thus presents a brief review of the elastic visco-plastic constitutive model and the numerical method used to predict the settlement and excess pore water pressure. A case based on the Väsby trial embankment data is then used to obtain the deterministic and probabilistic parameters. In the final step, the proposed probabilistic analysis and corresponding numerical results are presented and evaluated against field measurements so that a suitable cross correlation coefficient between selected random variables can be recommended.

Chapter 4 investigates the influence of spatial variability of the elastic visco-plastic model parameters, namely the elastic-plastic parameter (λ/V) and the initial creep coefficient (ψ_0/V) affecting the time-dependent behaviour of soft soils. For this purpose, a finite difference-based model is developed and then combined with Karhunen-Loeve (K-L) expansion method to generate the random field. Moreover, the finite difference model is combined with the Monte-Carlo simulation to conduct the single random variable (SRV) analysis for the sake of comparison with RF results. Then, by adopting the field measurements of Skå–Edeby trial embankment and determining the maximum probability of failure, the critical spatial correlation length is determined, which is required for a reliable design in the absence of sufficient data for model parameters.

Chapter 5 discusses how applying field monitoring results can reduce risks in predicting the long-term settlement of low embankments constructed on soft soils.

For this purpose, monitoring measurements of two case studies of Väsby and Skå-Edeby test fills are adopted. In this chapter, the elastic-plastic model parameter (λ/V) and the initial creep coefficient (ψ_0/V) are updated by adopting the Bayesian updating method and transitional Markov Chain Monte Carlo (TMCMC) algorithm. Then, the long-term settlement predictions obtained from updated parameters based on field data are compared with the predictions obtained from updated parameters based on oedometer test results.

Finally, in Chapter 6, a summary and key findings drawn from the current research are presented. It also provides a number of recommendations for future research.

2 Literature Review

2.1 Introduction

There are high degree of uncertainties in all disciplines of civil engineering; and among various professional fields, geotechnical engineers significantly rely on experience and judgment in their designs. The properties of soil and rock vary deeply in each site whereas in some other disciplines of civil engineering such as structural engineering, used materials are manufactured materials with reasonable control properties.

Urban areas and population have been increased unexpectedly in recent years, leading to land scarcity. Consequently, in some region reconstruction on soft soils is unavoidable. Construction on soft soils can cause substantial problems, including long-term settlement which can lead to damages to the superstructures. Although, research on the long-term settlement of soft soils has been developed during recent decades, there is not any particular and unified methods predicting long-term settlement or creep deformation of soft soils resulting in uncertainties in model and parameter determination. Consequently, presenting settlement distribution and performing reliability analysis play a vital role in predicting long-term settlement of soft soils. For this purpose, a brief introduction of various methods of geotechnical reliability and probabilistic analysis are presented in this chapter.

Subsequently, it is tried to collect the most important and relevant studies on long-term settlement of soft soils.

2.2 Introduction to Probability and Reliability Analysis Methods in Geotechnical Engineering

The main objective of this section is to introduce some basic methods and elements of reliability analysis applicable in geotechnical engineering. Traditional methods of geotechnical adequacy are expressed by a safety factor, which is the ratio of capacity to demand. In contrast to traditional method, probabilistic approach extends the concept of safety factor incorporating uncertainties in the parameters, which can be quantified by statistical analysis of existing data or judgment. It should be noted that even if in judgmentally assigned analysis the results would be more meaningful than deterministic analysis as result of incorporating uncertainties in judgment.

Reliability analysis in engineering means finding the reliability, R, or the probability of failure, Pr (f), of a system or structure (US Army Corps Engineers ,1995):

$$R + Pr(f) = 1 \tag{2.1}$$

In the following subsections the basic and the essential definitions and concepts for performing reliability analysis are presented.

2.2.1 Random Variables

Random variables are parameters with the most significant uncertainties and high significance in the analysis. Random variables have a range of values in accordance with probability density function or distribution which quantifies the likelihood that

a particular value lies in any given interval. In order to model random variables in Taylor's series, it is necessary to determine the magnitudes of expected values and standard deviations, which are the most important moments of several random variables. For dependent random variables, it is also necessary to assign correlation coefficients. The brief definitions of essential random variable moments are presented below according to US Army Corps Engineers (1995).

Mean value: The mean value (μ_X) of a set of N values for the random variable X is defined as:

$$\mu_X = \frac{\sum_{i=1}^{N} X_i}{N} \tag{2.2}$$

Expected value: The expected value, $E[X]$, of a random variable is obtained by multiplying the likelihood of occurrence of random variables by the values of random values:

$$E[X] = \mu_X = \int X f(X) dx \approx \sum X p(X_i) \tag{2.3}$$

where, $f(X)$ is the probability density function of X for continuous random variables, and $p(X_i)$ is the probability of the value X_i for discrete random variables.

Median value: The median value of the set of data ($x_{0.5}$) is the value for which half of the data is less and half is more. In other words, the median is the midpoint of the data sorted in increasing or decreasing order.

Mode value: The mode value of the set of data is the most common one which is obvious in theoretical distribution and unstable in sample data as a result of unexpected behaviour with which data appear.

Variance: Variance is defined as the expected value of the squared difference between the variable and its mean.

$$Var[X] = E[(X - \mu_X)^2] = \int (X - \mu_X)^2 f(X) dX = \frac{\sum[(X_i - \mu_X)^2]}{N} \quad (2.4)$$

N is the size of samples. In order to obtain the unbiased estimate of variance from finite samples, the *N* is replaced by *N*-1:

$$Var[X] = \frac{\sum[(X_i - \mu_X)^2]}{N - 1} \quad (2.5)$$

Standard deviation: Standard deviation σ_x is obtained as the square root of the variance which express the scatter of random variables about its expected value with the same unit of random variable:

$$\sigma_x = \sqrt{Var[X]} \quad (2.6)$$

Coefficient of variation: Coefficient of variation COV_X is calculated by dividing the standard deviation by the expected value which expresses uncertainty inherent in a random variable:

$$COV_X = \frac{\sigma_x}{E[X]} \times 100\% \quad (2.7)$$

In practice, if the existing random variable is not large enough, it is suggested to assume the correlation of variation from previously measure variable for the same parameter.

Correlation: In correlated random variable, the likelihood of occurrence random variable Y depends on the occurrence of random variable X. The covariance is the same as variance but measures how two variables vary together which is expressed as:

$$Cov[X,Y] = E[(X-\mu_X)(Y-\mu_Y)] = \iint (X-\mu_X)(Y-\mu_Y)f(X,Y)dYdX \tag{2.8}$$

where $f(X,Y)$ is the joint probability density function of random variables X and Y. The variance based on the data is calculated from the following equation:

$$Cov[X,Y] = \frac{1}{N}\sum (X_i-\mu_X)(Y_i-\mu_Y) \tag{2.9}$$

In order to provide a non-dimensional measurement of the correlation between X and Y, the correlation coefficient $\rho_{X,Y}$ is defined as dividing the covariance by the standard deviation:

$$\rho_{X,Y} = \frac{Cov[X,Y]}{\sigma_X \sigma_Y} \tag{2.10}$$

The correlation coefficient varies between -1 and 1. The value of -1 or 1 expresses the perfect linear correlation between two dependent variables, while the value of zero indicates no correlation and variables are independent. The positive value indicates the direct relation, meaning that the variables decrease or increase together; and the negative values shows that one value increases as the other decreases.

2.2.2 Probability Distribution

The term probability distribution and probability density function pdf or $f_X(X)$ is a function that indicates a continuous random variable. A probability density function has the characteristic that for any X, $f_X(X)$ describes the likelihood of X. As a result, the area under the probability density function is unity. The probability that the random variable X lies between X_1 and X_2 is obtained by integration of the probability density function between these two variables:

$$Pr(X_1 < X < X_2) = \int_{X_1}^{X_2} f_X(X)dx \tag{2.11}$$

The cumulative density function CDF or $F_X(X)$ is the probability that random variable X is less than the certain value x:

$$F_X(X) = \int_{-\infty}^{X} f_X(X)dx \tag{2.12}$$

There are six distributions, which are common in engineering applications, including Exponential, Gamma, Uniform, Weibull, Rayleigh, Normal, and Lognormal. Details of mentioned distributions can be found in Fenton and Griffiths (2008). Normal and Lognormal distributions are the most important distributions in geotechnical engineering, which are presented below:

Normal Distribution: Normal distribution is probably the most important in use distribution. The probability distribution of the random variable X following normal distribution is indicated as:

$$f_X(x) = \frac{1}{\sigma_x\sqrt{2\pi}} exp\left\{-\frac{1}{2}\left(\frac{x-\mu_x}{\sigma_x}\right)^2\right\} \tag{2.13}$$

According to Figure 2.1(a), normal distribution is symmetric about the mean and the maximum point, or mode, occurs at mean. Moreover, the inflection points are at $\mu \pm \sigma$.

Special case of normal distribution with $\mu_X = 0$ and $\sigma_X = 1$ is called standard normal distribution (Figure 2.1(b)). According to Fenton and Griffiths (2008), since the standard normal distribution is so important, the probability distribution of the standard normal Z is presented by special symbol $\emptyset_z(z)$:

$$\emptyset_z(z) = \frac{1}{\sqrt{2\pi}} exp\left\{-\frac{1}{2}z^2\right\} \tag{2.14}$$

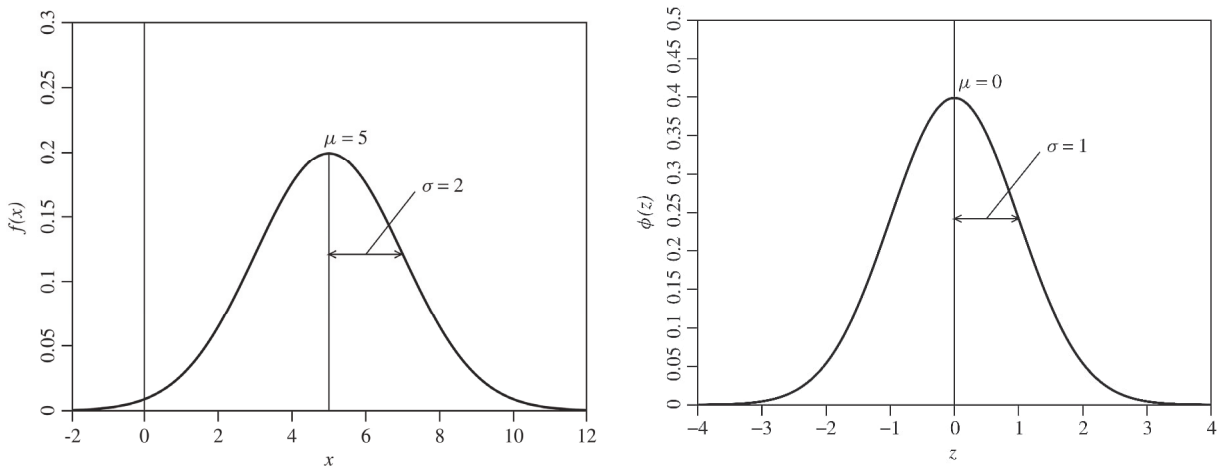

a) b)

Figure 2.1 Normal and standard normal distribution a) Normal distribution with $\mu = 5$ and $\sigma = 2$ b) Standard normal distribution (after Fenton and Griffiths, 2008)

Lognormal Distribution: Since in engineering, material properties and loads are commonly nonnegative, normal distribution suffers from disadvantages of modelling negative values. One simple way to solve this problem is introducing Lognormal distribution. The X random variable is Lognormally distributed random variable with a mean and standard deviation given by μ_X and σ_X, respectively. If X is Lognormally distributed, ln_X is normally distributed. Probability density function pdf or $f_X(X)$ for a lognormal distribution is given by:

$$f_X(x) = \frac{1}{x\sigma_{lnX}\sqrt{2\pi}} exp\left\{-\frac{1}{2}\left(\frac{lnX - \mu_{lnX}}{\sigma_{lnx}}\right)^2\right\} \tag{2.15}$$

The mean and standard deviation of the underlying normal distribution of ln_X is presented by:

$$\mu_{lnX} = ln\mu_X - \frac{1}{2}ln\{1 + v_X^2\} = ln\left(\frac{\mu_X}{\sqrt{1 + v_X^2}}\right) \tag{2.16.a}$$

$$\sigma_{lnX} = \sqrt{ln\{1 + v_X^2\}} \tag{2.16.b}$$

$$v_X = \frac{\sigma_X}{\mu_X} \tag{2.16.c}$$

Further relationships involving the lognormal distribution includes:

$$Median_X = exp(\mu_{lnX}) \tag{2.17.a}$$

$$Mode_X = exp(\mu_{lnX} - \sigma_{lnX}^2) \tag{2.17.b}$$

Figure 2.2 depicts the location of mean, mode, and median in lognormal distribution.

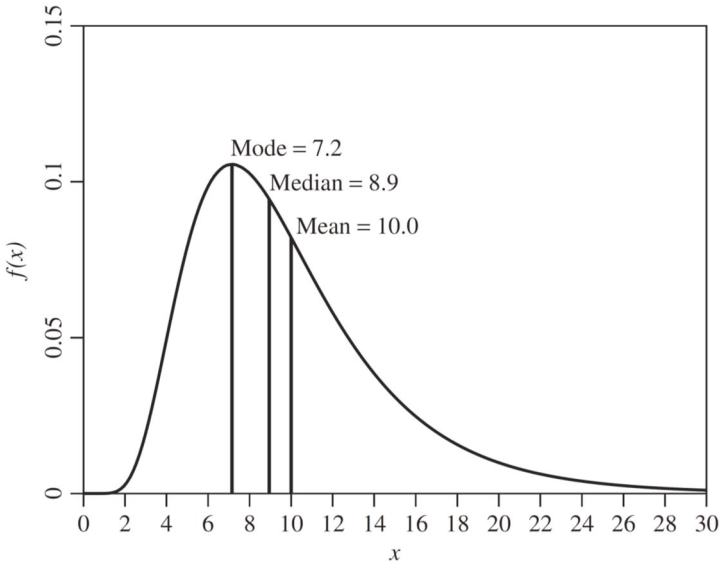

Figure 2.2 Lognormal distribution (after Fenton and Griffiths, 2008)

2.2.3 Reliability Index

Nowadays, the reliability is commonly expressed by reliability index which is related to the probability of failure. In general, reliability analysis is the relation between the applied loads (Q) and resistance of a system to those loads (R). Figure 2.3, shows the probability distribution of R and Q. According to this figure, the margin of safety is defined by:

$$M = R - Q \tag{2.18}$$

Based on Cornell (1969), reliability index β is expressed as the distance of the mean margin value from its failure or critical point (M =0) over or in units of standard deviation:

$$\beta = \frac{\mu_M}{\sigma_M} = \frac{\mu_R - \mu_Q}{\sqrt{\sigma_R^2 + \sigma_Q^2 - 2\rho_{RQ}\sigma_R\sigma_Q}} \tag{2.19}$$

As illustrated in Figure 2.4, probability of failure is the area in which the probability distribution of M is less than 0.0 or the intercept of the cumulative distribution function with vertical axis at $M = 0$.

Geotechnical engineers are more interested to work with factor of safety as a performance function in which failure occurs when F is less than one:

$$F = \frac{R}{Q}, \quad \beta = \frac{E[F] - 1}{\sigma_F} \tag{2.20}$$

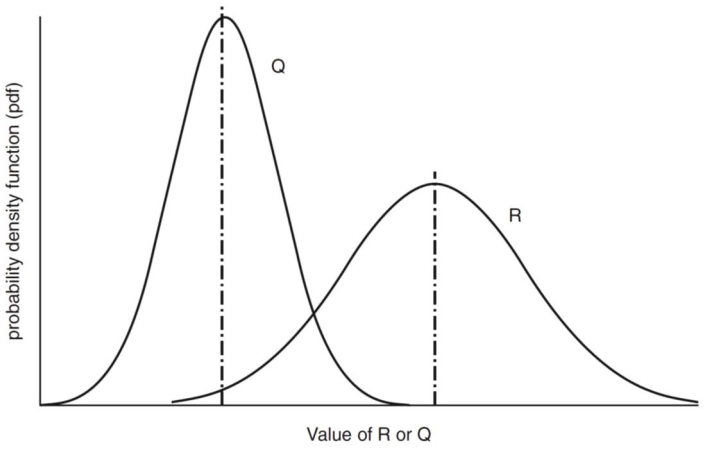

Figure 2.3 Probability distribution for load (Q) and resistance (R) (after Baecher and Christian, 2005)

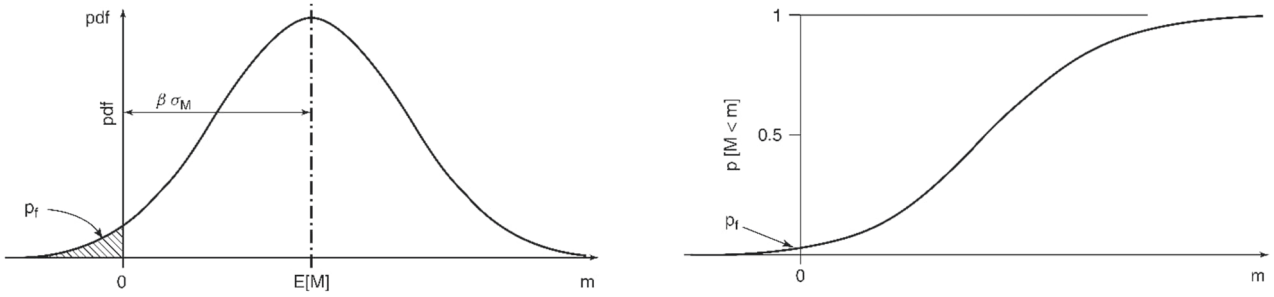

a) b)

Figure 2.4 Probability of failure a) Probability density, b) Cumulative distribution (after Baecher and Christian, 2005)

The values of probability of failure for normal and lognormal distribution (with various coefficients of variation, ν) are presented in Table 2.1 and Figure 2.5.

Table 2.1 Probability of failure for Normal and Lognormal Distributions (after Baecher and Christian, 2005)

Reliability index	Probability of failure			
	Normal distribution	Lognormal distribution		
		$\nu = 0.05$	$\nu = 0.10$	$\nu = 0.15$
0.0	5.000×10^{-1}	5.100×10^{-1}	5.199×10^{-1}	5.297×10^{-1}
0.5	3.085×10^{-1}	3.150×10^{-1}	3.212×10^{-1}	3.272×10^{-1}
1.0	1.586×10^{-1}	1.583×10^{-1}	1.571×10^{-1}	1.551×10^{-1}
1.5	6.681×10^{-2}	6.236×10^{-2}	5.713×10^{-2}	5.111×10^{-2}
2.0	2.275×10^{-2}	1.860×10^{-2}	1.437×10^{-2}	1.026×10^{-2}
2.5	6.210×10^{-3}	4.057×10^{-3}	2.298×10^{-3}	1.048×10^{-3}
3.0	1.350×10^{-3}	6.246×10^{-4}	2.111×10^{-4}	4.190×10^{-5}
3.5	2.326×10^{-4}	6.542×10^{-5}	9.831×10^{-6}	4.415×10^{-7}
4.0	3.167×10^{-5}	4.484×10^{-6}	1.977×10^{-7}	6.469×10^{-10}
4.5	3.398×10^{-6}	1.927×10^{-7}	1.396×10^{-9}	4.319×10^{-14}
5.0	2.867×10^{-7}	4.955×10^{-9}	2.621×10^{-12}	

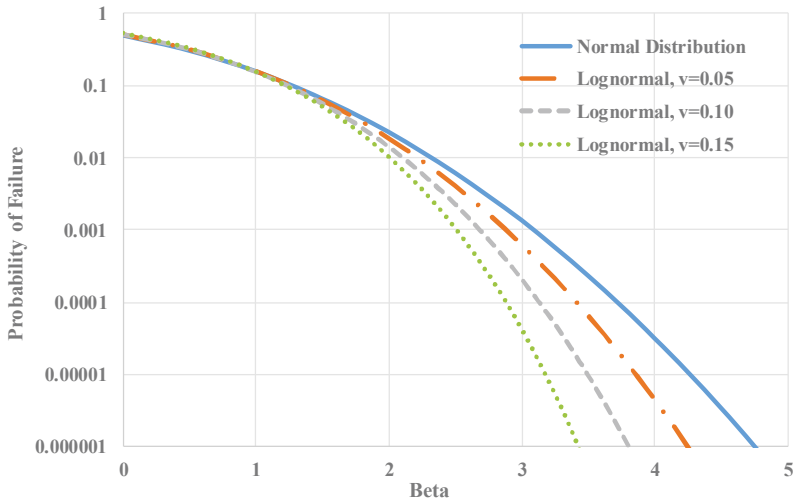

Figure 2.5 Probability of failure versus reliability index for Normal and Lognormal Distributions (after Baecher and Christian, 2005)

2.2.4 Reliability Analysis Methods

The main purpose of any reliability analysis is to estimate the probability of failure (p_f). In this regard, it is beneficial to set out the steps suggested by Baecher and Christian (2005):

- Establishing an analytical model to define the performance function in the form of margin of safety or factor of safety.
- Estimation statistical description of the parameters including mean, standard deviation, covariance, and the form of the distributions of the parameters.
- Calculation of the statistical moments of performance function such as mean and standard deviation
- Calculating the reliability index
- Estimating the probability of failure based on the obtained reliability index

There are various methods available in order to performing reliability analysis. Among them the most widely used are:

- First Order Second Moment (FOSM) method
- Point Estimate Method (PEM)
- First Order Reliability Method (FORM)
- Monte-Carlo simulation
- Random Field (RF) method
- Bayesian analysis

Among the above-mentioned methods, the Monte-Carlo simulation, RF method and Bayesian analysis have been applied in this research; and they are

described briefly in the following sections. The details of other methods (FOSM, PEM, and FORM) can be found in the literature (Baecher and Christian 2005; Fenton and Griffiths 2008).

2.2.4.1 Monte-Carlo simulation

Monte-Carlo methods are one of the most popular computational algorithms that rely on repeated random sampling to evaluate uncertainties and risks in quantitative decision making. In this method, a wide range of possible outcomes is obtained and consequently the probabilities of their occurrence can be calculated. For this purpose, models of possible results are built by substituting a range of random values (a probability distribution) for any variable. The outputs are calculated several times by applying a different set of random variables from the probability functions for each time. In this method, random variables are obtained randomly from the input probability distributions, and the outcomes are recorded and the probability distribution of possible outcome is provided. As a result, Monte-Carlo simulation gives a comprehensive perception of what may happen.

The required number of simulations runs depend on the extent of uncertainties and the ranges, specified for the variables, which leads to creating distributions of possible outcomes. It is obvious that a considerably long running time is required for a significant number of iterations, which is the greatest drawback of Monte-Carlo simulation. This issue can be solved by having access to modern computers and using special software packages. This method has been implemented in different geotechnical engineering problems. As an example, a probabilistic slope stability method, applying a spreadsheet computational approach in Microsoft Excel coupled with the software @Risk performed by El-Ramly et al. (2002).

2.2.4.2 Random Field method

Many features and phenomena in the worlds are random in time and space. The concept of random field is derived from capturing this variability into the model. As a result, a random field $H(x,\vartheta)$ is a continuous function in space which is consist of finite elements associating with random variables, where ϑ is a parameter capturing the random nature of $H(x,\vartheta)$ and x is a vector containing random variables. In order to introduce different methods for generation of random fields, it is necessary to become familiar with some basic concepts in random fields including, covariance function, correlation length and ergodicity.

Correlation function: Since it is common in reality that two points close to each other have approximately the same values or points with large distance are not correlated, the concept of correlation function is introduced describing the covariance between two points (x_1 and x_2) with certain distance to each other:

$$B(x_1,x_2) = Cov[X_1,X_2] = E[X_1X_2] - E[X_1]E[X_2] \tag{2.21}$$

where, $B(x_1,x_2)$ is covariance function, $X_1 = H(x_1)$ and $X_2 = H(x_2)$. Then, the correlation function is defined as:

$$\rho(x_1,x_2) = \frac{B(x_1,x_2)}{\sigma(x_1)\sigma(x_2)} \tag{2.22}$$

There are different correlation functions in literature (Li and Der Kiureghian 1993), the most commonly used ones are: (Note: the below equations are presented for one dimensional random field)

$$\rho(x_1, x_2)$$

$$= exp\left(-\frac{|x_1 - x_2|}{l_C}\right) \qquad Exponential\ Correlation\ Function \tag{2.23.a}$$

$$\rho(x_1, x_2) =$$

$$exp\left(-\frac{(x_1-x_2)^2}{{l_C}^2}\right)\ Squared\ exponental\ Correlation\ Function \tag{2.24.b}$$

$$\rho(x_1, x_2) = \frac{sin\left(\frac{2.2(x_1-x_2)}{L_C}\right)}{\frac{2.2(x_1-x_2)}{l_C}} Cardinal\ Sin\ Correlation\ Function \tag{2.25.c}$$

where, l_C is correlation length explained in the next section.

Correlation length: The correlation length or scale of fluctuation indicates the distance within which the probabilistic variables have a relatively strong correlation and has unit of the length. As defined by Vanmarcke (2010), the correlation length can be written in the form of:

$$l_C = \int_{-\infty}^{+\infty} \rho(x_1, x_2) d\Delta x = 2\int_{0}^{+\infty} \rho(x_1, x_2) d\Delta x \tag{2.26}$$

where Δx is the relative distance between two points x_1 and x_2.

Ergodicity: Random field could be considered as ergodic respecting any statistical properties. In order to illustrate the ergodicity feature, a simple example has been adopted to defined two different mean values in random field. The mean value for the single random field with domain of Ω is determined by:

$$\bar{H} = \frac{1}{\Omega}\int H(x)dx \tag{2.27}$$

Moreover, sample mean value for a certain position (x_1) can be defined as:

$$\bar{X}_1 = \frac{1}{N}\sum_{N} H(x_1) \tag{2.28}$$

where, N is the number of random field simulations. In the case that $\bar{H}$ is equal to $\bar{X}_1$, random field has ergodicity feature with respect to mean. As a consequence of ergodicity feature, all data related to joint PDF of a random field could be acquired by a single random field realization.

- **Generation of random field:**

The following steps have to be taken to generate a random field:

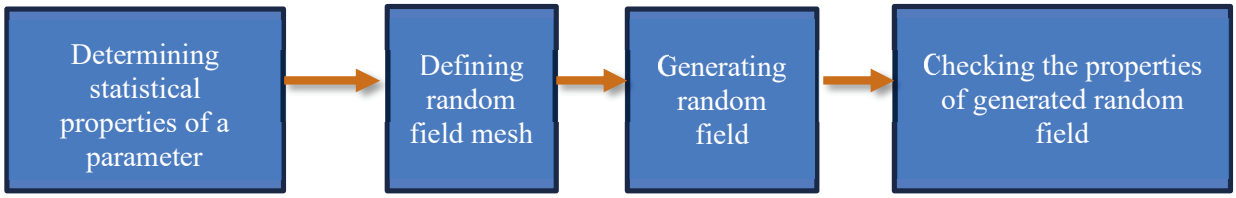

Figure 2.6 Steps of random field generation (after Van der Have, 2015)

- **Random field generators:**

There are various methods in literature to generate random fields. As can be seen in Table 2.2, Van der Have (2015) classified random field generators into two main classes.

Table 2.2 Various methods of random field generators (after Van der Have, 2015)

Random Field Generators	
Class 1	**Class 2**
Generators of spatial correlated variables	**Series expansion methods**
Covariance Matrix Decomposition (CMD)	Karhunen Loève expansion (K-L)
Moving Average (MA)	Orthogonal Series Expansion (OSE)
Discrete Fourier Transform (DFT)	Expansion Optimal Linear Estimation method (EOLE)
Fast Fourier Transform (FFT)	Nyström method
Turning Bands Method (TBM)	Galerking based methods (FEM & FCM)
Local Average Subdivision method (LAS)	Polynomial Chaos expansion (PC)

- **Class 1 generators:**

In class 1 generators, a random field is generated for every node which is correlated to the other nodes in the random field mesh. In order to allocate these spatially correlated random variables to an element in finite element or finite difference model, different discretization methods can be adopted. These discretization methods are classified into three groups. The firs group is the point discretization method causing a separated constant random field. The second group is also the point discretization method, but resulting in a continuous random field. The third group is the average discretization method. It should be mentioned that it is not possible to have all combinations between all methods of class 1 generators and discretization methods

which can be considered as one of the drawbacks of class 1 generators. Different methods in class 1 generators are explained briefly in Van der Have (2015).

- **Class 2 generators:**

In class 2 generators, the random field is expressed by a continuous function for the entire domain instead of describing the random field as a combination of discretized sections. Similar to other series representation methods such as Fourier series expansions, a continuous function is made through multiplying a constant by a set of deterministic functions. In the case of random field generation, these constants are random variables $c_i(\theta)$ with their own variance according to the basis function (f_i) contribution to series expansion (Van der Have 2015).

$$H(x,\theta) = \sum_{i=1}^{\infty} c_i(\theta) f_i(x) \tag{2.29}$$

To approximate a continuous random field (x, θ), the summation of truncated set of basis function is employed as:

$$\widehat{H}(x,\theta) = \sum_{i=1}^{N} c_i(\theta) f_i(x) \tag{2.30}$$

It is highly recommended to sort the constants and basis functions in a way that the first terms have the largest contribution to the expansion (Sudret and Der Kiureghian 2000).

As illustrated in Table 2.2, there are various methods for generation of random field based on series expansion methods, including:

- **Karhunen-Loeve expansion method**: This method is based on the spectral decomposition of its correlation function.
- **Orthogonal Series Expansion (OSE)**: In this method, there is an arbitrarily selection for the basis functions of series expansion.
- **Expansion Optimal Linear Estimation (EOLE)**: In this method, the eigenvalues and eigenfunctions of correlation function are chosen to approximate the corresponding values for the K-L expansion.
- **Nystrom method**: The method is based on numerical integration. As stated by Betz et al. (2014) if specific parameters are adopted, this method is equivalent to EOLE method.
- **Galerking base method**: This method includes Finite Element (FEM) and Finite Cell method (FCM) and is efficient for complex geometry (Betz et al. 2014).

The details of methods mentioned above can be found in Betz et al. (2014). In order to select to most suitable and accurate expansion method, the used correlation function and geometry of random field domain are crucial factors. Among the mentioned methods, Karhunen-Loeve expansion method (K-L) and EOLE method are commonly used methods particularly for simple geometry of random field (Sudret and Der Kiureghian 2000). In this research, Karhunen-Loeve expansion method (K-L) is used and will be explained in Chapter 4.

2.2.4.3 Bayesian analysis

Bayesian analysis is a conditional reliability analysis which addresses the question (Christian 2004), “If I have before me a set of data, what is now the probability that my view of the subject is true?”. Bayesian method begins with prior probability and analyst must first evaluate the state of the nature before getting the new data.

In order to explain Bayesian procedure more easily, a simple example of determining a liquefiable zone is presented. The following questions are considered to be answered based on the results of either standard penetration test or cone penetration tests (it should be mentioned that the design earthquake has been determined in advance):

- What is the probability of the liquefiable zone existence?
- How does the result of successive borings affect the probability?

Referring to Christian (2004), to answer the above questions, the following procedure should be adopted:

If the liquefiable zone exists, consider the probability of finding it 0.3 for any one boring. Therefore, the probability of not finding it is 0.7. The probability of false positive is assumed 0.05 which implies that the probability of not finding it if it does not exist is 0.95. F shows that the liquefiable zone is found and E indicates that the zone exists, and a complement is shown by the superimposed bar, hence the conventional probability is:

$$P[F|E] = 0.3, P\left[\overline{F}\middle|E\right] = 0.7, P[F|\bar{E}] = \ 0.05, P\left[\overline{F}\middle|\bar{E}\right] = 0.95$$

According to the basic of Bayes' theory, if there is some prior probability that the liquefiable zone exists, $\mathrm{P}_0[\mathrm{E}]$, the posterior probability that it exists if the zone is found in one boring is $\mathrm{P}_1[E|F]$:

$$P_1[E|F] = \frac{P[E|F]P_0[E]}{P[F|E]P_0[E] + P[F|\bar{E}]P_0[\bar{E}]} \tag{2.31}$$

The posterior probability that the liquefiable zone exists if the zone is not found in one boring is $P_1[E|\bar{F}]$:

$$P_1[E|\bar{F}] = \frac{P[\bar{F}|E]P_0[E]}{P[\bar{F}|E]P_0[E] + P[\bar{F}|\bar{E}]P_0[\bar{E}]} \tag{2.32}$$

It is assumed that there are two equals of minds whether or not the zone exists:

$$P[E] = P[\bar{E}] = 0.5$$

Hence:

$$P_1[E|F] = \frac{(0.3)(0.5)}{(0.3)(0.5) + (0.05)(0.5)} = 0.86$$

The obtained result shows a sharp increase in the assumption that the zone exists. Furthermore, if the boring did not find the liquefiable zone:

$$P_1[E|\bar{F}] = \frac{(0.7)(0.5)}{(0.7)(0.5) + (0.95)(0.5)} = 0.42$$

Indicating the decrease in the degree of belief that the existence of liquefiable zone exists. Figure 2.7 illustrates the all possible results from additional borings in the case that the initial prior probability of existence is 0.5.

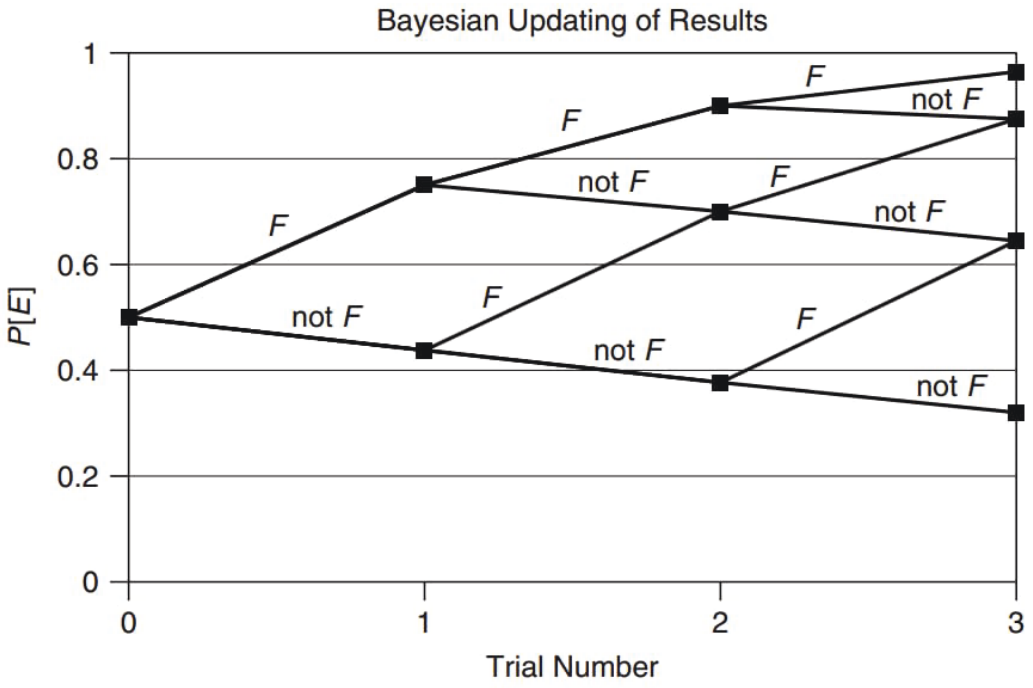

Figure 2.7 Posterior probability of existence of liquefiable zone by Bayesian method based on three borings when initial prior probability is 0.5. (after Christian 2004) (Note: upper branch corresponds to 'Find' and lower to 'not Find')

2.3 Literature Review on Long-term Settlement of Soft Soils

Based on laboratory results and filed measurements, settlement of soft soils occurs during and after the dissipation of excess pore water pressure. There are two components of settlements including "primary settlement" which is the settlement due to flowing out water from voids and transferring loads from pore water to soil particles and "secondary compression" due to the constant effective loads which is also called creep. Since settlement may occur during the dissipation of excess pore water pressure, the creep should be considered different from settlement under constant effective stress.

There are two main hypothesis predicting time dependent of soft soils, including:

- **Hypothesis A:** The void ratio at the end of primary consolidation (e_{EOP}) is unique for thin and thick samples (Mesri 2003; Mesri et al. 1994). In this hypothesis settlement is divided into two parts: during the dissipation of excess pore water pressure (primary settlement) followed by creep settlement in which the excess pore water pressure is significantly small.

- **Hypothesis B:** Since the primary consolidation includes creep, e_{EOP} is not unique for thin and thick samples (Yin and Graham 1996). In this hypothesis the soil settlement is calculated based on a constitutive model considering dissipation of excess pore water pressure and creep simultaneously. Therefore, in thick samples (longer duration of primary consolidation) the difference between hypothesis A and B is more considerable (Figure 2.8).

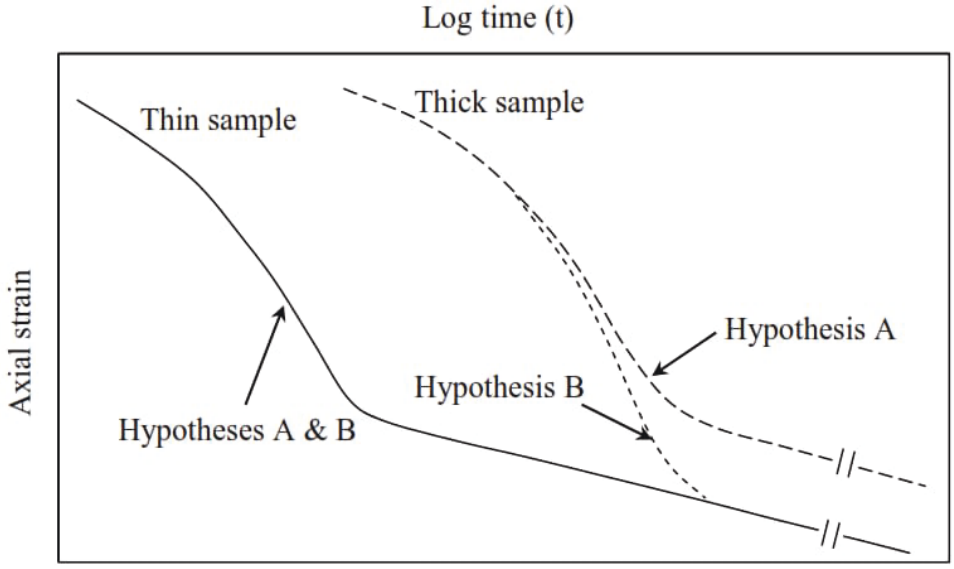

Figure 2.8 Effect of sample thickness on the behaviour of time-dependent settlement of normally consolidated clay (after Ladd et al. 1977)

In this section the mechanism of creep is presented and a summary of previous studies on long-term settlement based on Hypothesis B is reviewed briefly. Then, the elastic visco-plastic model with non-linear creep function (Yin, 1999) model is described in detail applied in this study as a model coupled with consolidation theory aim to performing reliability analysis on long-term settlement of soft soils.

2.3.2 Mechanism of Creep Deformation

As stated by Taylor and Merchant (1940) and Terzaghi (1941), compression settlement of soft soils is defined based on the transferring the stress and adjusting soil structure. There are various studied relevant to creep mechanism in soft soils and the most important of them is explained briefly as follows.

The breakdown of interparticle bonds: There are a variety of factors contributing to the breakdown of interparticle bonds, including relative movement of particles induced by shear displacement or variation of particle spacing (Mesri 1973). This breakdown may cause soil structure rearrangement and further settlement.

Jumping of molecules bonds: Creep settlement may be due to the movement of atoms and molecules to reach a new equilibrium under constant effective stress. As explained by Mitchell et al. (1968), the activation energy required to overcome the berries resists the movement of atoms and molecules depends on deviatoric stress and elapsed time of creep.

Sliding between particles: Kuhn and Mitchell (1993) pointed out creep settlement may be due to the sliding movement between the particles. The sliding movement is due to the tangential component of the contact forces between soil particles because of the nature of viscous friction. The movement of particles is

caused by the relationship between the sliding force, the sliding velocity, and the friction ratio between tangential and normal forces.

Double porosity: De Jong and Verruijt (1965) proposed creep deformation as a result of transferring pore waters from micropores to macropores. This flow of water can impose compression inside clay clusters as a result of decreasing spaces between clay minerals or relative movement of clay particles.

Structural viscosity: This school of thought is based on the opinion that viscosity has a considerable effect on soil creep. Viscosity is explained as the resistance of the fluid to flow or deformation under applied stress. As suggested by Yin (2003) creep is mainly due to the combination of two process, including:

a) Viscous flow of adsorbed double layer water on clay particles

b) Viscous rearrangement of clay particles to reach a new equilibrium under applied effective stresses.

As a result, creep continues as long as the effective stress exists and creep is not due to the free pore water flow which is caused by hydraulic gradient.

2.3.3 Creep Deformation Based on Hypothesis A

As mentioned before, although there is a creep deformation during primary consolidation in Hypothesis A, the void ratio at the end of primary consolidation is assumed constant and not related to the thickness of the sample. One of the significant methods for calculating soft soil settlement based on Hypothesis A is the concept of creep ratio, in which soil settlement is divided into the primary settlement followed by the secondary settlement.

Mesri and Choi (1985) proposed the following equation as a principle equation for predicting the primary consolidation:

$$(\Delta e)_p = \int_0^{t_{EOP}} \left[\left(\frac{\partial e}{\partial \sigma_v'} \right)_t \frac{d\sigma_v'}{dt} \left(\frac{\partial e}{\partial t} \right)_{\sigma_v'} \right] dt \tag{2.33}$$

where, $(\Delta e)_p$ is void ratio changes during primary consolidation, e is void ratio, σ_v' vertical effective stress, t elapsed time, t_{EOP} is time needed for primary consolidation, $\left(\frac{\partial e}{\partial \sigma_v'} \right)_t$ stands for compressibility of the soil at time t, and $\left(\frac{\partial e}{\partial t} \right)_{\sigma_v'}$ stands for compressibility of the soil at σ_v'.

Moreover, as reported by Mesri and Choi (1985), the secondary compression is estimated as follows:

$$(\Delta e)_s = \int_{t_{EOP}}^{t} \left(\frac{\partial e}{\partial t} \right)_{\sigma_v'} dt \tag{2.34}$$

where, $(\Delta e)_s$ stands for the void ratio changes during the secondary compression, e is the void ratio, σ_v' denotes the vertical effective stress, t is the elapsed time, and t_{EOP} is the time needed for the primary consolidation.

Based on the experimental results, Mesri (2003) suggested the secondary compression can be predicted by the creep ratio as follows:

$$(\varepsilon_v)_t = \frac{C_c'}{1 + e_0} log \frac{\sigma_v'}{\sigma_p'} + \frac{C_c}{1 + e_0} \left[\frac{C_\alpha}{C_c} \right] log \frac{t}{t_{EOP}} \tag{2.35}$$

where, $(\varepsilon_v)_t$ is the total vertical strain, e_0 is the initial void ratio, t denotes the elapsed time for secondary compression, t_{EOP} is the time needed for primary consolidation, C_α is the secondary compression index indicates the slope of $e - logt$, C_c is the primary compression index represents for the slope of $e - log\sigma'_v$, and C'_c stands for the secant compression index which is defined as the slope of the lines between point *P* to different point on the compression curve (Figure 2.9). As can be seen in Figure 2.9, point *P* is defined by the recompression line from point (e_0, σ'_{v0}) with the slope C_r at the preconsolidation pressure (σ'_p).

Azari (2015) pointed out that the values of $\frac{C_\alpha}{C_c}$ varies between 0.025 and 0.1 based on the data collected by Mesri and Godlewski (1977a) for some natural soil deposits.

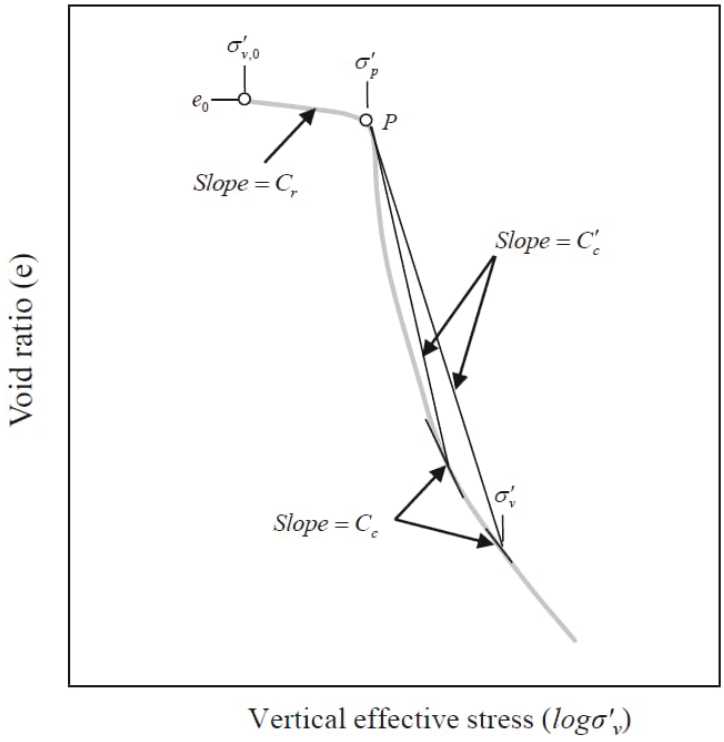

Figure 2.9 Definition of C_r, C_c, and C'_c (after Mesri et al. 1994)

2.3.4 Creep Deformation Based on Hypothesis B

Based on Hypothesis B, the void ratio at the end of primary consolidation is not the same for the thick and thin samples. This hypothesis comes from the assumption that creep occurs during primary consolidation. Leroueil (1996) conducted extensive laboratory and in-situ observations showing that the stress-strain curve followed by a soil element during primary consolidation depends on drainage conditions, strain rate and temperature. The analysis undertaken by Leroueil (1996) confirmed the validity of Hypothesis B.

There are a diversity number of constitutive model for supporting hypothesis B categorized into: empirical models, rheological models, and general stress-strain-time model. These models are explained briefly in this section. Among the existing models, since Yin's model originally proposed by Yin and Graham (1989) in category of empirical models is a simple and reliable model, it is applied for reliability analysis of soft soils in this research. Yin's model is the elastic visco-plastic (EVP) model with the non-linear creep function which is described in detail in Chapter 3.

2.3.4.1 Empirical models

Empirical models are generally based on fitting creep experimental results, stress relaxation, and constant rate of strain tests. As a result, they are mostly proposed by closed form solutions or differential equations. Moreover, by applying boundary condition in laboratory experiments, the empirical solutions would be more practical.

In order to include creep deformation to Terzaghi's consolidation theory, Taylor and Merchant (1940) suggested a method to contain a time dependent

effective stress model. Moreover, Suklje (1957) proposed a model relied on a system of void ratio-effective stress lines at constant stress rate, named isotaches. In this study, a graphical consolidation curves were presented merging into the same linear $e - logt$ and compared with the results obtained by Terzaghi's theory of consolidation.

In another model in empirical models named Bjerrum's model, the clay settlement by including secondary compression were formulated by Buisman (1936). In this study, settlement and logarithm of time were correlated linearly based on the results of oedometer tests on clay and peat after about one day and one minute, respectively. Bjerrum (1967) proposed a theory of time dependent settlement based on two main concepts: 1) parallel time lines or curves in a system of vertical effective stress. 2) a constant relationship between vertical effective stress, void ratio, and time. A family of curves called "time lines" first introduced by Taylor (1942) for the one-dimensional consolidation of clay. In order to define the time lines, the effective stress versus void ratio graph in logarithm scale was used in which each time line is related to a given duration of loading. Figure 2.10 illustrates a sample of time line system. Based on the time lines, Garlanger (1972) presented a formulation expressing void ratio changes as a result of loading from σ_0' to σ_f':

$$e_0 - e = C_r log\frac{\sigma_c'}{\sigma_0'} + C_c log\frac{\sigma_f'}{\sigma_c'} + C_\alpha log\frac{t_i + t}{t_i} \tag{2.36}$$

where, t_i is the reference time line assigned to the instant compression (Garlanger 1972), t is the time from applying the load, σ_c' stands for the critical pressure, and σ_f' is the final vertical effective stress.

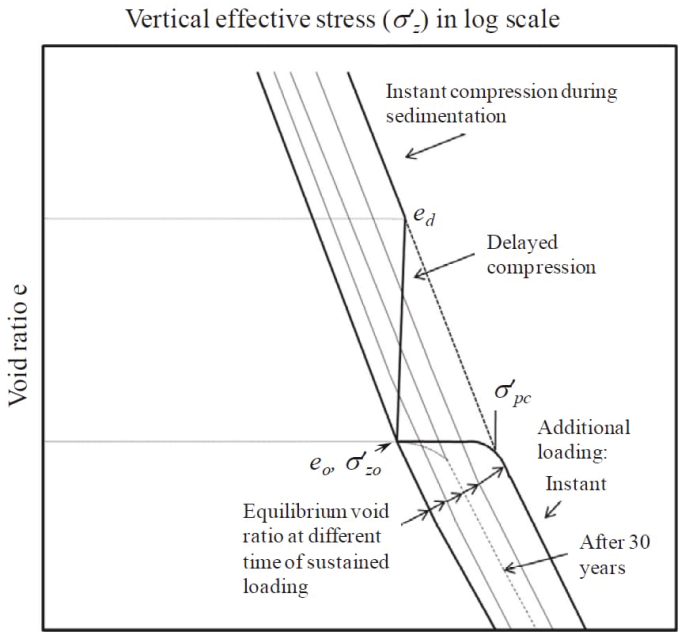

Figure 2.10 Time-line system (after Bjerrum, 1967)

Kabbaj (1985) used the theory of time lines in order to evaluate the effect of the strain rate on the value of the preconsolidation pressure. In Kabbaj's study, the linear relationship between the logarithm of preconsolidation pressure and the logarithm of plastic strain rate, and also a linear relationship between the logarithm of effective stress and the plastic strain were assumed resulting in proposing a model equation to obtain the plastic strain rate. In addition, an elastic visco-plastic empirical model based on equivalent time line concept called Yin's model were proposed first by Yin and Graham (1989) which is explained in detail in Chapter 3.

2.3.4.2 Rheological models

In rheological models, in order to simulate the soil behavior, an appropriate combination of springs, dashpots, and sliders is used. This model is developed by some researchers aim to evaluate the time dependent behavior of soils which are briefly explained.

Gibson and Lo (1961) simulated the compressibility of the soil with the Kelvin element of linear spring and modified Terzaghi's (1923) consolidation theory in order to calculate secondary compression. In this model, the primary compressibility is defined by the instantaneous compression generated by linear springs while the response of Kelvin elements corresponds to the secondary compression.

Wahls (1962) reported that the secondary compression may be calculated by the rate of void ratio change per logarithm of the time ($C_{\alpha e} = -\frac{\Delta e}{\Delta log t}$) concluded by the results of oedometer tests on the samples of calcareous organic silt. Based on the obtained results, Wahls (1962) pointed out that $C_{\alpha e}$ is independet of the load increment and load increment ratio, and the required time for starting the secondary compression is defined by the required time for the completion of primary consolidation. Wahls (1962) modelled the primary consolidation by applying infinite series of Kelvin elements, while creep settlement was simulated by infinite series of nonlinear dashpots. Wahls (1962) used analytical solution of Terzaghi's consolidation theories as a reference in his model.

In another research, Barden (1965) addressed three facts not considered in Terzaghi's (1923) consolidation theory, including (i) the rate of pore water dissipation in the early stages of oedometer test is more than predicted value based on consolidation coefficient, (ii) secondary compression occurs during primary consolidation, (iii) loading condition is the influential factor on the total settlement. As a result, Barden (1965) proposed a rheological model with non-linear springs and dashpots simplified then by adopting linear springs and Kelvin's elements (Figure

2.11). It should be mentioned that in this model the relation between the secondary compression and the logarithm of the time is non-linear.

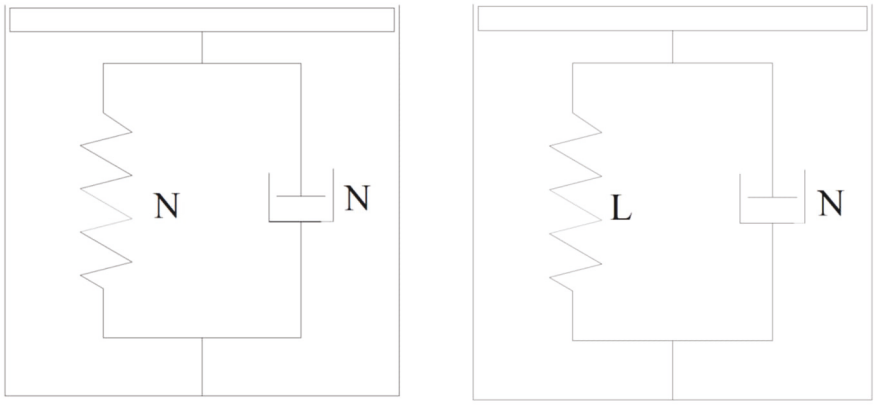

a) Barden's proposed method **b) Model solved by Barden**

Figure 2.11 Rheological models proposed by Barden (after Barden, 1965) (Note: N and L stands for Non-linear and Linear, respectively)

Aboshi (1973), carried out a set of oedometer tests on sample of different sizes in order to evaluate the similarity between field and laboratory deformation on soft soils. The most significance outcomes of Aboshi's (1973) investigations are that the consolidation coefficient (c_v), and the amount of deformation at the end of primary consolidation are dependent to sample thicknesses, while the creep strain rate is independent of sample thickness and it decreases with time to a minimum constant value. As illustrated in Figure 2.12, although the deformation curves become parallel by increasing the time, but they do not reach to a single line. In addition to, Aboshi stated that the primary deformation is dependent to the effective stress loading in time, whereas the secondary compression rate depends on the loading history.

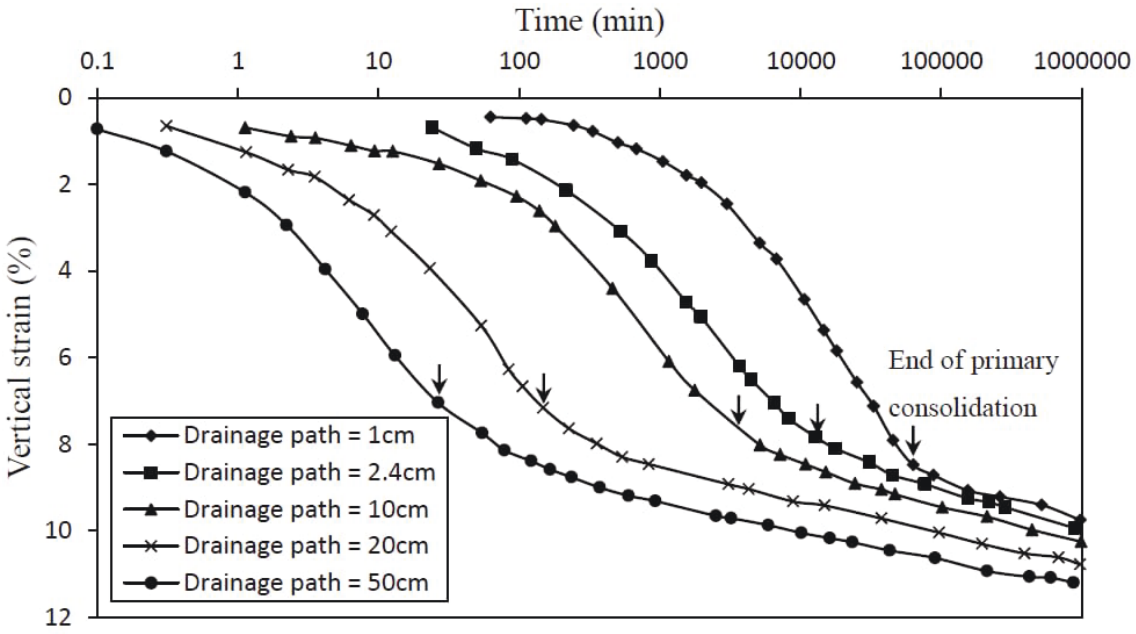

Figure 2.12 Variation of vertical strain with drainage Path (after Aboshi, 1973)

In another rheological model proposed by Rajot (1993), the time dependent constitutive relationship is formulated by a combination of two springs, a dashpot and a slider which is presented in Figure 2.13. In this proposed model, the yield stress and creep are related and the slider properties are a function of the creep value and creep rate.

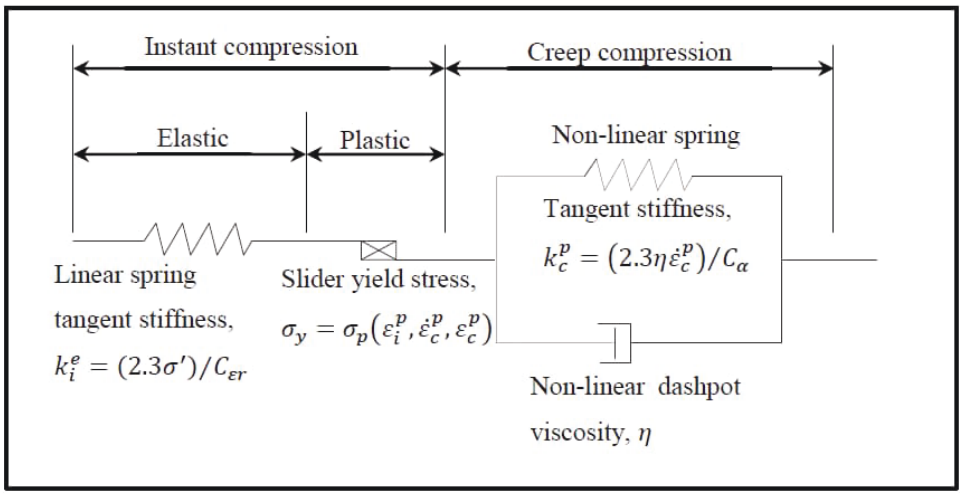

Figure 2.13 Rajot's rheological mechanical (after Aboshi, 1973)

Leroueil et al. (1985) carried out various types of oedometer tests on different samples of Champlain sea clays and proposed a simple rheological clay model which was a particular case of isotache model proposed by Suklje (1957). The model showed the clay behaviour under one-dimensional compression is controlled by a unique effective stress-strain-strain rate.

2.3.4.3 General stress-strain-time models

General stress-strain-time models consider both viscous effect and the rate behavior of soils under various loading conditions. Elastic visco-plastic approach combines the rate dependent elastic and time-dependent plastic behavior of soft soils. As reported by Liingaard et al. (2004), there are three categories of elastic visco-plastic models, including overstress theory, non-stationary flow surface theory, and others.

Based on the Perzyna (1963) visco-plastic overstress theory, the elastic visco-plastic approach applied in one dimensional visco-plastic models for multi-dimensional stress space. As depicted in Figure 2.14, there can be visco-plastic strains when the stress state reaches the yield surface. Otherwise, while visco-plastic

strains are below the yield surface, they can be ignored. It should be mentioned that in Perzyna's (1963) theory, aging effects are not considered. As a result, the yield surface does not change when the visco-plastic strains are unchanged. Furthermore, in the condition of zero over-stress, the visco-plastic strain rate is also zero.

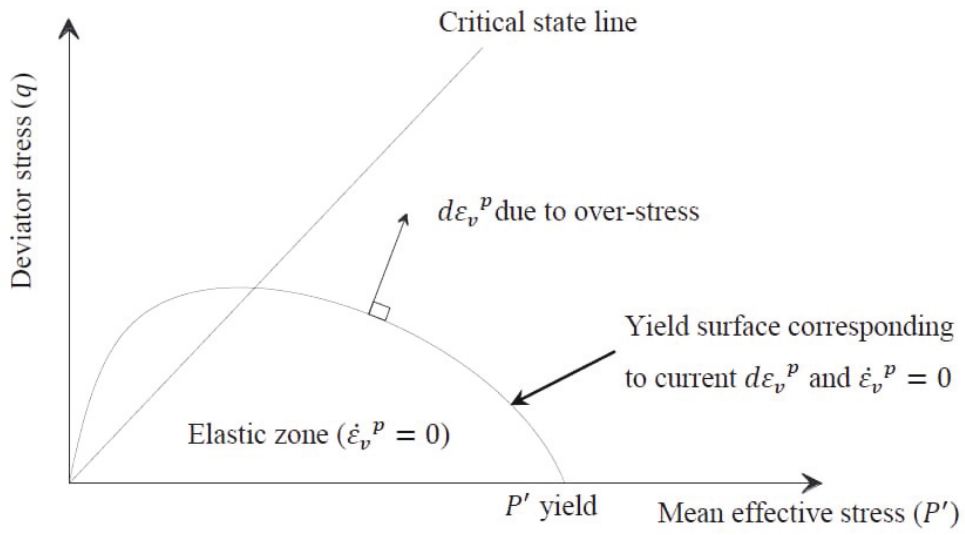

Figure 2.14 Perzyana's (1963) visco-plastic theory (after Perrone, 1998)

In order to modify Perzyna's (1963) theory, Olszak and Perzyna (1966b) proposed a visco-elastic theory named a non-stationary flow surface theory in which the concept of changing the yield surface with time is considered. As can be seen in Figure 2.15, the yield surface is time dependent and represents a specific visco-plastic strain rate.

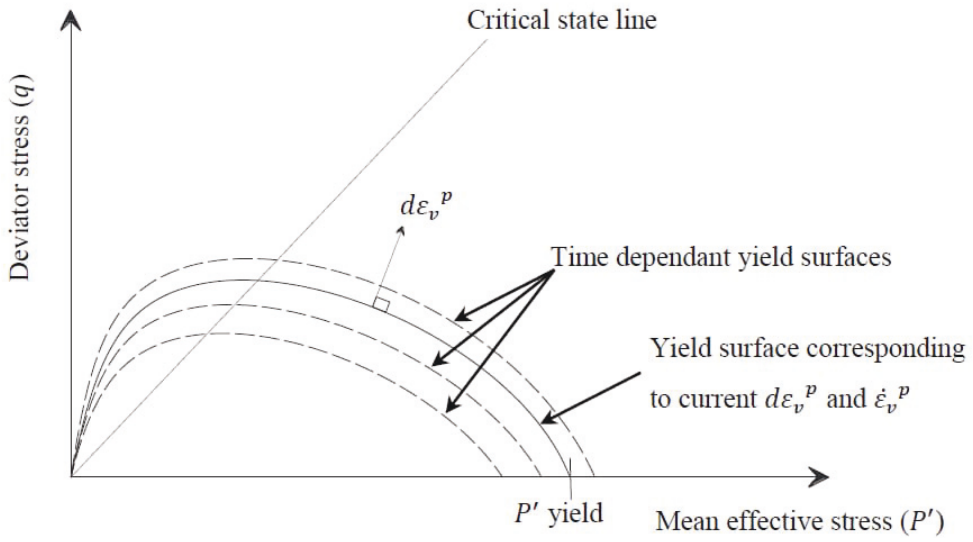

Figure 2.15 Olszak and Perzyna (1963) visco-plastic theory (after Perrone, 1998)

2.4 Literature Review on Probabilistic Analysis in Geotechnical Engineering

At each site the properties of soil and rock vary depending on the lithological heterogeneity of the soil and its inherent spatial variability (Elkateb et al. 2003) in contrast to manufactured materials with controlled properties. Morgenstern (1995) classified geotechnical uncertainties as either parameters, models, or human uncertainties (Zhao and Deng 2019). To quantify these uncertainties, probabilistic or reliability analysis was introduced to distinguish conditions with high or low uncertainties (Duncan 2000).

In recent decades, reliability analysis has been significantly recognized as a great importance in various engineering projects such as nuclear plant (Tosoni et al. 2019; Zheng and Deng 2018) and structural engineering (Coccon et al. 2017; Feng and Zhang 2020; Kim and Song 2019; Ni et al. 2020; Zhou, Li, et al. 2018). Moreover, a great deal of research has adopted probabilistic analysis to manage and control the risks associated with uncertainties in soil for geotechnical problems such

as bearing capacity (Fenton et al. 2008; Griffiths and Fenton 2000; Malhotra et al. 2020; Pramanik et al. 2020), settlement of foundations (Bungenstab and Bicalho 2016), slope stability (Christian et al. 1994; Goh et al. 2019; Jiang et al. 2018), piling (Huang et al. 2016) tunnelling (Feng and Zhang 2020), and seepage (Griffiths and Fenton 1994). The probabilistic methods can also be used for back analysis and updating parameters based on the existing data. Some of these methods include the maximum likelihood method and Bayesian probabilistic method incorporated for geotechnical engineering problems such as characterization of sub surface profiles (Wang 2020; Wang 2016), the model and parameter updating based on measured data with or without considering spatial variability of soil parameters (Jung et al. 2009; Lo and Leung 2019; Zhou, Tan, et al. 2018; Zhou, Li, et al. 2018), as well as the determination of generic transformation and site specific correlation models (Ching et al. 2018; Ching and Phoon 2020a, 2020b).

In addition, there is an array of research studies which consider the uncertainties of soil parameters in probabilistic analysis concerning soil consolidation and settlement (Bari and Shahin 2014; Bari and Shahin 2015; Bari et al. 2013; Bari et al. 2016; Houmadi et al. 2012; Huang et al. 2010). For instance, Huang et al. (2010) combined the coupled Biot (1941) consolidation theory with the random finite element method to investigate how the spatial variability of the coefficient of volume compressibility (m_v) and soil permeability (k) would affect the prediction of settlement and degree of consolidation in one dimensional and two dimensional spaces. In another study, Houmadi et al. (2012) used the Collocation-based Stochastic Response Surface Method (CSRSM) for the probabilistic analysis of a one-dimensional soil consolidation problem by considering Young's modulus

(E), Poisson's ratio (υ), the hydraulic conductivity (k_h) and uniform surcharge loading (q) as random variables. The responses of the probabilistic system considered in the study by Houmadi et al. (2012) were surface settlement and consolidation time. Moreover, Bong et al. (2014) analysed the consolidation of soil by considering the spatial variability of vertical and horizontal coefficients of consolidation while using the Stochastic Response Surface Method (SRSM).

In another study, the effects of spatial varability of soil permeability and coefficient of cosolidation on soil consolidation by prefabricated vertical drains (PVDs) were investigated stocahtically and the uncertainites accosciated with degree of consildation were analysed (Bari and Shahin 2014; Bari et al. 2013). In addition, Bari and Shahin (2015) integrated the local average subdivision of random field method with Monte Carlo simulation to investigate the impact of spatial variability of soil permability and volume compressibility in the smear zone on soil consolidation by PVDs compered with the corresponding impact in the undisturbed zone. The results indicated that the spactial variabitiy of soil permeability in the smear zone has a siginifcant impact on soil consolidation over that on the undisturbed zone. Bari et al. (2016) extended the undrtetaken probabilistic analyses by Bari and Shahin (2015) to soil consolidation by prifabricated vertical drain for single-drain and multi drain systems. Note that while these research studies addressed the time-dependent consolidation deformation of soft soil, they omitted the uncertainties in creep parameters. Liu et al. (2018) reported a probabilistic analysis for predicting the time-dependent settlement and horizontal displacement and pore water pressure of the Ballina test embankment in New South Wales, Australia. In this case study, the probabilistic predictions were combined with the finite element program PLAXIS

2D, adopting Soft Soil Creep Model (SSCM) to simulate the behaviour of the estuarine clay.

It is evident that soil is a heterogeneous material with spatial variable properties stemmed from different factors such as environmental, geological, and physical-chemical processes during soil formation or deposition (Li et al. 2016; Li et al. 2017; Wang et al. 2016). In the random field (RF) method, the soil variability in different directions in space is captured (Ahmed and Soubra 2012; Bari and Shahin 2014; Bari and Shahin 2015; Bari et al. 2013; Bari et al. 2016; Bong et al. 2014; Cassidy et al. 2013; Fenton and Griffiths 2005; Huang et al. 2010; Kasama and Whittle 2016; Van der Have 2015; Wang et al. 2020). Wang et al. (2020) investigated the probability of failure for multi-stage slopes by assuming cohesion and friction angle as spatially random variables. According to the results reported by Wang et al. (2020), the deterministic analysis at the mean values of the strength parameters can result in a non-conservative prediction of factor of safety indicating the significance of performing random field analysis.

One of the inherent essentials in random field analysis (RF) is the introduction of correlation length. In natural soil deposits, two points close to each other may possess approximately the same values, while points widely spaced apart most likely remain uncorrelated. Thus, the concept of spatial correlation length or scale of fluctuation (l_c) is deemed necessary to describe the distance within which the random variables are correlated. A larger correlation length indicates that soil properties vary more smoothly within the layer, while a smaller correlation length implies ragged fluctuation of soil properties in the layer and thus soil is more heterogeneous (Van der Have 2015). Since the in-situ experimental data are often scattered and limited,

establishing a reliable spatial correlation length for a design parameter is a quite challenging task. Consequently, it is highly recommended to perform parametric study to determine the spatial correlation length with maximum risk or probability of failure, referred to as the critical spatial correlation length. For example, referring to the slope stability analysis results, reported in the literature (Allahverdizadeh et al. 2015; Li et al. 2017), the critical spatial correlation length was determined to be 0.5H to 1H, where H is the height of slope. Moreover, in the other research studies reported in the literature, the critical spatial correlation length for the block compression problem was reported to be 0.1B to 2B, where B in the square block dimension (Allahverdizadeh et al. 2016), and for shallow foundation bearing capacity, the critical spatial correlation length was estimated to be between 2B and 10B, where B is the width of the strip footing (Allahverdizadeh Sheykhloo 2015).

2.5 Summary and Gap Identification

In infrastructure projects constructed on top of soft soils, predicting the time-dependent behaviour of soft soils is one of the most important challenges. There are two schools of thought on predicting the time dependent settlement of soft soil, namely Hypotheses A and B. Hypothesis A divides settlement into primary settlement that occurs as excess pore water pressure dissipates, followed by secondary compression settlement (explicitly related to creep) after the excess pore water pressure has dissipated (Mesri 2003; Mesri et al. 1994). According to Yin and Graham (1996), in Hypothesis B however, soil settlement is calculated based on a constitutive model where primary consolidation and creep are considered simultaneously.

There are various constitutive models that support Hypothesis B for predicting the time-dependent behaviour of soft soils classified into empirical models (Bjerrum 1967; Garlanger 1972; Kabbaj 1985; Suklje 1957; Taylor and Merchant 1940; Yin and Graham 1989), rheological models (Aboshi 1973; Barden 1965; Gibson 1961; Gibson and Lo 1961; Leroueil et al. 1985; Rajot 1993; Wahls 1962), and general stress-strain models (Olszak and Perzyna 1966b; Perzyna 1963).

Among the existing models, the category of constitutive models developed by Yin and co-workers is one of the widely accepted approaches to describe the time-dependent behaviour of soft soils. Initially, Yin (1990) proposed a model based on elastic visco-plastic (EVP) behaviour that applied a linear logarithmic function for creep compression to provide an infinite creep settlement as time approaches infinity. However, it is presumed that creep settlement will eventually cease after a very long time when there are no more accessible voids to be compressed. On this basis, Yin (1999) improved the proposed elastic visco-plastic (EVP) model by introducing a non-linear creep function with a creep strain limit, but in order to calculate the creep settlement of soft soil using the EVP model, the model parameters must be determined in advance, which limits its practicality. There are several common methods based on curve fitting to the experimental data to determine the model parameters (Yin 1999; Yin and Graham 1994; Yin et al. 2002). These methods enable the creep parameters to be obtained based on the data measured in the laboratory after completing the primary consolidation stage. For multi-stage loading tests, the time required for excess pore water pressure to dissipate (i.e. end of primary consolidation) varies with the applied stress causing difficulties and uncertainties in evaluating the visco-plastic parameters. This procedure may also violate the concept

whereby the reference-time line may include a large viscous strain, particularly for thicker soil samples or materials with a high creep rate such as organic soils.

To overcome the limitations of these curve fitting methods, an optimisation method was proposed based on the trust-region reflective least square method in which the model parameters are obtained simultaneously based on the test data, while assuming a reference time parameter as the unit value (Le et al. 2017; Le et al. 2016). Yin et al. (2017) also adopted an enhanced genetic algorithm to determine the creep model parameters of soft soils based on an efficient optimisation method. Note that when the experimental data are limited the curve fitting and optimisation methods can lead to uncertainties in determining the visco-plastic parameters. Furthermore, the main concern with determining the parameters in the optimisation methods is finding the best fit between the predicted and observed experimental data, regardless of the statistical characteristics, the measurements, and the model uncertainties. In order to consider uncertainties in determining the model parameters, Zhou, Tan, et al. (2018) adopted the Bayesian model class selection approach and the transitional Markov Chain Monte Carlo (TMCMC) method to select the model and corresponding model parameters best suited to predict the creep behaviour of soft soil using laboratory measurements. In the research conducted by Zhou, Tan, et al. (2018), the uncertainties of soil parameters were quantified via the posterior probabilistic distributions that were obtained based on the Bayesian probabilistic method. In this method, similar to traditional curve fitting and optimisation methods, a limited set of experimental data was used to determine the creep parameters by introducing significant uncertainties. Since it is not practical and cost-effective to carry out long term creep tests to capture creep nonlinearities, the method proposed

by Zhou, Tan, et al. (2018) can be used to determine the optimised creep parameters, but while it will provide a probabilistic evaluation of model predictions based on the given data, it will not address the uncertainties of model parameters due to the lack of sufficient long term test data.

Furthermore, there are another source of uncertainties due to spatial variability of soil parameters due to its inherent variability. Among the existing probabilistic methods, random field analysis (RF) quantifies spatial variability of soil parameters. In random field analysis (RF), introduction of a stablished spatial correlation length is a quite challenging task due to the scattered and limited experimental data. Cho (2007) and Javankhoshdel and Bathurst (2014) claimed that since the highest probability of failure (PF) corresponds to an infinite spatial correlation length ($l_c = \infty$), it is not essential to perform random field analysis. In other words, they claimed that the single random variable (SRV) method is adequate for conservative analysis, in which soil properties are fully correlated and uniform across the site with randomly selected values. In contrast, recent studies undertaken by Li et al. (2017), Allahverdizadeh et al. (2015), Jha and Ching (2013), and Griffiths et al. (2009) confirmed that SRV method can result in over or under estimation of the probability of failure. Therefore, RF analysis and determining the critical spatial correlation length is deemed necessary in the absence of good quality data.

In this research, an elastic visco-plastic creep model is combined with the Monte-Carlo probabilistic method to investigate the effects of uncertainties in the elastic visco-plastic model parameters on time-dependent settlement and the distribution of excess pore water pressure in soft soils under applied loads. The impacts of spatially variable elastic visco-plastic model parameters on long-term

settlement predictions are evaluated through random field analysis (RF) with different spatial correlation lengths to determine the critical spatial correlation length. The Bayesian updating method and transitional Markov Chain Monte Carlo (TMCMC) algorithm are also adopted to update the visco-plastic model parameter based on field monitoring data.

3 Reliability Assessment for Time-Dependent Behaviour of Soft Soils Considering Cross Correlation between Elastic Visco-Plastic Model Parameters

3.1 Introduction

This chapter presents an elastic visco-plastic creep model combined with the Monte-Carlo probabilistic method. The proposed model incorporates multivariate copula and nonlinear analysis to investigate the effects of uncertainties in the elastic visco-plastic model parameters on one-dimensional (1D) time-dependent settlement and the distribution of excess pore water pressure in soft soils under applied loads. It is not practical and cost-effective to carry out long term creep tests to capture creep nonlinearities and determine creep parameters. As a result, the elastic-plastic model parameter (λ/V) and creep coefficient (ψ_0/V) are considered as random variables with lognormal distribution, while considering the cross correlation between these two random variables. A case study based on the Väsby test data (a trial embankment in Sweden) is used to obtain the deterministic and probabilistic parameters. The proposed probabilistic analysis and corresponding numerical results are presented and evaluated against field measurements so that a suitable cross correlation coefficient between selected random variables can be recommended.

This chapter also provides a practical insight into selecting the most suitable cross correlation coefficient between elastic visco-plastic model parameters, while adopting reliability-based design approach that captures the time-dependent deformation of embankments and structures built on soft soils.

3.2 Adopted Elastic Visco-plastic Model

Yin (1999) applied the time-line concept proposed by Bjerrum (1967); it consists of an instant time line, a reference time line, a limit time line, and a system of parallel time lines to develop an elastic visco-plastic model for soils, as shown in Figure 3.1. The vertical strain ε_z, at the effective stress σ'_z, is generally calculated using Equation (3.1):

$$\varepsilon_z = \varepsilon_{z_0}^r + \frac{\lambda}{V} ln\left(\frac{\sigma'_z}{\sigma'_{z_0}}\right) + \frac{\frac{\psi_0}{V}}{1+\frac{\psi_0}{V\varepsilon_{lm}^{vp}} ln\frac{t_0+t_e}{t_0}} ln\frac{t_0+t_e}{t_0} = \varepsilon_z^r + \frac{\frac{\psi_0}{V}}{1+\frac{\psi_0}{V\varepsilon_{lm}^{vp}} ln\frac{t_0+t_e}{t_0}} \quad (3.1)$$

where, $\varepsilon_{z_0}^r$ is the reference strain at the vertical effective stress σ'_{z_0}, and $\varepsilon_z^r = \varepsilon_{z_0}^r + \frac{\lambda}{V} ln\left(\frac{\sigma'_z}{\sigma'_{z_0}}\right)$, σ'_{z_0} and t_0 are the model parameters, t_e denotes the equivalent time, ε_{lm}^{vp} is the creep strain limit, λ/V is the elastic-plastic model parameter, ψ_0/V is the initial creep parameter, and V is the specific volume. In this research, as Yin et al. (2002) pointed out, the creep strain limit was assumed to be $\varepsilon_{lm}^{vp} = \frac{e_0}{1+e_0}$ (where e_0 is the initial void ratio); this corresponds to a condition where there are no more voids left to compress and soil compression would cease.

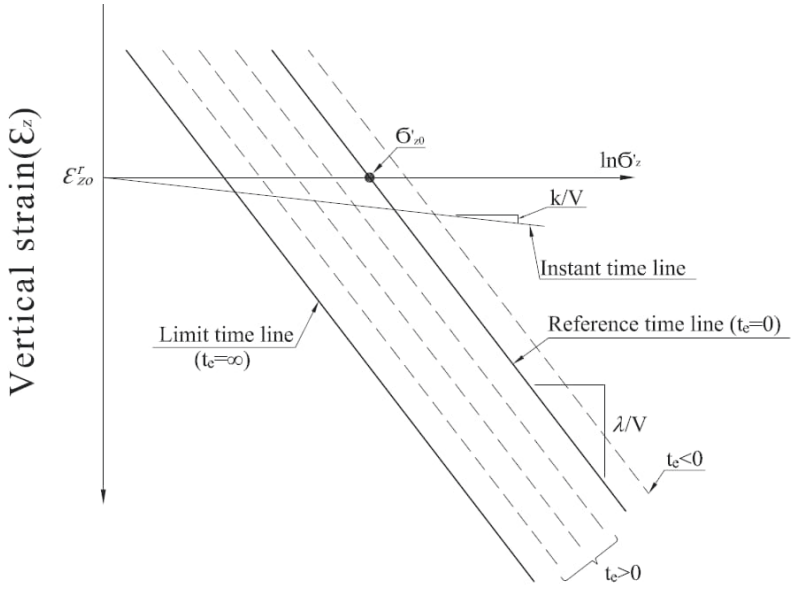

Figure 3.1 The time-line system including instant time line, reference time line, equivalent time lines, and limit time line (data taken from Yin and Graham, 1996)

As Terzaghi (1941) recommended, the continuity equation for saturated soil should be satisfied by aiming to obtain the coupled governing equations for vertical strain and excess pore water pressure:

$$\frac{k}{\gamma_w}\frac{\partial^2 u}{\partial z^2} = -\frac{\partial \varepsilon_z}{\partial t} \tag{3.2}$$

where, k is the coefficient of hydraulic conductivity, γ_w is the water unit weight, u is the pore water pressure equal to sum of the excess pore water pressure (u_e) and the initial equilibrium water pressure (u_0), z is the depth, ε_z is the vertical strain, and t is the elapsed time. Referring to Yin and Graham (1996), by substituting Equation (3.1) into Equation (3.2) and assuming u_0 is constant during consolidation (i.e. $\frac{\partial^2 u}{\partial z^2} = \frac{\partial^2 u_e}{\partial z^2}$), the following equations can be obtained:

- For any (σ'_z, ε_z) point below the limit time-line:

$$\frac{k}{\gamma_w}\frac{\partial^2 u_e}{\partial z^2} = -\frac{\kappa}{V\sigma'_z}\left(\frac{\partial \sigma_z}{\partial t} - \frac{\partial u_e}{\partial t}\right) \tag{3.3.a}$$

- For any $(\sigma'_z, \varepsilon_z)$ point above the limit time-line:

$$\frac{k}{\gamma_w}\frac{\partial^2 u_e}{\partial z^2} = -\left(\frac{\kappa}{V\sigma'_z}\left(\frac{\partial \sigma_z}{\partial t} - \frac{\partial u_e}{\partial t}\right) + \frac{\left(\frac{\psi_0}{V}\right)}{t_0}\left(1 + \frac{\varepsilon_z^r - \varepsilon_z}{\varepsilon_{lm}^{vp}}\right)^2 exp\left(\frac{1}{\left(\frac{\psi_0}{V}\right)}\left(\frac{\varepsilon_z^r - \varepsilon_z}{1 + \frac{\varepsilon_z^r - \varepsilon_z}{\varepsilon_{lm}^{vp}}}\right)\right)\right) \tag{3.3.b}$$

where, κ/V is the elastic model parameter, and t_0 is the model parameter that expresses the time value corresponding to the adopted reference time line. The coefficient of volume compressibility $m_v = \frac{\partial \varepsilon_z}{\partial \sigma'_z}$, and the consolidation coefficient $c_\mathrm{v} = k/(m_v\gamma_w)$, are depth and time dependent. Substituting Equation (3.3) into Equation (3.2) and incorporating $m_v = \frac{\partial \varepsilon_z}{\partial \sigma'_z}$ and $c_\mathrm{v} = k/(m_v\gamma_w)$ leads to the following coupled partial differential equations:

$$c_v\frac{\partial^2 u_e}{\partial z^2} = -\left(\frac{\partial \sigma_z}{\partial t} - \frac{\partial u_e}{\partial t}\right) - \frac{1}{m_v}\ g(\varepsilon_z, \sigma'_z) \tag{3.4.a}$$

$$\frac{\partial \varepsilon_z}{\partial t} = m_v\left(\frac{\partial \sigma_z}{\partial t} - \frac{\partial u_e}{\partial t}\right) + g(\varepsilon_z, \sigma'_z) \tag{3.4.b}$$

where

$$g(\varepsilon_z, \sigma'_z) = \left[\frac{\left(\frac{\psi_0}{V}\right)}{t_0} \left(1 + \frac{\varepsilon_z^r - \varepsilon_z}{\varepsilon_{lm}^{vp}}\right)^2 \; exp\left(\frac{1}{\left(\frac{\psi_0}{V}\right)} \left(\frac{\varepsilon_z^r - \varepsilon_z}{1 + \frac{\varepsilon_z^r - \varepsilon_z}{\varepsilon_{lm}^{vp}}} \right) \right) \right]$$

Similar to Yin and Graham (1996) and Le et al. (2017), the Crank-Nicolson method is used to solve the partial differential equations so that the variations of strains and excess pore water pressures with time and depth could be obtained. The Crank-Nicolson method is based on the central difference and trapezoidal approximation in space and time, respectively; this method is fully implicit and stable without any need for a selected time step (Crank and Nicolson 1947). The following equations illustrate the finite difference form of the above mentioned differential equations for two-way drainage system; they are coded in MATLAB software in this research:

$$-0.5r_{(i,j)}u_{e_{(i-1,j+1)}} + \left(1 + r_{(i,j)}\right)u_{e_{(i,j+1)}} - 0.5r_{(i,j)}u_{e_{(i+1,j+1)}} = 0.5r_{(i,j)}u_{e_{(i-1,j)}} + \left(1 - r_{(i,j)}\right)u_{e_{(i,j)}} + 0.5r_{(i,j)}u_{e_{(i+1,j)}} + h_{(i,j)} \quad (3.5.a)$$

$$\text{with } r_{(i,j)} = (c_v)_{(i,j)}\frac{\Delta t}{\Delta z},\; h_{(i,j)} = \Delta t \frac{1}{(m_v)_{(i,j)}} g(\varepsilon_z, \sigma'_z)_{i,j} + \left((\sigma_z)_i^{j+1} - (\sigma_z)_i^j\right)$$

$$\varepsilon_{z_{(i,j+1)}} = \varepsilon_{z_{(i,j)}} + (m_v)_{(i,j)}\left[\left(\sigma_{z_{(i,j+1)}} - \sigma_{z_{(i,j)}}\right) - \left(u_{e_{(i,j+1)}} - u_{e_{(i,j)}}\right)\right] + \Delta t g(\varepsilon_z, \sigma'_z)_{i,j} \quad (3.5.b)$$

where Δt and Δz are time and depth increments, respectively. As Figure 3.2 shows, the subscript $i = 2, 3, \dots, n$ indicates the variation in depth, and the subscript $j = 1, 2, \dots, m$ describes the variation of time. The boundary conditions used in this study are pervious at the top and bottom layers, as shown in Figure 3.2. By applying a two-way drainage boundary condition, the tridiagonal matrix can be obtained to solve Equation (3.5):

$$\begin{bmatrix} \mathbf{1+r} & \mathbf{-0.5r} & \mathbf{0} & . & \mathbf{0} & \mathbf{0} \\ \mathbf{-0.5r} & \mathbf{1+r} & \mathbf{-0.5r} & . & \mathbf{0} & \mathbf{0} \\ \mathbf{0} & \mathbf{-0.5r} & \mathbf{1+r} & . & \mathbf{0} & \mathbf{0} \\ . & . & . & . & . & . \\ \mathbf{0} & \mathbf{0} & \mathbf{0} & . & \mathbf{1+r} & \mathbf{-0.5r} \\ \mathbf{0} & \mathbf{0} & \mathbf{0} & . & \mathbf{-0.5r} & \mathbf{1+r} \end{bmatrix} \begin{bmatrix} \begin{bmatrix} \boldsymbol{u_{e2}} \\ \boldsymbol{u_{e3}} \\ \boldsymbol{u_{e4}} \\ . \\ \boldsymbol{u_{en-2}} \\ \boldsymbol{u_{en-1}} \end{bmatrix}_{j+1} \end{bmatrix}$$

$$= \begin{bmatrix} \mathbf{1-r} & \mathbf{0.5r} & \mathbf{0} & . & \mathbf{0} & \mathbf{0} \\ \mathbf{0.5r} & \mathbf{1-r} & \mathbf{0.5r} & . & \mathbf{0} & \mathbf{0} \\ \mathbf{0} & \mathbf{0.5r} & \mathbf{1-r} & . & \mathbf{0} & \mathbf{0} \\ . & . & . & . & . & . \\ \mathbf{0} & \mathbf{0} & \mathbf{0} & . & \mathbf{1-r} & \mathbf{0.5r} \\ \mathbf{0} & \mathbf{0} & \mathbf{0} & . & \mathbf{0.5r} & \mathbf{1-r} \end{bmatrix} \begin{bmatrix} \begin{bmatrix} \boldsymbol{u_{e2}} \\ \boldsymbol{u_{e3}} \\ \boldsymbol{u_{e4}} \\ . \\ \boldsymbol{u_{en-2}} \\ \boldsymbol{u_{en-1}} \end{bmatrix}_{j} + \begin{bmatrix} \boldsymbol{h_2} \\ \boldsymbol{h_3} \\ \boldsymbol{h_4} \\ . \\ \boldsymbol{h_{n-2}} \\ \boldsymbol{h_{n-1}} \end{bmatrix}_{j} \end{bmatrix} \quad (3.6)$$

In order to obtain the ground surface settlement at time t by adopting the vertical strain, the following equation is applied:

$$S_t = \int_{z=0}^{z=H} (\varepsilon_z)_t \, dz \quad (3.7)$$

where, H is the total depth of the soil layer.

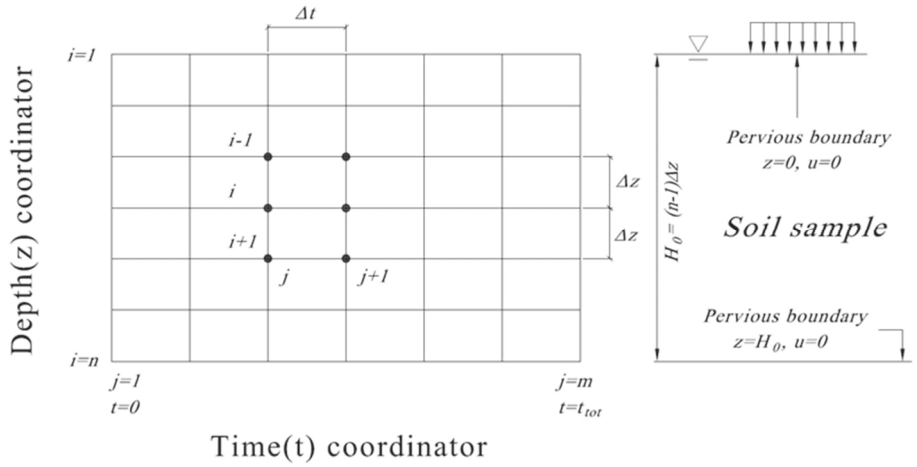

Figure 3.2 Adopted grid and boundary conditions of the Crank-Nicolson finite difference

3.3 Probabilistic Analysis

3.3.1 Adopted Probabilistic Method

It is common to adopt approximate reliability methods including, first order methods, first order second moment reliability methods, responses surface methods and Monte-Carlo simulation in engineering practice. As reported by Wang et al. (2019), among different reliability analysis methods, Monte-Carlo simulation is straightforward to use, and suitable for nonlinear and complex functions. The Monte-Carlo simulation is a powerful technique that simulates uncertainties and stochastic properties, using random values for each uncertain parameter in a model, and then quantifies its probability density function. In this study, a series of probabilistic analyses are carried out using the Monte-Carlo approach incorporating multivariate data and nonlinear analysis relying on repeated random sampling to evaluate uncertainties and risks in quantitative decision making. The random variables considered in this research are the elastic-plastic parameter (λ/V) and the initial creep coefficient (ψ_0/V), which are comparable to the conventional values of primary compression ($C_C/ln10$) and secondary compression coefficient ($C_\alpha/ln10$).

The statistical characteristics of lognormally distributed random variables of λ/V and ψ_0/V are the mean ($\mu_{\lambda/V}, \mu_{\psi_0/V}$) and standard deviation ($\sigma_{\lambda/V}, \sigma_{\psi_0/V}$). In order to indicate the mean and standard deviation in terms of a dimensionless parameter, the coefficients of the variations of selected random variables are determined as follows (Baecher and Christian 2005):

$$COV_X = \frac{\sigma_X}{\mu_X}, \quad (for\ X = \frac{\lambda}{V}, \frac{\psi_0}{V}) \tag{3.8}$$

The coefficient of variation (COV_X) indicates that the confidence level related to uncertainties with input parameters, such that a high COV_X expresses the low confidence level of soil parameters and vice versa.

Since the selected random variables are non-negative, the elastic-plastic parameter (λ/V) and initial creep coefficient (ψ_0/V) are assumed to be characterised statistically by lognormal distribution having a simple relationship with normal distribution, as recommended by Fenton and Griffiths (2002) and Liu et al. (2018). The mean (μ_{lnX}) and the standard deviation (σ_{lnX}) of the transformed Gaussian (normal) random variables $ln\lambda/V$ and $ln\psi_0/V$ can be obtained as:

$$\mu_{lnX} = ln\mu_X - \frac{1}{2} ln\{1 + (COV_X)^2\} = ln\left(\frac{\mu_X}{\sqrt{1+(COV_X)^2}}\right), \ (for\ X = \lambda/V, \psi_0/V) \tag{3.9}$$

$$\sigma_{lnX} = \sqrt{ln\{1 + (COV_X)^2\}}, \quad (for\ X = \lambda/V, \psi_0/V) \tag{3.10}$$

When the selected random variables λ/V and ψ_0/V are correlated, it is implied that the likelihood of the random variable ψ_0/V occurring depends on the occurrence of random variable λ/V, hence establishing the joint cumulative density function (CDF) of these two random variables is not straightforward. Referring to Feng and Zhang (2020), the Gaussian copula function in the series of elliptical copulas were adopted to generate correlated random variables. It is essential to determine the cross correlation coefficient between two random variables in the Gaussian copula model. For this purpose, two methods namely the Pearson and Kendall's rank correlation methods are adopted in this study to measure the selected random variables dependency and the cross correlation coefficient. Referring to Nelsen (2007), the covariance $Cov[\lambda/V, \psi_0/V]$ and the Pearson cross correlation coefficient ($\rho_{p_{\lambda/V,\psi_0/V}}$) can be introduced as follows:

$$Cov[\lambda/V, \psi_0/V] = \frac{1}{N}\sum(\lambda/V_i - \mu_{\lambda/V})(\psi_0/V_i - \mu_{\psi_0/V}) \tag{3.11}$$

$$\rho_{p_{\lambda/V,\psi_0/V}} = \frac{Cov[\lambda/V,\psi_0/V]}{\sigma_{\lambda/V}\sigma_{\psi_0/V}} \tag{3.12}$$

where N is the number of samples.

The Kendall's rank correlation coefficient is also adopted to measure λ/V and ψ_0/V dependency. According to this method, the Kendall's rank correlation coefficient (τ_k) can be obtained as follows (Feng and Zhang 2020; Nelsen 2007):

$$\tau_k = \frac{2}{N(N-1)} \sum_{i<j} sign\left[\left(\frac{\lambda}{V_{1i}} - \frac{\lambda}{V_{1j}}\right)\left(\frac{\psi_0}{V_{2i}} - \frac{\psi_0}{V_{2j}}\right)\right] \; i,j = 1,2,\ldots,N \tag{3.13.a}$$

$$sign\left[\left(\frac{\lambda}{V_{1i}} - \frac{\lambda}{V_{1j}}\right)\left(\frac{\psi_0}{V_{2i}} - \frac{\psi_0}{V_{2j}}\right)\right] = \begin{cases} 1 & if\ \left(\lambda/V_{1i} - \lambda/V_{1j}\right)\left(\psi_0/V_{2i} - \psi_0/V_{2j}\right) > 0 \\ -1 & if\left(\lambda/V_{1i} - \lambda/V_{1j}\right)\left(\psi_0/V_{2i} - \psi_0/V_{2j}\right) < 0 \end{cases} \tag{3.13.b}$$

The Kendall's rank cross correlation coefficient ($\rho_{k_{\lambda/V,\psi_0/V}}$) are derived from τ_k as expressed in Equation (3.14):

$$\tau_k = \frac{2}{\pi}\, arcsin\left(\rho_{k_{\lambda/V,\psi_0/V}}\right) \tag{3.14}$$

In order to generate cross correlated random variables based on Gaussian copula method, the probability density function $f(X,\mu,\Sigma)$ of the d dimensional multivariate normal distribution can be used, as recommended by Genz and Bretz (2002):

$$f(X,\mu,\Sigma) = \frac{1}{\sqrt{|\Sigma|(2\pi)^d}} \exp\left(-\frac{1}{2}(Y-\mu)\Sigma^{-1}(Y-\mu)'\right) \tag{3.15}$$

where d is the number of random variables, Y is the $1 \times d$ vectors of random variables, μ is the mean value, and Σ is a $d \times d$ symmetric positive definite matrix of covariance. The diagonal elements of Σ consist of the variances for variables, while the off-diagonal elements of Σ include the covariance between variables. In the

next step, the generated random variables should be converted to the cumulative density function with standard normal distribution ($i.e.\ \mu_Z = 0, \sigma_Z = 1$) as:

$$normcdf(Z) = \frac{1}{\sqrt{\pi}} \int_{-\frac{Z}{\sqrt{2}}}^{\infty} e^{-t^2} dt \tag{3.16}$$

where Z is a $1 \times d$ vector of correlated random variables with zero mean and one standard deviation.

The following function is then applied to convert the generated cumulative density function of cross correlated random variables with a standard normal distribution to a lognormal distribution:

$$X = F^{-1}(normcdf(Z)|\mu, \sigma) =$$

$$F^{-1}\left(\frac{1}{\sigma\sqrt{2\pi}} \int_0^X \frac{e^{\frac{-(\ln(t)-\mu)^2}{2\sigma^2}}}{t} dt \right) (for\ X = \lambda/V, \psi_0/V) \tag{3.17}$$

where, X is the 1×2 vector of correlated random variables λ/V and ψ_0/V, μ and σ are the mean and the standard deviation of underlying normal distribution; indeed they are obtained using Equation (3.9) and Equation (3.10).

Figure 3.3 summarises an adopted probabilistic method by a flowchart.

3.3.2 Adopted Case Study

Long term consolidation settlements beneath several test fills were monitored at Väsby, Sweden (Chang 1981a). The Väsby study area is located near Uplands Väsby

village, 30 km north of Stockholm on the east coast of Sweden. As Chang (1981a) reported, these three test fills, including one with vertical drains and two without vertical drains, were built in the Väsby area to study the long term behaviour of Swedish clays by evaluating the suitability of the site for airport construction. The first undrained test fill of gravel with a density of 1700 kg/m^3, a height of 2.5 m, and bottom dimensions of 30m×30m and slope of 1(V): 1.5 (H) was constructed in 1947 over 25 days. In this study, only the first 2.5 m high test fill, constructed with no vertical drains, is investigated and discussed. The stress applied at the ground surface due to the fill weight was 40.6 kPa and the mean water level was 0.8m below the ground surface, with minor seasonal variations (Larsson and Mattsson 2003). Figure 3.4 shows that the 14 m deep subsoils in layers I, II, and III consist of post glacial clays, while layer IV consists of glacial clay.

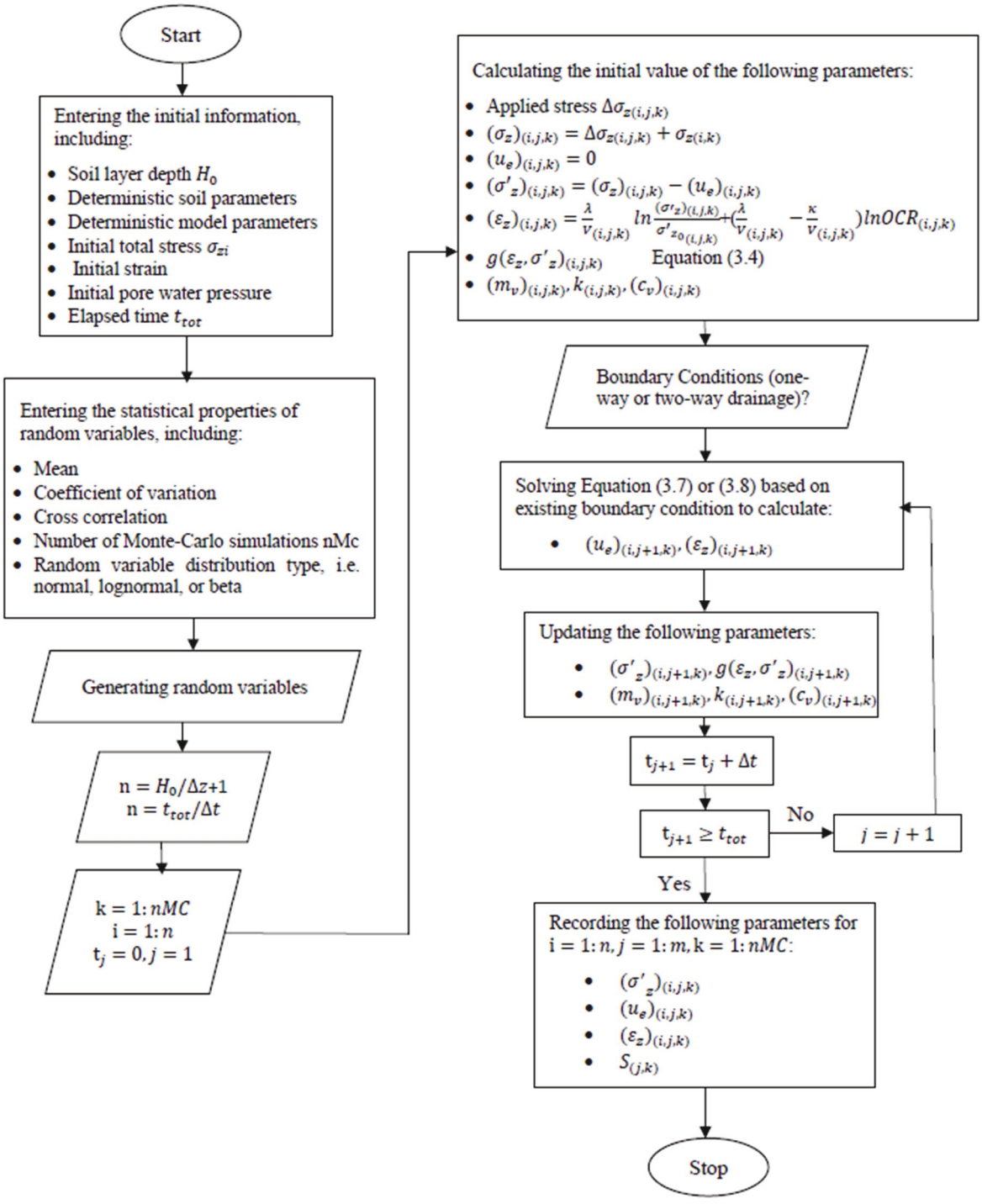

Figure 3.3 Flowchart for probabilistic analysis of time-dependent behaviour of soft soils based on EVP model

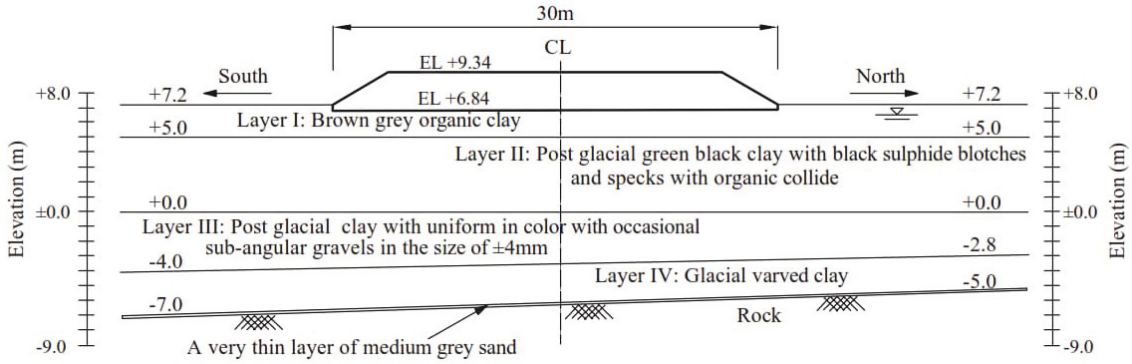

Figure 3.4 Subsoil layer for Väsby test fill (Data taken from Chang, 1981)

The properties of this soil, including the void ratio, the permeability, the water content, the soil compressibility indices, the soil unit weight, and Atterberg limits, are obtained by carrying out a series of laboratory investigations Chang (1981a). Figure 3.5 shows the soil parameters, used for the numerical simulation, are based on the laboratory test results, and included the void ratio, the soil unit weight, the soil permeability, and the over consolidated ratio (OCR). To determine elastic visco-plastic model parameters, the curve fitting methods are used (Le 2015; Yin 1999; Yin and Graham 1994; Yin et al. 2002). As Figure 3.6 shows, model parameters such as the initial creep coefficient (ψ_0/V) and the time independent elastic-plastic parameters (κ/V, σ'_{z_0}, and λ/V), are obtained using the results of the oedometer test continuing after almost complete dissipation of excess pore water pressure (i.e. end of primary consolidation).

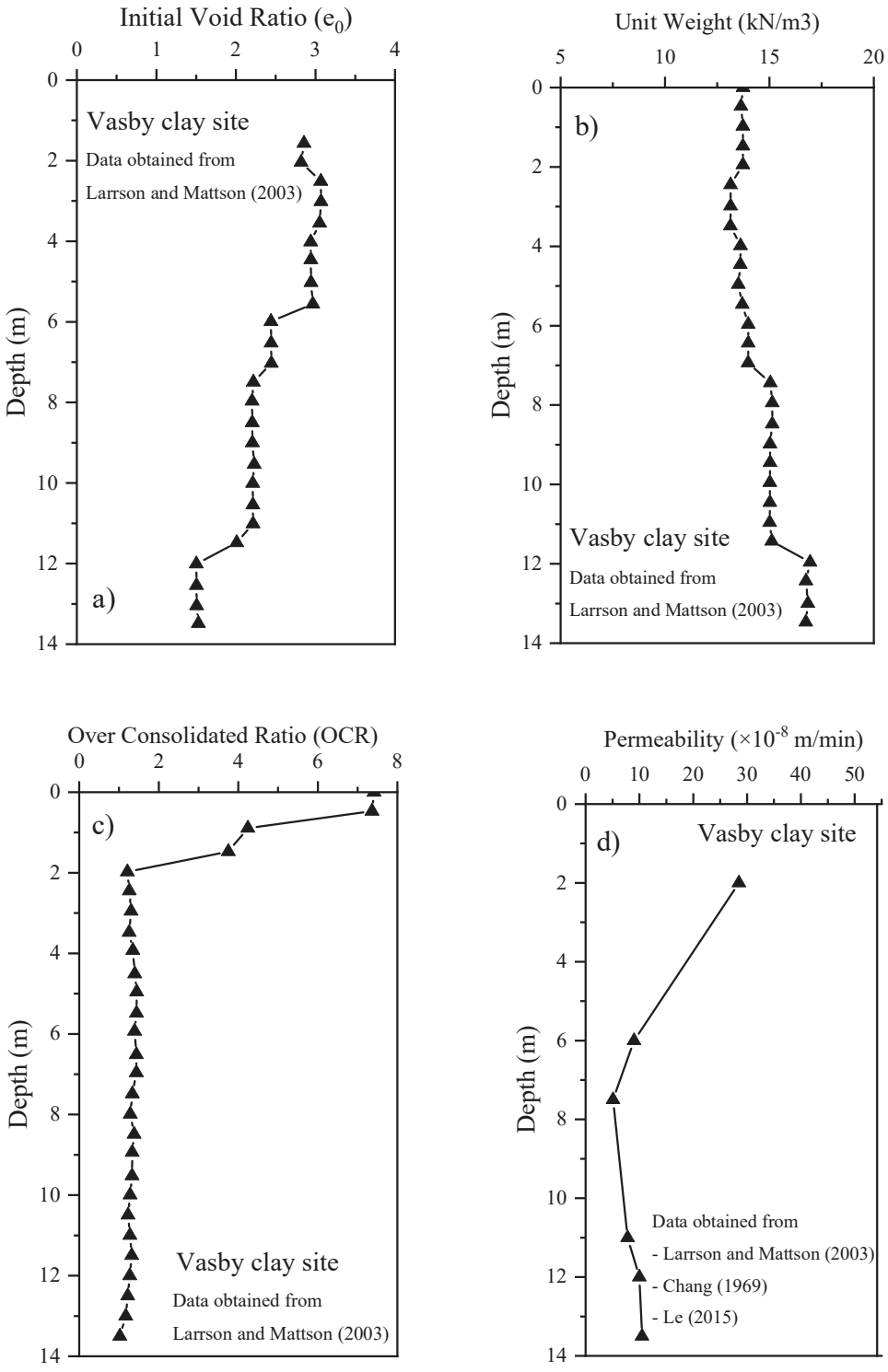

Figure 3.5 Deterministic adopted soil properties of Väsby test fill for numerical modelling for Väsby test fill (a) initial void ratio (b) total unit weight (c) over-consolidated ratio (d) permeability

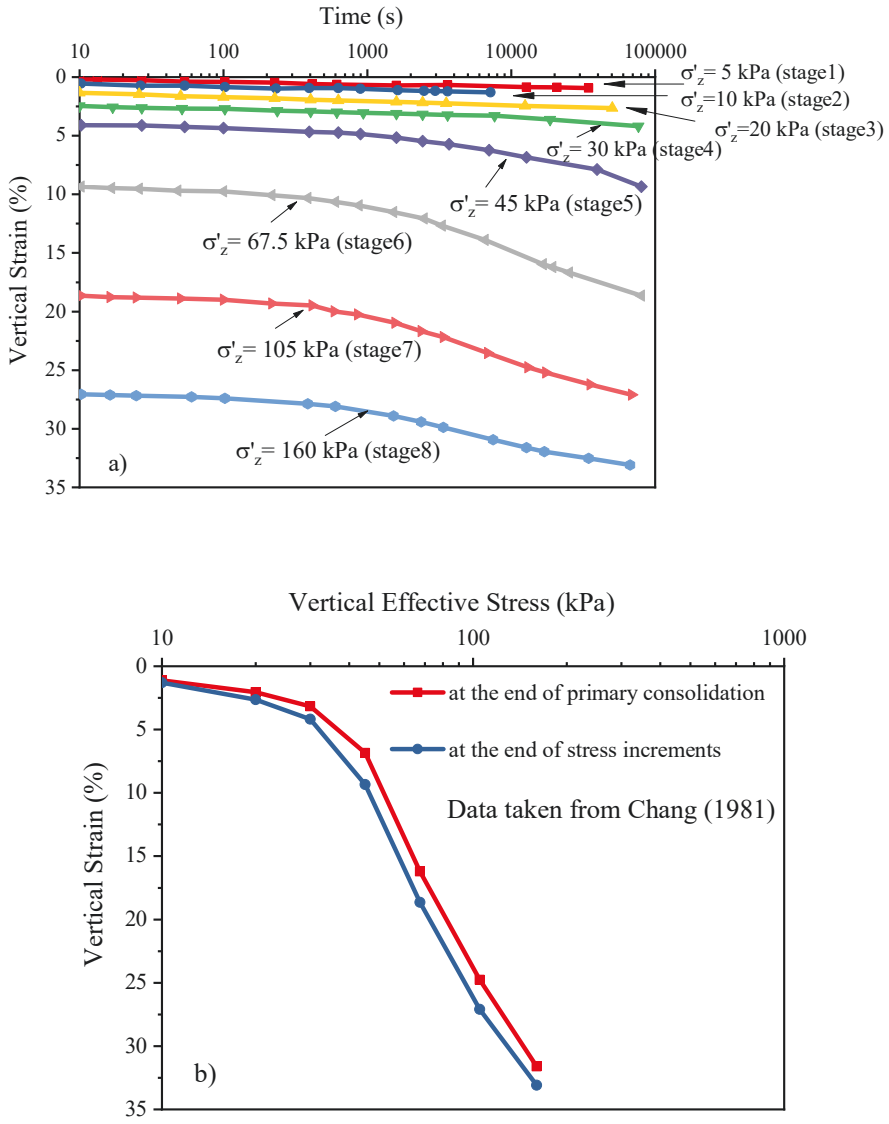

Figure 3.6 Oedometer test results of Väsby test (a) vertical strain versus time and (b) vertical strain versus vertical effective stress (Data taken from Chang, 1981)

To obtain more reliable creep parameters, long term oedometer tests are needed, but very long creep tests are neither feasible nor cost effective, so the lack of long term creep tests can lead to uncertainties in estimating the model parameters as well as uncertainties caused by soil heterogeneity on site. As a result, the initial creep coefficient (ψ_0/V) and elastic-plastic parameter (λ/V) are considered as

probabilistic values. As Yin et al. (2002) proposed, the creep strain limit (ε_{lm}^{vp}) is determined based on the initial void ratio, to be equal to $\frac{e_0}{1+e_0}$.

To obtain the initial creep coefficient (ψ_0/V) and also cover uncertainties stemming from the methods of interpretation, a method based on the conventional approach proposed by Yin (1999) is adopted. The procedure for determining the initial creep coefficient (ψ_0/V) and the creep strain limit (ε_{lm}^{vp}) begins with selecting the Yin model parameter t_0. In this study, t_0 is the time when the excess pore water pressure in the small laboratory sample has almost completely dissipated, so any further strain beyond this time would be due to creep only. To determine the creep parameters, Equation (3.1) is rearranged to obtain Equation (3.18), and this yielded a linear function, where $y = x + a$, in which a is the inverted values of the initial creep coefficient (ψ_0/V), and x and y are equal to $\frac{1}{\varepsilon_{lm}^{vp}} ln\left(\frac{t_0+t_{vp}}{t_0}\right)$ and $\frac{ln\frac{t_0+t_{vp}}{t_0}}{\varepsilon_z^{vp}}$, respectively.

$$\frac{ln\frac{t_0+t_{vp}}{t_0}}{\varepsilon_z^{vp}} = \frac{1}{\frac{\psi_0}{V}} + \frac{1}{\varepsilon_{lm}^{vp}} ln\left(\frac{t_0+t_{vp}}{t_0}\right) \tag{3.18}$$

where, t_{vp} is the creep time determined by subtracting the loading time from the end of primary compression time (t_{EOP}) for the small laboratory sample.

By referring to the values reported in Table 3.2, the mean and coefficient of variation for the initial creep coefficient (ψ_0/V) are determined to be 0.0135 and 0.3, respectively.

Two methods are used to determine the elastic-plastic parameter (λ/V) and the elastic-visco plastic model parameter (σ'_{z_0}). In the first method, referring to Yin (1999), the slope of vertical strain versus vertical effective stress (semi-logarthmic scale) is used as the slope of the reference time-line (i.e. λ/V). In the second method, to define the reference time line parameters, Equation (3.1) is used by assuming that the reference point equals the point where the excess pore water pressure has almost completely dissipated. Referring to Yin and Graham (1994), it is convenient to select a point where $\sigma'_z = \sigma'_{z_0}$ and $\varepsilon^r_{z_0} = 0$, so the elastic-plastic parameter (λ/V) could be defined Equation (3.19):

$$\varepsilon^r_z = \varepsilon^r_{z_0} + \frac{\lambda}{V} ln\left(\frac{\sigma'^r_z}{\sigma'_{z_0}}\right) \tag{3.19}$$

where, ε^r_z and σ'^r_z are the vertical strain and effective stress at the reference point known and obtained from the oedometer test results, respectively.

Another loading stage is then selected in the normally consolidated range and called point 2. The vertical strain at point 2 due to the effective stress at this stage (σ'_{z_2}) is defined based on Equation. (3.20):

$$\varepsilon_{z2} = \frac{\lambda}{V} ln\left(\frac{\sigma'_{z_2}}{\sigma'_{z_0}}\right) + \frac{\frac{\psi_{02}}{V}}{1 + \frac{\psi_{02}}{V\varepsilon^{vp}_{lm}} ln\frac{t_0 + t_{e2}}{t_0}} ln\frac{t_0 + t_{e2}}{t_0} \tag{3.20}$$

where, t_{e2} denotes the equivalent time at stage 2, $\frac{\psi_{02}}{V}$ is the initial creep coefficient determined at stage 2, and the creep strain limit (ε_{lm}^{vp}) is constant and equal to $\frac{e_0+1}{e_0}$.

In Equation (3.20), the equivalent time at stage 2 (t_{e2}), the elastic-plastic parameter (λ/V), and the elastic-visco plastic model parameter (σ'_{z_0}) are unknown parameters. By defining the equivalent time at stage 2 (t_{e2}), the elastic-plastic parameter (λ/V) and the elastic-visco plastic model parameter (σ'_{z_0}) can be obtained using Equation (3.19) and (3.20). Referring to Le et al. (2017), the equivalent time at stage 2 (t_{e2}) can be defined via an intermediate and instant elastic point under the effective stress increments from stage 1 to stage 2. This point is called point $2'$ and the vertical strain at this point can be obtained based on Equation (3.21):

$$\varepsilon_{z2'} = \varepsilon_{z1} + \frac{\kappa}{V} ln\left(\frac{\sigma'_{z_2}}{\sigma'_{z_1}}\right) = \frac{\lambda}{V} ln\left(\frac{\sigma'_{z_2}}{\sigma'_{z_0}}\right) + \frac{\frac{\psi_{02}}{V}}{1+\frac{\psi_{02}}{V\varepsilon_{lm}^{vp}} ln\frac{t_0+t_{e2'}}{t_0}} ln\frac{t_0+t_{e2'}}{t_0} \tag{3.21}$$

By rearranging Equation (3.21), the value of $t_{e2'}$ is computed as follows:

$$t_{e2'} = t_0 exp\left(\frac{\frac{\varepsilon_{lm}^{vp}}{\frac{\psi_{02}}{V}} \left(\varepsilon_{z1} + \frac{\kappa}{V} ln\left(\frac{\sigma'_{z_2}}{\sigma'_{z_1}}\right) - \frac{\lambda}{V} ln\left(\frac{\sigma'_{z_2}}{\sigma'_{z_0}}\right)\right)}{1 - \left(\frac{1}{\varepsilon_{lm}^{vp}}\left(\varepsilon_{z1} + \frac{\kappa}{V} ln\left(\frac{\sigma'_{z_2}}{\sigma'_{z_1}}\right) - \frac{\lambda}{V} ln\left(\frac{\sigma'_{z_2}}{\sigma'_{z_0}}\right)\right)\right)}\right) - t_0 \tag{3.22}$$

The total loading time required for stress increment is from point $2'$ to point 2 because the stress increment from point 1 to point $2'$ is time-independent.

Consequently, the equivalent time at stage 2 (t_{e2}) is calculated based on Equation (3.23):

$$t_{e2} = t_{e2'} + \Delta t$$

$$= t_0 exp\left(\frac{\varepsilon_{lm}^{vp}}{\frac{\psi_{02}}{V}} \frac{\left(\varepsilon_{z1} + \frac{\kappa}{V} ln\left(\frac{\sigma'_{z_2}}{\sigma'_{z_1}}\right) - \frac{\lambda}{V} ln\left(\frac{\sigma'_{z_2}}{\sigma'_{z_0}}\right)\right)}{1 - \left(\frac{1}{\varepsilon_{lm}^{vp}}\left(\varepsilon_{z1} + \frac{\kappa}{V} ln\left(\frac{\sigma'_{z_2}}{\sigma'_{z_1}}\right) - \frac{\lambda}{V} ln\left(\frac{\sigma'_{z_2}}{\sigma'_{z_0}}\right)\right)\right)}\right) - t_0 + \Delta t_2 \quad (3.23)$$

where, Δt_2 is the loading time at stage 2.

Substituting Equation (3.23) into Equation (3.20) forms an equation with two unknowns (λ/V and σ'_{z_0}); this equation can then be combined with Equation (3.19) to yield a system of two equations and two unknowns.

A set of data for the elastic-plastic parameter (λ/V) and the elastic-visco plastic model parameter (σ'_{z_0}) is obtained by adopting the above-mentioned methods. Note that since the reference time line parameters ($\sigma'_{z_0}$and λ/V) are interdependent, a relationship between the elastic-plastic parameter (λ/V) and the elastic-visco plastic model parameter (σ'_{z_0}) must be found so that by generating random values for the elastic-plastic parameter (λ/V) the corresponding elastic-visco plastic model parameter (σ'_{z_0}) could be determined. This is why the regression analysis to find the best fit curve with minimum error is adopted. As can be seen in Table 3.2, the logarithmic regression can be considered as the most appropriate curve fitting between the elastic-plastic parameter (λ/V) and the elastic-visco plastic model parameter (σ'_{z_0}). Furthermore, to have a larger range of data for the elastic-plastic

parameter (λ/V), a set of data such as the compression index ($C_{c\varepsilon} = \frac{\lambda}{V} ln10$), as calculated by Perrone (1998) from 24-hour oedometer tests, is adopted; these values are summarised in Table 3.1.

Table 3.1 Adopted values for $C_{c\varepsilon}$ and λ/V based on oedometer test results

Layer Number	Disturbed Sample		Undisturbed Sample		Notes
	$C_{c\varepsilon}$	λ/V	$C_{c\varepsilon}$	λ/V	
I	0.4	0.17	0.51-0.74	0.22-0.32	Data taken from Perrone (1998)
II	0.4-0.6	0.17-0.26	0.36-0.74	0.16-0.32	
III	0.6	0.26	0.36-0.74	0.16-0.32	
IV	0.55	0.24	0.36	0.16	

Random variables and corresponding statistical properties such as the mean and standard deviation, and the cross correlation coefficient generated by existing data, are presented graphically in Figure 3.7. The deterministic and random model parameters, and the corresponding statistical properties, are summarized in Table 3.2. Table 3.2 reveals that the calculated ratio of $\mu_{\frac{\lambda}{V}}/\mu_{\frac{\psi_0}{V}}$ is 0.06, which is similar to the corresponding ratio of $\frac{C_{\varepsilon\alpha}}{C_{\varepsilon C}} = 0.06$ for the undisturbed Väsby clay reported by Mesri and Choi (1985). Mesri (2003) further pointed out that the secondary compression can be predicted by adopting the creep ratio $\frac{C_{\varepsilon\alpha}}{C_{\varepsilon C}}$, which is a constant ratio for each soil. This ratio varies with the type of soil between 0.025 and 0.1 based on the data collected by Mesri and Godlewski (1977b) for some natural soil deposits. Therefore, the elastic-plastic parameter (λ/V) and the initial creep coefficient (ψ_0/V) should be considered as correlated random variables. The cross correlation coefficient between λ/V and ψ_0/V are determined by adopting both Pearson and Kendall's rank method

as discussed in Section 3.3.1. Figure 3.7 shows that based on the existing data, the calculated cross correlation coefficient between the elastic-plastic parameter (λ/V) and the initial creep coefficient (ψ_0/V) is 0.5; however, since the existing number of oedometer test results might not be sufficient to generate a more precise cross correlation coefficient, a parametric study is carried out to investigate the most suitable cross correlation coefficient by comparing the predicted results with the measured field data.

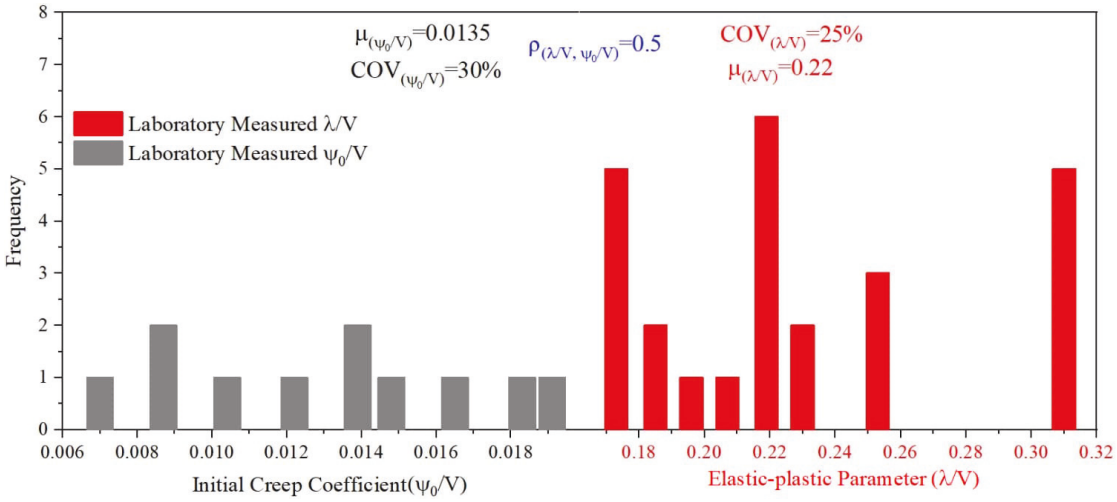

Figure 3.7 Generated random variables of elastic-plastic parameter (λ/V) and initial creep coefficient (ψ_0/V)

Table 3.2 Adopted deterministic and probabilistic model parameters for Väsby test fill

Model parameter	Type	Mean (μ)	Coefficient of Variation (υ_X)	Distribution
λ/V	random	0.22	0.25	Lognormal
ψ_0/V	random	0.0135	0.3	Lognormal
$\sigma'_{z_0}(kPa)$	deterministic	$\sigma'_{z_0} = 33\ln(\lambda/V) + 85$	-	-
κ/V	deterministic	0.0177	-	-
$t_0(s)$	deterministic	12000	-	-

3.4 Results and Discussion

Time-dependent settlement is usually a key concern when constructing on top of soft soils due to the risks associated with excessive post-construction settlement and instability. Therefore, the uncertainties related to model parameters in predicting time-dependent deformation must be quantified by a simple and understandable procedure. The first step in this study is to carry out an array of probabilistic analysis with the elastic-plastic and creep model parameters (λ/V , ψ_0/V) as random variables to obtain a range of possible time-dependent settlements for the Väsby test fill built on soft soil. Then the influence of the cross correlation coefficient between the elastic-plastic parameter (λ/V) and the initial creep coefficient (ψ_0/V) are evaluated by considering these parameters as random variables correlated with different degrees, then the settlement and excess pore water pressure are compared with the field measurements.

3.4.1 Influence of Uncertainties in λ/V and ψ_0/V on Predicted Time-dependent Deformations

A set of predicted ground surface settlement of Väsby test fill at different time stages are obtained from Monte-Carlo simulations by capturing uncertainties in the elastic-plastic model parameter (λ/V). To ensure that the proposed probabilistic method would be efficient and reliable, the sensitivity of the results to the number of Monte-Carlo simulations must be evaluated. For this purpose, the optimal number of Monte-Carlo simulations is presumed to be the minimum number of simulations that will result in convergence in the standard deviation of the ground surface settlement. Figure 3.8 shows the standard deviation of ground surface settlement versus the number of Monte-Carlo simulations that correspond to the various consolidation

times such as PCY5, PCY10, PCY20, PCY40, and PCY56 (Note: PCY means post construction time in years). It can be concluded from the above mentioned convergence curves that standard deviation remains almost unchanged when there are more than 1000 simulations. Based on the simulation results, the probability density function of ground surface settlement at different times is shown in Figure 3.9, when $\mu_{\lambda/V}$ = 0.22 and $COV_{\lambda/V} = 25\%$ is considered. As Figure 3.9 depicts, by increasing the time, the mean value and the standard deviation of time-dependent ground surface settlement increase. These results indicate that the probability density function of ground surface settlement becomes more scattered over time because the uncertainties in the predicted time-dependent ground surface settlement gradually accumulate with time.

Figure 3.10 shows the variation of the mean and the standard deviation, and the coefficient of variation for predicted ground surface settlement with time. Figure 3.10 also indicates that the mean value and standard deviation of ground surface settlement gradually increase over time. The effect of uncertainties in elastic-plastic model parameter (λ/V) over time are evaluated using the coefficient of variation (COV). Figure 3.10 shows how the coefficient of variation decreases over time from 0.19 to 0.10, thus indicating that as consolidation progresses the uncertainties in the elastic-plastic model parameter (λ/V) have less impact on the uncertainties in the predicted time-dependent ground surface settlement. This observation is due to the fact that the elastic-plastic model parameter (λ/V) is the model parameter for predicting the elastic-plastic strain, which occurs at initial stages of consolidation. As a result, the contribution of (λ/V) to the predicted long-term settlement decreases with time.

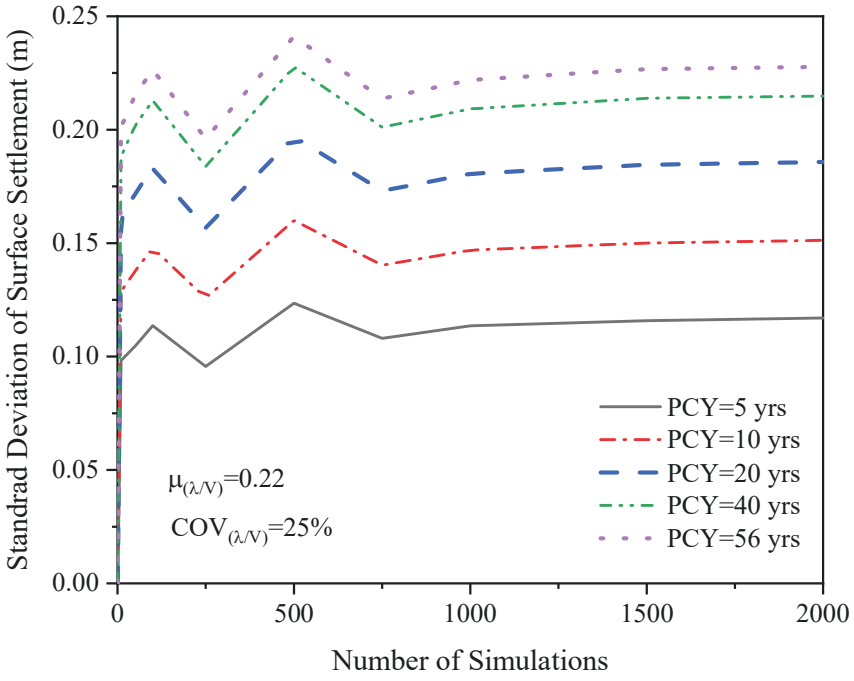

Figure 3.8 Convergence of the number of simulations for the surface settlement considering the elastic-plastic parameter (λ/V) as random variable

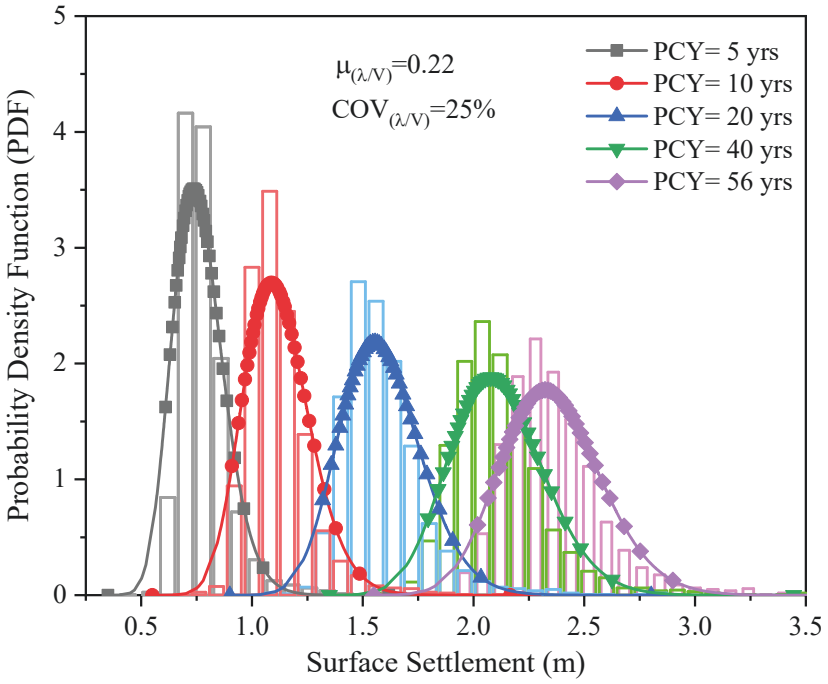

Figure 3.9 Probability distribution of surface settlement at different post construction years (PCY) considering the elastic-plastic parameter (λ/V) as a random variable

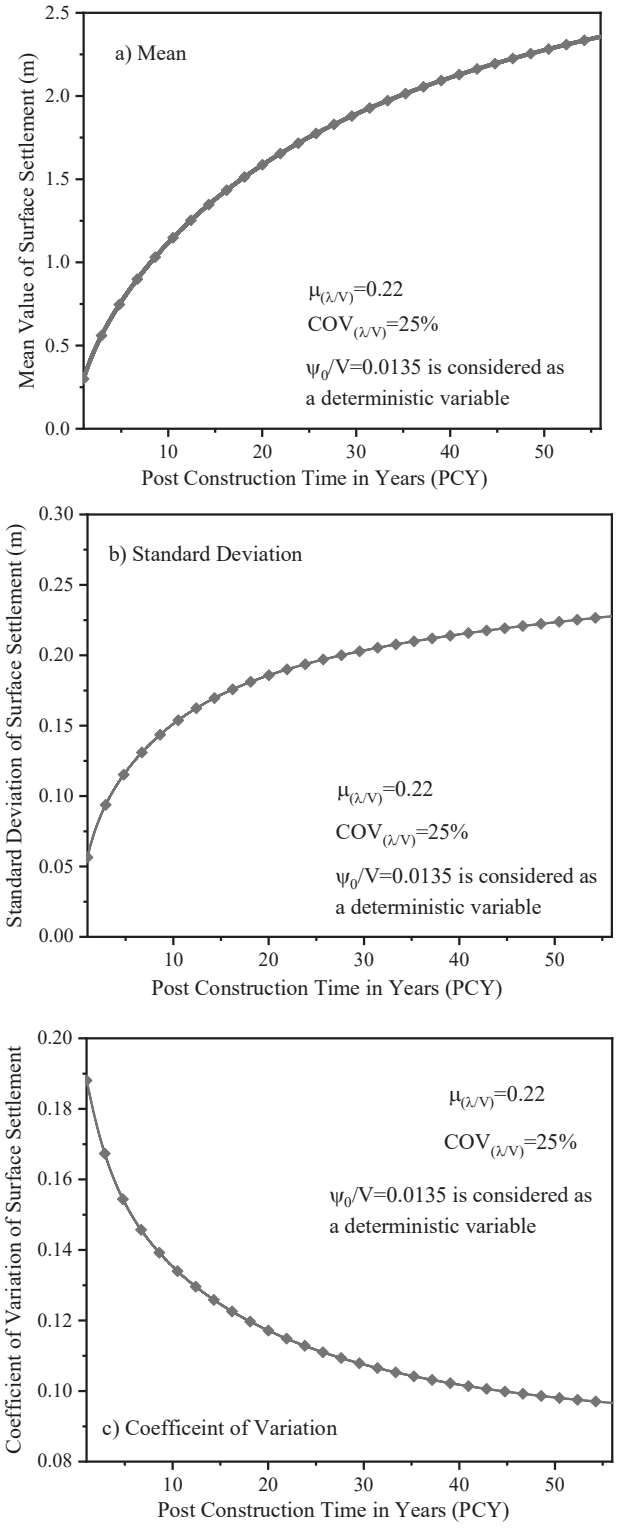

Figure 3.10 Statistical dispersions of surface settlement versus post construction time considering the elastic-plastic parameter (λ/V) as random variable (a) mean, (b) standard deviation and (c) coefficient of variation

To evaluate the influence of uncertainties that the initial creep coefficient (ψ_0/V) has on time-dependent deformation, the optimal number of Monte-Carlo simulations should be established while considering the initial creep coefficient (ψ_0/V) as a random variable. Figure 3.11 shows the standard deviation curves of ground surface settlement for various consolidation periods, predicted with respect to the number of simulations. In this instance, the standard deviation remains approximately constant after 1000 Monte-Carlo simulations, so 2000 Monte-Carlo simulations are used in the follow up analyses for the sake of computational efficiency and accuracy. A probability analysis is also carried out to obtain a set of predicted time-dependent ground surface settlements, while capturing any uncertainties related to determining the initial creep coefficient (ψ_0/V). Figure 3.12 shows the probability density function of time-dependent ground surface settlement at different time stages by adopting $\mu_{\psi_0/V}$ = 0.0135 and $COV_{\psi_0/V} = 30\%$. This shows that the mean and standard deviation of predicted surface deformations gradually increase with time. Figure 3.13 (c) shows that the level of confidence for ground surface settlement decreases with time, which indicates that uncertainties in the time-dependent ground surface settlement increase over time when the initial creep coefficient (ψ_0/V) is considered as a random variable. Since the initial creep coefficient (ψ_0/V) is the main model parameter contributing to the creep settlement, it can be concluded that, the uncertainties in predicting long-term settlement of soft soils increase with time. Moreover, comparing Figure 3.10 (c) with Figure 3.13 (c) shows that as consolidation progresses, the level of confidence for the predicted ground surface settlement depends more on uncertainties in the initial creep coefficient (ψ_0/V), unlike the corresponding feature for the elastic-plastic model

parameter (λ/V); this indicates a higher contribution of ψ_0/V uncertainties in predicting settlement over the long term.

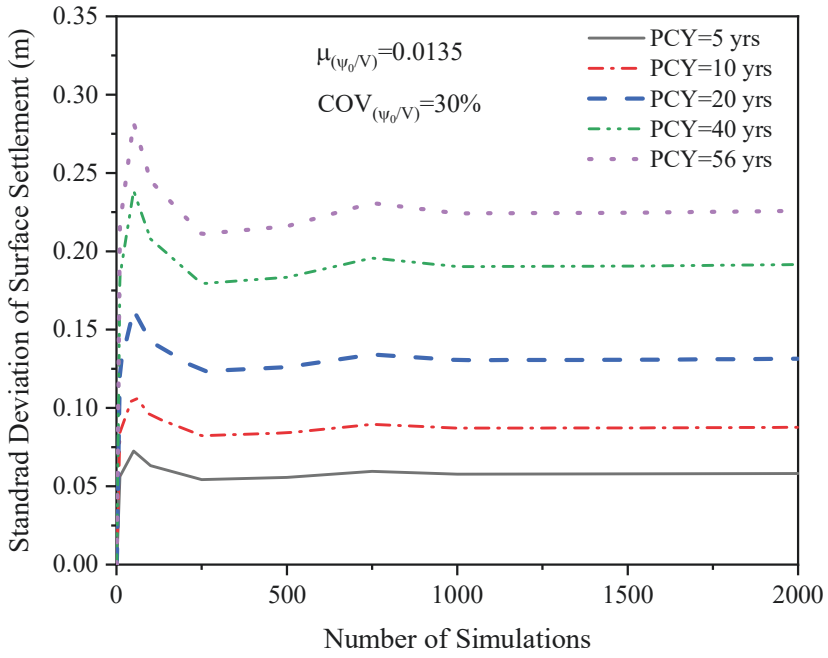

Figure 3.11 Convergence of the number of simulations for the surface settlement considering the initial creep coefficient (ψ_0/V) as random variable

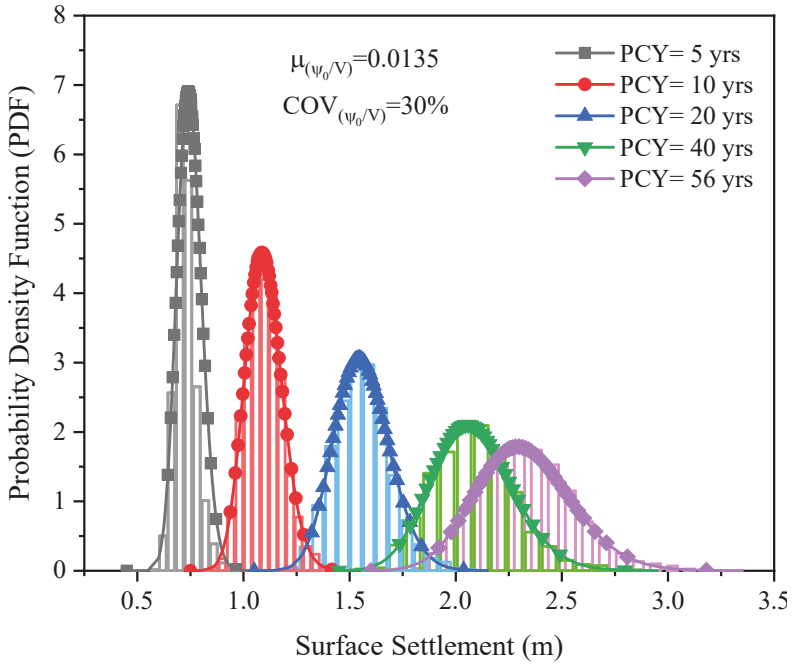

Figure 3.12 Probability distribution of surface settlement at different post construction years (PCY) considering the initial creep coefficient (ψ_0/V) as random variable

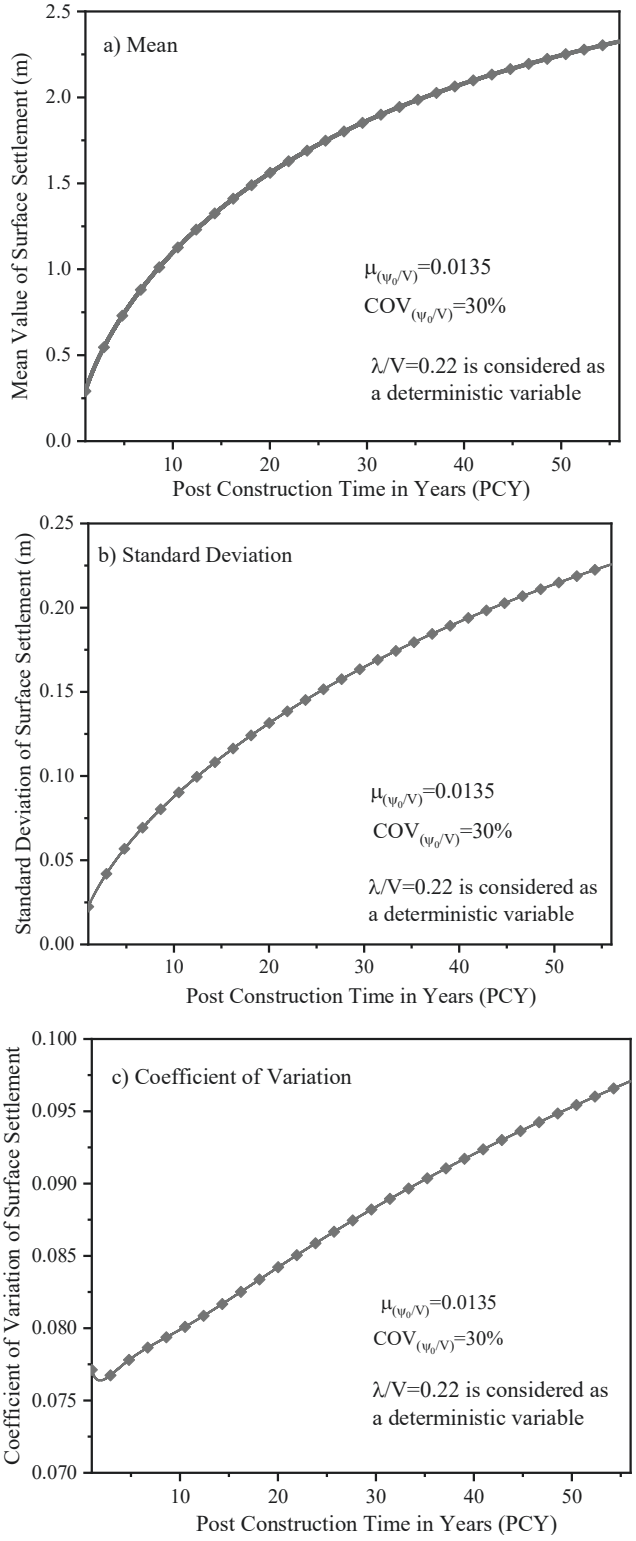

Figure 3.13 Statistical dispersions of surface settlement versus post construction time considering the initial creep coefficient (ψ_0/V) as random variable (a) mean, (b) standard deviation and (c) coefficient of variation

3.4.2 Influence of the Cross Correlation Coefficient between ψ_0/V and λ/V on PDFs of Time-dependent Settlement

Figure 3.14 shows how the cross correlation coefficient between the elastic-plastic model parameter (λ/V) and the initial creep coefficient (ψ_0/V) impacted on the probability density function (PDFs) of the predicted ground surface settlement at PCY5, PCY10, PCY20, PCY40, and PCY56. Figure 3.14 also indicates that the cross correlation coefficient between the initial creep coefficient (ψ_0/V) and the elastic-plastic model parameter (λ/V) has a significant effect on the time-dependent ground surface deformation of soft soil in the Väsby test fill. Table 3.3 provides the statistical properties of ground surface settlement at different time steps for various cross correlation coefficients. Note here that when the elastic-plastic model parameter (λ/V) and the initial creep coefficient (ψ_0/V) are fully correlated (i.e. $\rho = 1$), the standard deviation and the coefficient of variation of surface settlement exceeds the corresponding values for uncorrected random variables (i.e. $\rho = 0$). As a consequence, the uncertainties in predicting settlement increase as the cross correlation coefficient between λ/V and ψ_0/V increased, thus reducing the level of risk. Moreover, by comparing the interval between the maximum and minimum values (range) of soil surface settlement, it can be concluded that when the cross correlation coefficient increased, the range is wider. This observation indicates that time-dependent ground surface settlement would be more scattered and the maximum predicted settlement would slightly over predict settlements when $\rho = 1$ is adopted.

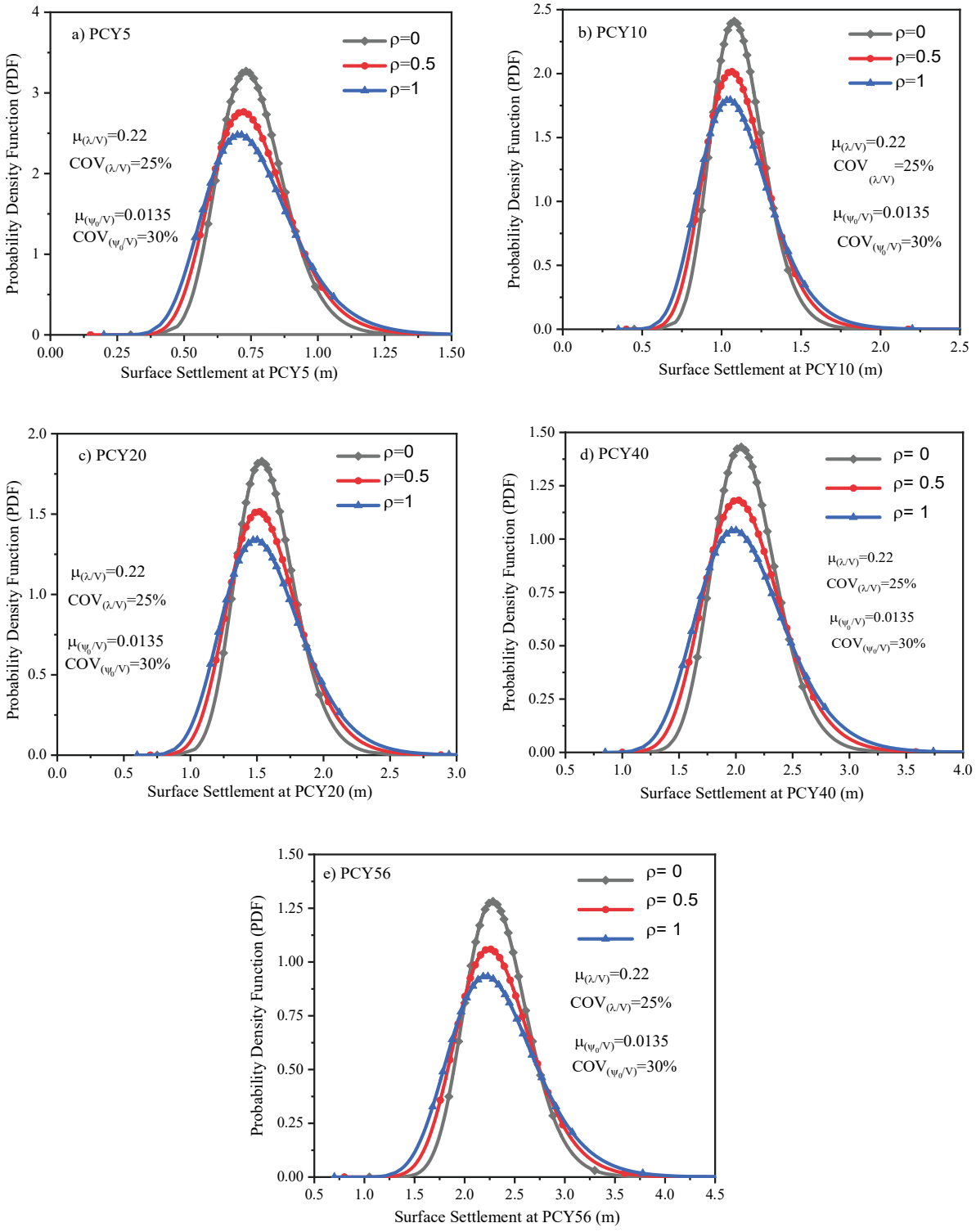

Figure 3.14 Influence of cross correlation coefficient between the elastic-plastic parameter (/) and the initial creep coefficient ($_0$/) for various time stages (a) PCY5, (b) PCY10, (c) PCY20, (d) PCY40 and (e) PCY56

Table 3.3 Statistical properties of surface settlement at different time steps for various cross correlation coefficients between the elastic-plastic parameter (λ/V) and the initial creep coefficient (ψ_0/V)

PCY (years)	$\rho(\frac{\lambda}{V},\frac{\psi_0}{V})$	Mean (m)	Standard deviation (m)	Coefficient of variation (%)	Minimum Settlement, S_{min} (m)	Maximum Settlement, S_{max} (m)	Range (S_{max} - S_{min}) (m)
56	0	2.34	0.32	0.14	1.51	3.71	2.2
	0.5	2.34	0.39	0.17	1.25	4.35	3.1
	1	2.33	0.45	0.19	1.12	5.33	4.22
40	0	2.10	0.29	0.14	1.32	3.40	2.08
	0.5	2.10	0.35	0.17	1.13	4.02	2.89
	1	2.09	0.40	0.19	0.99	4.92	3.93
20	0	1.58	0.22	0.14	0.91	2.74	1.83
	0.5	1.58	0.27	0.17	0.84	3.29	2.45
	1	1.58	0.31	0.20	0.72	4.03	3.31
10	0	1.12	0.17	0.15	0.61	2.09	1.48
	0.5	1.11	0.21	0.19	0.57	2.56	1.99
	1	1.11	0.23	0.21	0.49	3.17	2.67
5	0	0.76	0.13	0.17	0.41	1.55	1.15
	0.5	0.76	0.15	0.20	0.38	1.93	1.57
	1	0.76	0.17	0.22	0.33	2.40	2.07

The statistical dispersion of surface settlement for various cross correlation coefficients between the elastic-plastic model parameter (λ/V) and the initial creep coefficient (ψ_0/V) are shown in Figure 3.15. As expected, the mean value of predicted surface settlement is almost constant for the different cross correlation coefficients adopted in this study. Indeed, the slight differences observed in the

predicted mean could be due to a computational approximation in generating random numbers. Moreover, in the case of non-correlated random variables (i.e. $\rho = 0$), the standard deviation of surface settlement at PCY56 is about 0.26 m, while the corresponding value for fully correlated random variables (i.e. $\rho = 1$) is about 0.37 m, which shows the difference in the dispersion of the predicted ground surface settlement. Furthermore, the coefficient of variation for predicted surface settlement for fully correlated random variables (i.e. $\rho = 1$) is 0.185 which is higher than the corresponding 0.13 for non-correlated (i.e. $\rho = 0$) or 0.16 for partially correlated random variables (i.e. $\rho = 0.5$). This result indicates higher uncertainties in settlement prediction when the random variables are fully correlated. In Figure 3.15 (c), the results confirm that when the adopted random variables ψ_0/V and λ/V are fully correlated (i.e. $\rho = 1$), the confidence level of settlement prediction is rather low ($COV_s = 0.19$ at PCY56 as shown in Table 3). However, when the random variables are assumed fully correlated (i.e. $\rho = 1$), the predicted settlements captured a wider range, thus leading to a more reliable design and a more conservative assumption in the absence of adequate input data.

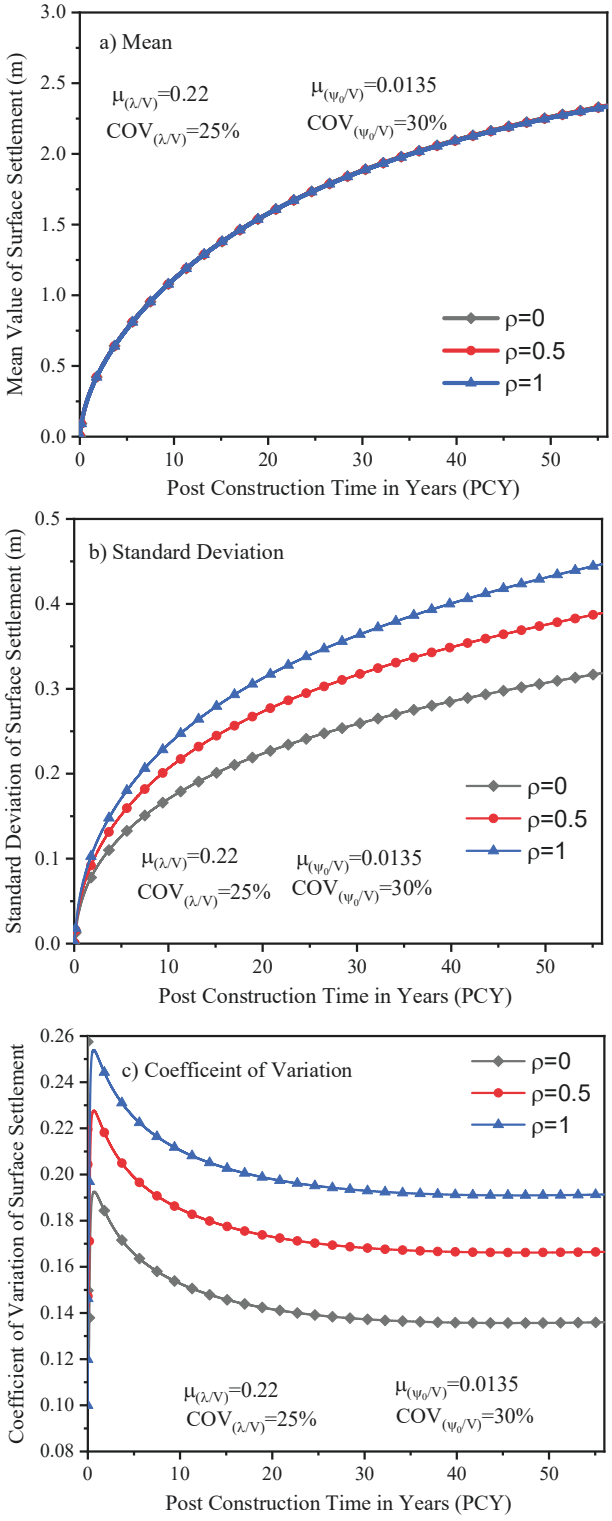

Figure 3.15 Statistical dispersions of surface settlement versus post construction time considering various cross correlation coefficients (ρ) between the elastic-plastic parameter (λ/V) and the initial creep coefficient (ψ_0/V) (a) mean, (b) standard deviation and (c) coefficient of variation

3.4.3 Comparison of Settlement Predictions with Field Measurements

In order to address the potential measurement of uncertainties, a wide range of field measurements at different depths and the field measurements of excess pore water pressures (EPWP) at PCY21 and PCY30 are adopted and compared with predictions. Two different settlement plates were installed in the Väsby test fill to monitor ground surface and sub-ground settlement. As described by Chang (1981a), settlement plates consisted of square steel plates with a perpendicular welded rod to measure ground surface settlements and installed directly below the embankment fill. Screw type settlement markers with a vertical steel rod were used to monitor sub-ground settlement at depths of 2.5 m, 5.0 m, and 7.5 m. A flexible sleeve was used to protect the steel rod from soil hanging during settlement. Perrone (1998) reported that field measurements were made regularly from 1947 until the mid-1950's. Note here that the settlement markers in sub-ground layer malfunctioned over time so the distribution of settlement with depth was calculated from changes in the water content from 1967 to 2002 (Chang 1981a; Perrone 1998).

The values of the characteristics in the probabilistic analysis should be labelled as 'lower bound' (LB), 'most probable' (MP), and 'upper bound' (UB); which is why the mean of the calculated settlements was considered to be the most probable value (MP). To define the upper and lower bounds, boundaries with a 95% confidence interval (CI) were used, as recommended by Zhou, et al. (2018) and Muhammed et al. (2020); these upper and lowers boundaries for lognormal distribution correspond to approximately $\mu_s \pm 1.96\sigma_s$ (where μ_s is the mean and σ_s is the standard deviation of predicted settlement, respectively). Figure 3.16 to Figure 3.19 show a comparison between data for settlement measured at different depths in the field with the mean

value, and the boundaries of 95% CI. This took place while investigating the impact made by the cross correlation coefficient on the elastic-plastic model parameter (λ/V) and the initial creep coefficient (ψ_0/V). According to Figure 3.16 to Figure 3.19, all the field settlements are located between the lower bounds (i.e. $\mu_s - 1.96\sigma_s$) and upper bounds (i.e. $\mu_s + 1.96\sigma_s$) of predicted settlement for all the cross correlation coefficients between the elastic-plastic model parameter (λ/V) and the initial creep coefficient (ψ_0/V); thus confirming the reliability of the predictions. However, Figure 3.16 shows that the settlement measured at surface is located between the predicted mean values and lower bound. Evidently, by performing deterministic analysis and only considering the mean value of input data, the predicted surface settlement would be more than what actually occurred in the field, thus leading to overestimated predictions. It is therefore recommended that a probabilistic analysis which includes uncertainties and engineering judgment should be carried out when a more economical prediction of time dependent settlement is required. Figure 3.17 shows that at a depth of 2.5 m, the data measured earlier (before 15 years) are between the mean value and upper bound values, whereas at later stages the predictions are between the mean and lower bound values (i.e. $\mu_s + 1.96\sigma_s$). Figure 3.18 shows that at a depth of 5.0 m, settlement measured after 5 years is between the mean and upper bounds (i.e. $\mu_s + 1.96\sigma_s$) for all adopted cross correlation coefficients; this is closer to the case where random input variables are not correlated (i.e. $\rho = 0$). Note here that the reported field monitoring is not smooth and consistent due to seasonal and environmental effects. Figure 3.19 shows that at lower depths (i.e. 7.5 m deep), the field measurements agree with the mean values and are between the mean values and upper bound. Therefore, at lower depths, the

field measurements are generally located between the mean value and upper bounds (i.e. $\mu_s + 1.96\sigma_s$), while at the surface the opposite trend is observed and the field measurements are between the mean values and lower bounds (i.e. $\mu_s - 1.96\sigma_s$) of predicted settlement for all the cross correlation coefficients.

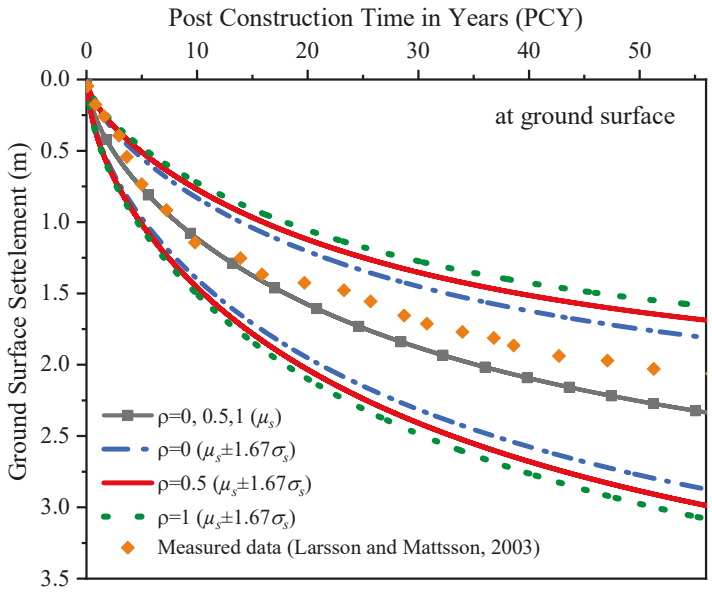

Figure 3.16 Comparison of measured and predicted settlement with 95% confidence interval considering various cross correlation coefficients (ρ) between the elastic-plastic parameter (λ/V) and the initial creep coefficient (ψ_0/V) at ground surface

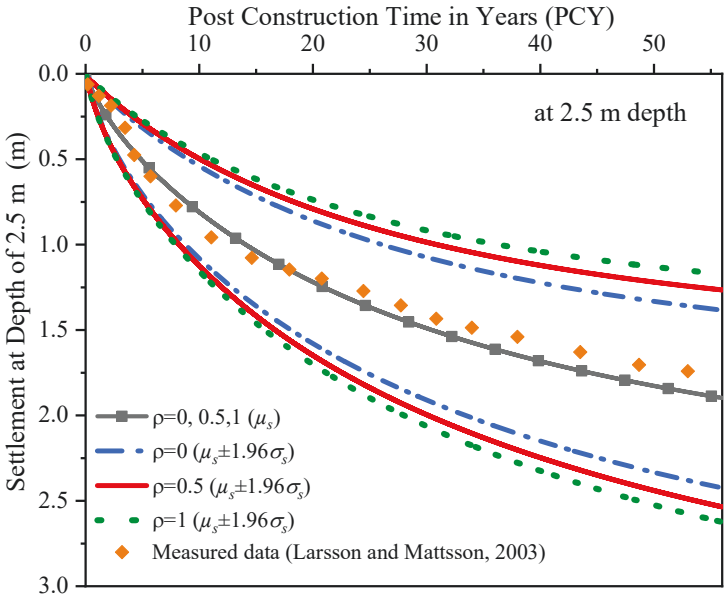

Figure 3.17 Comparison of measured and predicted settlement with 95% confidence interval considering various cross correlation coefficients (ρ) between the elastic-plastic parameter (λ/V) and the initial creep coefficient (ψ_0/V) at depth of 2.5 m

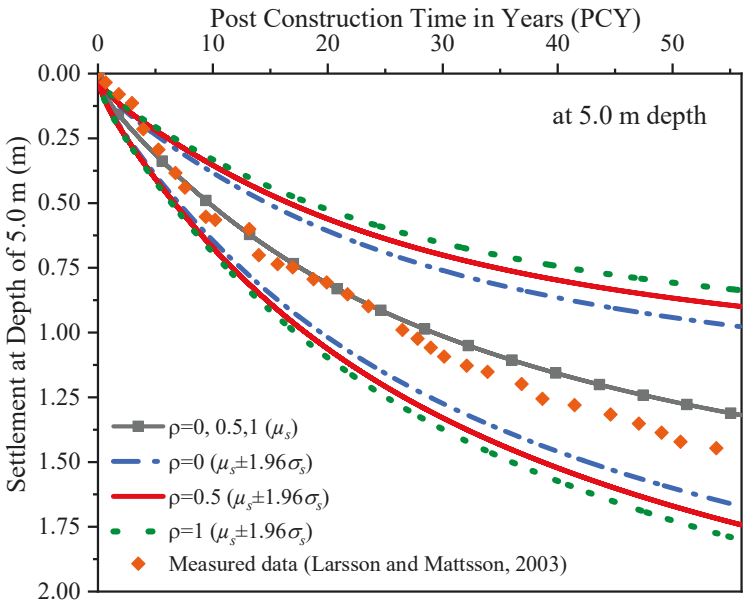

Figure 3.18 Comparison of measured and predicted settlement with 95% confidence interval considering various cross correlation coefficients (ρ) between the elastic-plastic parameter (λ/V) and the initial creep coefficient (ψ_0/V) at depth of 5.0 m

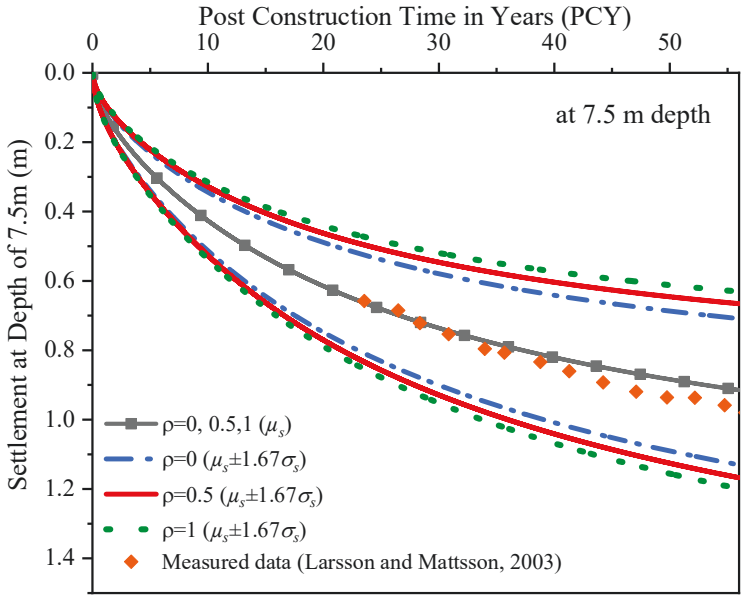

Figure 3.19 Comparison of measured and predicted settlement with 95% confidence interval considering various cross correlation coefficients (ρ) between the elastic-plastic parameter (λ/V) and the initial creep coefficient (ψ_0/V) at depth of 7.5 m

3.4.4 Discrepancy Evaluation

Various factors contribute to uncertainties in settlement and deviations from the field measurements. Obviously, uncertainties in random input variables lead to uncertainties in predicting settlement (output), and discrepancies between settlement predictions and measurements can also be attributed to the model uncertainties used to predict settlement. To evaluate the performance of the cross correlation coefficient between selected random variables (i.e. ψ_0/V and λ/V), a quantitative comparison must be made between the predictions and field measurements. This is why the three indicators that are commonly used to evaluate discrepancy, namely the root mean square error ($RMSE$) index, the mean absolute error (MAE), and the coefficient of determination (R^2), are adopted in this study.

$$RMSE = \sqrt{\frac{1}{N}\sum_{i=1}^{N}\left(Y_m - Y_p\right)^2} \tag{3.24}$$

$$MAE = \frac{1}{N}\sum_{i=1}^{N}\left|Y_m - Y_p\right| \tag{3.25}$$

$$R^2 = \frac{\sum_{i=1}^{N}(Y_m)^2 - \sum_{i=1}^{N}\left(Y_m - Y_p\right)^2}{\sum_{i=1}^{N}(Y_m)^2} \tag{3.26}$$

where, Y_m and Y_p are the measured and predicted values, respectively and N stands for the number of available data. Indeed, lower values of $RMSE$ and MAE or higher R^2 values indicate better compliance and agreement between the numerical predictions and field measurements.

As discussed earlier and as shown in Figure 3.16 to Figure 3.19, the mean value of the predicted settlement is almost the same for all the cross correlation coefficients adopted, and the field measured settlements are positioned between the upper and

lower bounds (i.e. $\mu_s \pm 1.96\sigma_s$). Therefore, to evaluate any errors in the values of predicted settlement for different cross correlation coefficients, the mean, upper bound, and lower bound values are utilised. Table 3.4 summarises the corresponding indicators to compare the most probable (i.e. MP) upper bound (i.e. UB) and lower bound (i.e. LB) settlement predictions with the measured data for various cross correlation coefficients. According to the indices presented in Table 3.4, the mean values of the error indicators $RMSE$ and MAE for adopted 95% confidence interval at different depths (i.e. $RMSE$ and MAE) are lower for the non-correlated random variables (i.e. $\rho = 0$), and thus confirm a better agreement with the field observations. Therefore, by referring to the common statistical measures to calculate error, it is evident that the predicted settlements better conform to data measured in the field when the selected random variables (i.e. ψ_0/V and λ/V) are assumed to be non-correlated (i.e. $\rho = 0$). Moreover, the error indicators at depth were less than the surface values for all adopted cross correlation coefficients, because the surface settlement is an accumulation of settlement of all the sub-layers below, where the errors also accumulated. To further discuss this increase in error from the depth to the surface, the variations of mean, standard deviation and the coefficient of variation with depth at PCY56 and PCY20 are plotted for the different cross correlation coefficients as shown in Figure 3.20. As expected, the mean predicted settlements increase from depth of 14 m to the surface, but they are rather independent of the cross correlation coefficients. Moreover, the standard deviation of the predicted settlement decreases with depth for all the cross correlation coefficients adopted, thus confirming that at the surface the uncertainties of settlement prediction is an accumulation of the uncertainties in the sub-layers. Figure 3.21 (c) however shows

that the coefficient of variation (i.e. COV) only changes slightly with rather minor variations between PCY56 and PCY20. However, the highest confidence level of settlement prediction (i.e. the minimum value of COV) occurs around the middle of soil layer because the maximum strains occur near the drainage boundaries, which results in more uncertainties in settlement prediction at the upper and lower depths and less uncertainties in the middle layers (i.e. furthest away from the drainage boundaries) due to least excess pore water pressure dissipation rate. As explained earlier, by adopting fully correlated random variables (i.e. $\rho = 1$ between λ/V and ψ_0/V), the standard deviation and coefficient of variation (i.e. COV) are the largest, irrespective of the depth or the consolidation time.

It is important to mention that while evaluating errors using $RMSE$, MAE, and R^2, the absolute distance between the predicted and measured data can be determined, but since an underestimated settlement prediction can lead to an unsafe analysis, a criterion is needed to evaluate whether all the predicted settlements are equal to or more than the measured settlements. For this purpose, a prediction bias or settlement error can be represented by the settlement ratio (SR_X), which is defined as the ratio of predicted settlement to measured settlement:

$$SR_X = \frac{S_{P-X}}{S_{M-X}} \tag{3.27}$$

where S_{P-X} and S_{M-X} are the predicted and measured settlement values at depth X. In fact, an SR_X value of more than unity (i.e. $SR_X > 1$) indicates a conservative and thus overestimated prediction, otherwise they are underestimated. Figure 3.21 to Figure 3.24 show the settlement ratio versus time for predicted settlements at different depths and for various cross correlation coefficients. It is

worth mentioning that since the $\mu_s - 1.96\sigma_s$ (i.e. LB) values of predicted settlement were less than the measured data, this comparison is made between μ_s (i.e. MP) and $\mu_s + 1.96\sigma_s$ (i.e. UB).

At the ground surface (Figure 3.21), the settlement ratio vs time ($SR_0 - t$) curve is above 1 for the mean and upper bound settlement predictions for all the cross correlation coefficients adopted. It should be noted that an ideal value for the settlement ratio is 1, where the predicted and measured settlements match the ideal conditions but without any uncertainties in data gathered during field monitoring, or input parameters and modelling procedures. Hence, by referring to Muhammed et al. (2020) and Liu et al. (2018), in the presence of uncertainties, it is better to adopt a settlement ratio more than one. However, when the settlement ratio is more than one, the predicted settlement is more conservative but less economical. Figure 3.21 shows that although the settlement ratio for the upper bounds of predicted settlement is more than one for various cross correlation coefficients, the ground surface settlement ratio SR_0 for the case where the random variables are not correlated (i.e. $\rho = 0$), is less than the corresponding values for partially (i.e. $\rho = 0.5$) and fully correlated (i.e. $\rho = 1$) input random variables. In other words, when the elastic-plastic model parameter (λ/V) and the initial creep coefficient (ψ_0/V) are fully correlated (i.e. $\rho = 1$), the predicted settlement is on conservative side. Figure 3.22 to Figure 3.24 indicate that the settlement ratios at depths of 2.5 m, 5.0m and 7.5m (i.e. $SR_{2.5}$, $SR_{5.0}$, and $SR_{7.5}$), are close to but less than one for the mean values of predicted settlement, which is considered to be aggressive in the presence of uncertainties. However, for all adopted cross correlation coefficients, $SR_{2.5}$, $SR_{5.0}$, and $SR_{7.5}$ for the upper bound predictions are more than one; thus indicating conservative and rather reliable predictions.

Therefore Figure 3.21 to Figure 3.24 show that as the cross correlation coefficients between the random variables ψ_0/V and λ/Vincrease, the settlement ratio increases, resulting in more conservative and thus safer predictions.

Table 3.4 Summary of settlement indicators for all adopted cross correlation coefficients (ρ) between the elastic-plastic parameter (λ/V) and the initial creep coefficient (ψ_0/V)

Cross Correlation Coefficient	Indicator	Boundaries	at Surface	at 2.5 m depth	at 5.0 m depth	at 7.5 m depth
$\boldsymbol{\rho = 0}$	$\boldsymbol{RMSE}$	$\mu_s - 1.96\sigma_s$	0.29	0.3	0.25	0.25
		μ_s	0.17	0.08	0.06	0.03
		$\mu_s + 1.96\sigma_s$	0.61	0.41	0.15	0.15
		Mean of *RMSE*	0.36	0.26	0.16	0.16
	$\boldsymbol{MAE}$	$\mu_s - 1.96\sigma_s$	0.27	0.27	0.2	0.24
		μ_s	0.15	0.07	0.05	0.03
		$\mu_s + 1.96\sigma_s$	0.57	0.36	0.13	0.19
		Mean of *MAE*	0.33	0.25	0.13	0.15
	$\boldsymbol{R^2}$	$\mu_s - 1.96\sigma_s$	0.95	0.93	0.97	0.92
		μ_s	0.99	0.99	0.99	0.99
		$\mu_s + 1.96\sigma_s$	0.82	0.88	0.91	0.95
		Mean of R^2	0.92	0.93	0.96	0.95
$\boldsymbol{\rho = 0.5}$	$\boldsymbol{RMSE}$	$\mu_s - 1.96\sigma_s$	0.39	0.37	0.30	0.29
		μ_s	0.17	0.08	0.07	0.03
		$\mu_s + 1.96\sigma_s$	0.71	0.48	0.19	0.23
		Mean of *RMSE*	0.42	0.31	0.19	0.19
	$\boldsymbol{MAE}$	$\mu_s - 1.96\sigma_s$	0.36	0.34	0.23	0.28
		μ_s	0.15	0.07	0.05	0.03
		$\mu_s + 1.96\sigma_s$	0.65	0.42	0.17	0.23
		Mean of *MAE*	0.39	0.30	0.15	0.18
	$\boldsymbol{R^2}$	$\mu_s - 1.96\sigma_s$	0.93	0.90	0.87	0.88
		μ_s	0.99	0.99	0.99	0.99
		$\mu_s + 1.96\sigma_s$	0.76	0.83	0.94	0.92
		Mean of R^2	0.89	0.91	0.94	0.93
$\boldsymbol{\rho = 1}$	$\boldsymbol{RMSE}$	$\mu_s - 1.96\sigma_s$	0.47	0.42	0.33	0.33
		μ_s	0.17	0.08	0.07	0.04
		$\mu_s + 1.96\sigma_s$	0.79	0.53	0.23	0.27
		Mean of *RMSE*	0.48	0.34	0.21	0.21
	$\boldsymbol{MAE}$	$\mu_s - 1.96\sigma_s$	0.43	0.38	0.26	0.32
		μ_s	0.15	0.07	0.05	0.03
		$\mu_s + 1.96\sigma_s$	0.73	0.47	0.19	0.26
		Mean of *MAE*	0.44	0.33	0.17	0.21
	$\boldsymbol{R^2}$	$\mu_s - 1.96\sigma_s$	0.89	0.87	0.84	0.85
		μ_s	0.99	0.99	0.99	0.99
		$\mu_s + 1.96\sigma_s$	0.70	0.79	0.92	0.90
		Mean of R^2	0.86	0.87	0.92	0.92

Note: $RMSE$ is the root mean square error, MAE denotes the mean absolute error, and R^2 is the coefficient of determination.

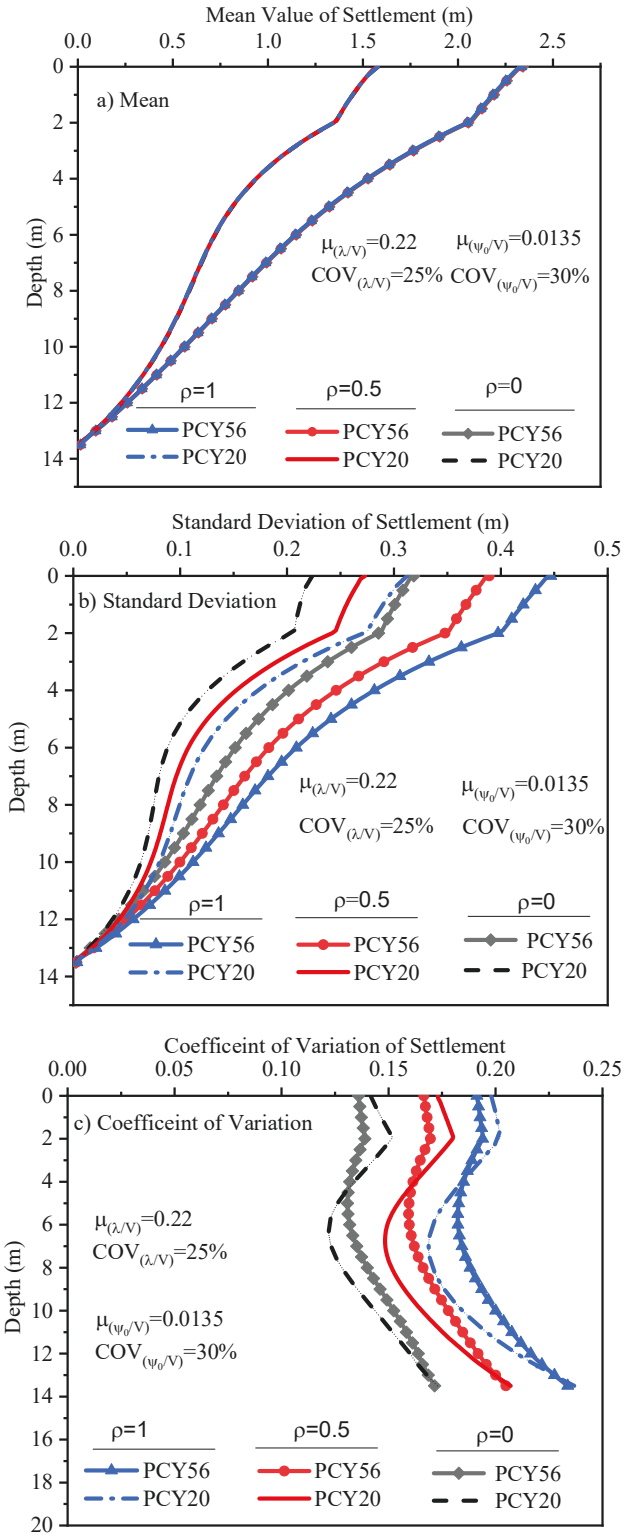

Figure 3.20 Statistical dispersions of settlement versus depth at PCY56 and PCY20 considering various cross correlation coefficients (ρ) between the elastic-plastic parameter (λ/V) and the initial creep coefficient (ψ_0/V) (a) mean, (b) standard deviation and (c) coefficient of variation

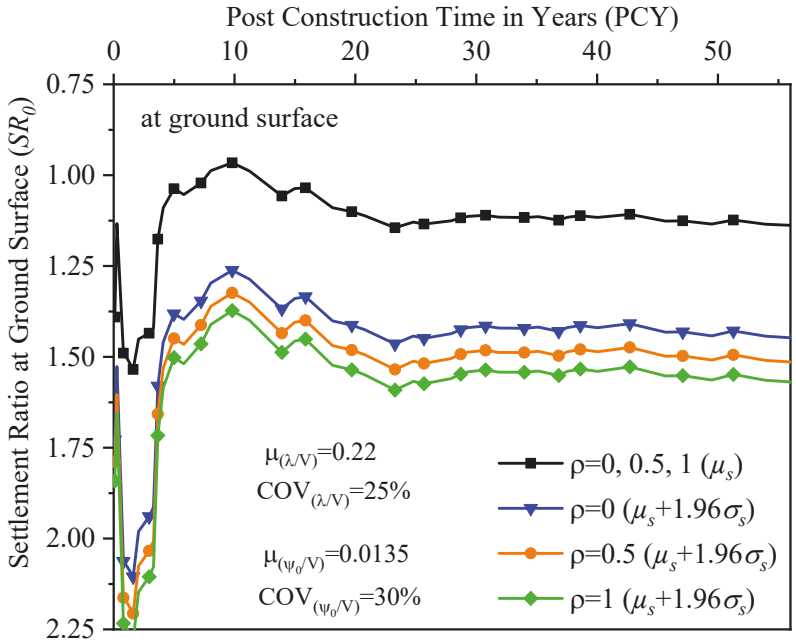

Figure 3.21 Settlement ratio versus time at ground surface for various cross correlation coefficients (ρ) between the elastic-plastic parameter (λ/V) and the initial creep coefficient (ψ_0/V)

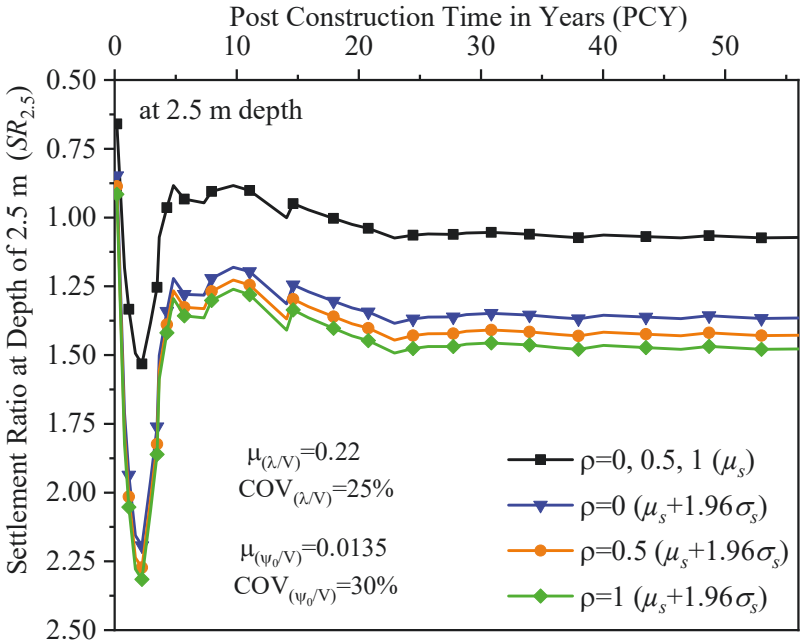

Figure 3.22 Settlement ratio versus time at depth of 2.5 m for various cross correlation coefficients (ρ) between the elastic-plastic parameter (λ/V) and the initial creep coefficient (ψ_0/V)

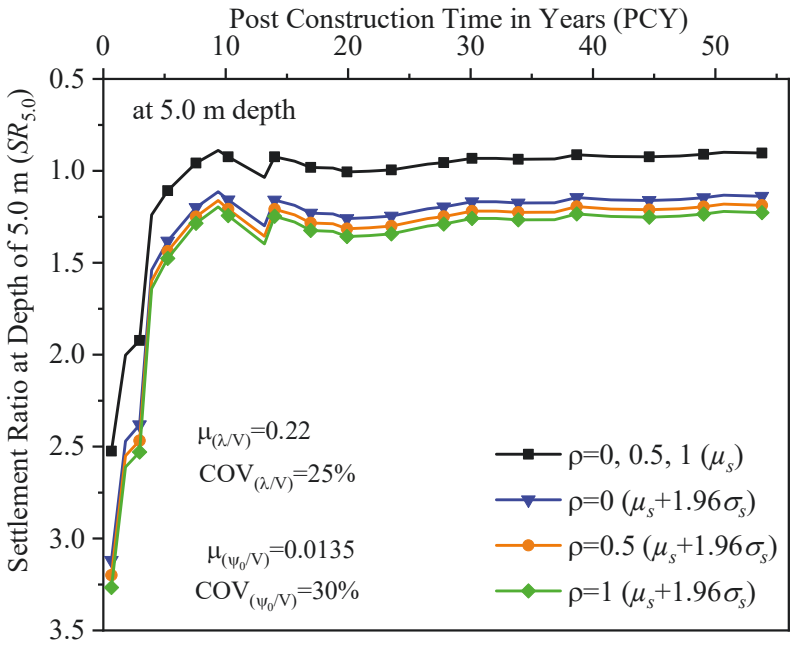

Figure 3.23 Settlement ratio versus time at depth of 5.0 m for various cross correlation coefficients (ρ) between the elastic-plastic parameter (λ/V) and the initial creep coefficient (ψ_0/V)

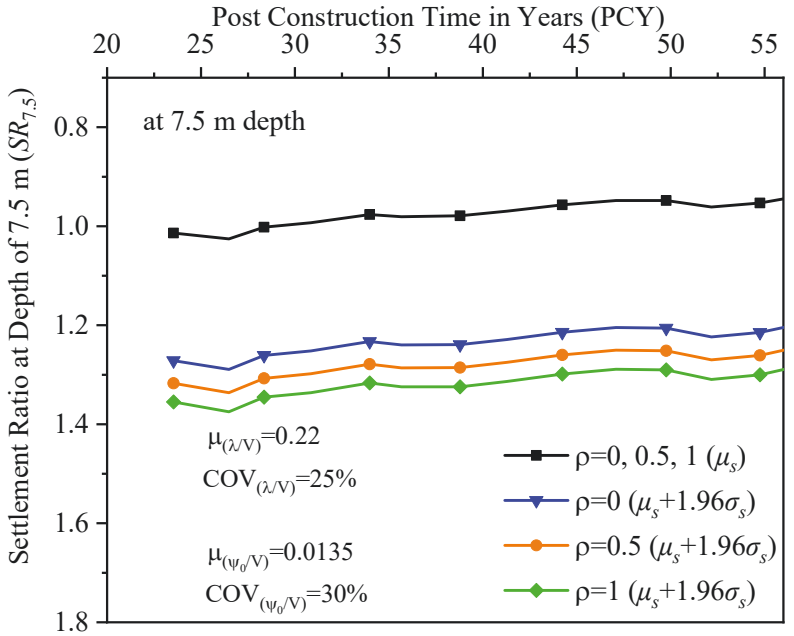

Figure 3.24 Settlement ratio versus time at depth of 7.5 m for various cross correlation coefficients (ρ) between the elastic-plastic parameter (λ/V) and the initial creep coefficient (ψ_0/V)

Table 3.5 shows the risk associated with unsatisfactory settlement prediction while considering λ/V and ψ_0/V as random variables. The risk can be assessed by determining the probability that the field measurements exceed the design values. In this risk analysis, the cost of repair or maintenance is assumed \$10M. As can be concluded from Table 3.5, when λ/V and ψ_0/V are considered fully correlated (i.e. $\rho = 1$), the risk of unsatisfactory prediction is the lowest at all different post-construction times which resulted in safer design.

Table 3.5 Risks associated with unsatisfactory prediction for all adopted cross correlation coefficients (ρ) between the elastic-plastic parameter (λ/V) and the initial creep coefficient (ψ_0/V)

		PCY5	PCY10	PCY20	PYC40	PCY56
Probability of Exceedance	$\boldsymbol{\rho = 0}$	0.53	0.55	0.73	0.77	0.81
	$\boldsymbol{\rho = 0.5}$	0.5	0.53	0.69	0.71	0.75
	$\boldsymbol{\rho = 1}$	0.48	0.5	0.66	0.69	0.72
Risk (\$M)	$\boldsymbol{\rho = 0}$	5.3	5.5	7.3	7.5	8.1
	$\boldsymbol{\rho = 0.5}$	5.0	5.3	6.9	7.1	7.5
	$\boldsymbol{\rho = 1}$	4.8	5.0	6.6	6.9	7.2

3.4.5 Assessment of Excess Pore Water Pressure

As well as predicting settlement, predicting excess pore water pressure plays an important role in investigating the long-term behaviour of soft soils because it affects the stress, stiffness, and shear strength of soil. Therefore, the field measurements of excess pore water pressures (EPWP) at PCY21 and PCY30 are compared with predictions in Figure 3.25. The Figure shows the predicted upper and lower bounds of excess pore water pressures $\mu_u \pm 1.96\sigma_u$ (boundaries for 95% confidence

interval) which are obtained while considering different cross correlation coefficients between λ/V and ψ_0/V. Figure 3.25 shows that 21 years and 30 years post construction of the embankment on Väsby clay, the mean values of predicted EPWP for all cross correlation coefficients indicate discrepancies from measured data, but when the probabilistic approach is adopted and a reliability analysis is carried out the predicted excess pore water pressures are between the upper bound (i.e. $\mu_u + 1.96\sigma_u$) and lower bound (i.e. $\mu_u - 1.96\sigma_u$). This observation highlights the significance of carrying out a probabilistic analysis while predicting the excess pore water pressure profile.

Figure 3.25 shows that unlike the settlement prediction, the dispersion of excess pore water pressure when the elastic-plastic model parameter (λ/V) and the initial creep coefficient (ψ_0/V) are non-correlated random variables (i.e. $\rho = 0$), is much higher than the corresponding observations for fully-correlated random variables (i.e. $\rho = 1$); this is due to the fact that the remaining excess pore water decreases as settlement increases. Hence, with non-correlated random variables (i.e. $\rho = 0$), the excess pore water pressure covers a wider range, and envelopes all the data measured at PCY21 and most of the data measured at PCY52. Figure 3.26 shows the statistical properties of predicted excess pore water pressure at PCY21 and PCY30 for different cross correlation coefficients between λ/V and ψ_0/V. As expected, the mean predicted EPWP for different adopted cross correlation coefficients is almost the same, but the standard deviation and coefficient of variation of predicted EPWP are higher for the non-correlated random variables (i.e. $\rho = 0$), followed by partially correlated (i.e. $\rho = 0.5$) and then fully correlated (i.e. $\rho = 1$) cases. This indicates that non-correlated random variables (i.e. $\rho = 0$) could result in

more uncertainties in the predicted excess pore water pressure predictions. In Figure 3.26 (c), the coefficient of variation (COV) for the predicted EPWP decreases with depth and achieves a minimum value at the mid-depth because the rate of excess pore water pressure variations is least in the mid-depth (for two-way drained condition) and there are more strains closer to the drainage boundaries resulting in more uncertainties in strain predictions. Since excess pore water pressure and strain are inter-related variables, higher uncertainties in EPWP prediction can lead to higher uncertainties in predicted strain. As a result the uncertainties in EPWP prediction is much higher (COV is higher) closer to the drainage boundaries than the mid-depth layers. Figure 3.27 shows the statistical dispersions of predicted EPWP over time for different adopted cross correlation coefficients between the selected random variables (i.e. ψ_0/V and λ/V). Here the coefficient of variation (COV) for the predicted excess pore water pressure increases with time, which confirmed that errors and uncertainties in predicting excess pore water pressure accumulate as soil consolidates. Moreover, during consolidation the uncertainties in predicting excess pore water increase as the cross correlation coefficient, decreases, which indicates a lower confidence level in predicting EPWP when the selected random variables are not correlated (i.e. $\rho = 0$) (Note: time in horizontal axis is construction years (CY) and post construction years (PCY)).

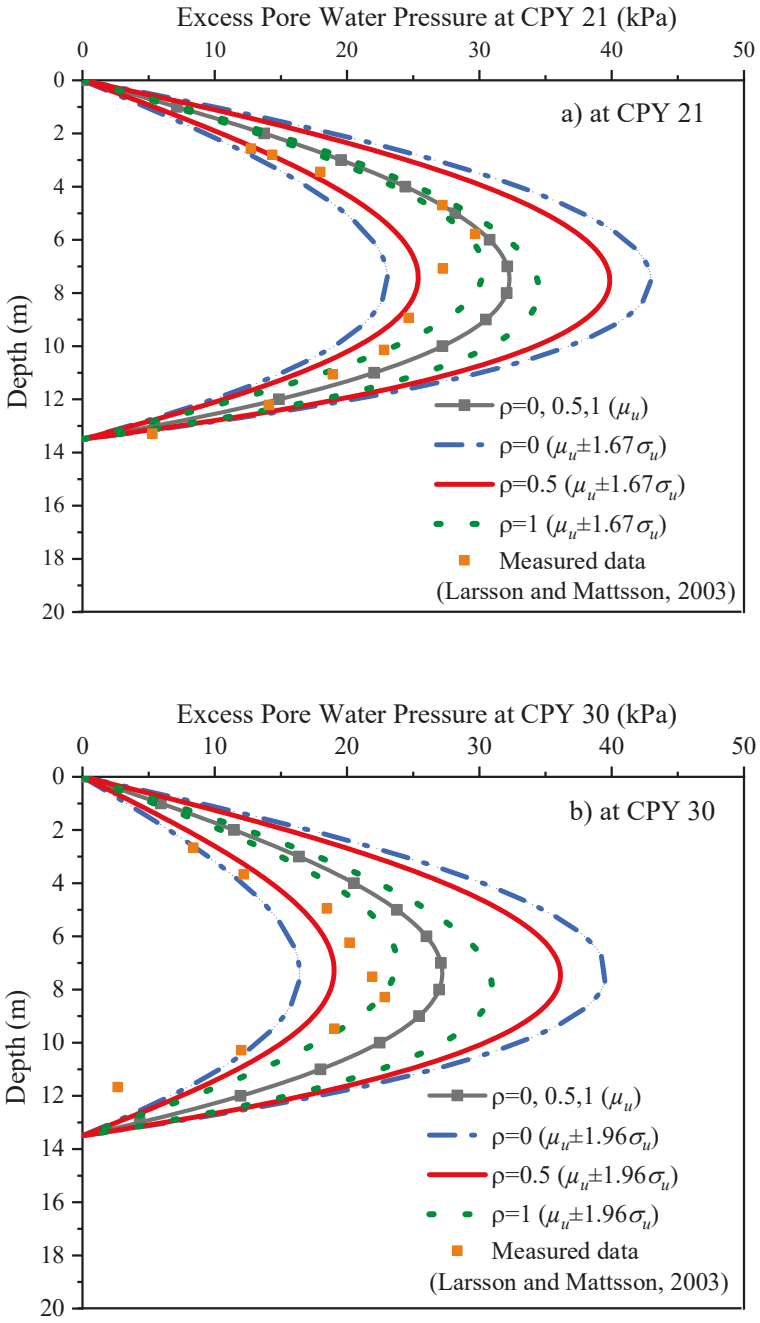

Figure 3.25 Comparison of measured and predicted excess pore water pressures with 95% confidence of interval considering various correlation coefficients between ψ_0/V and λ/V at (a) at CPY21, (b) at CPY30

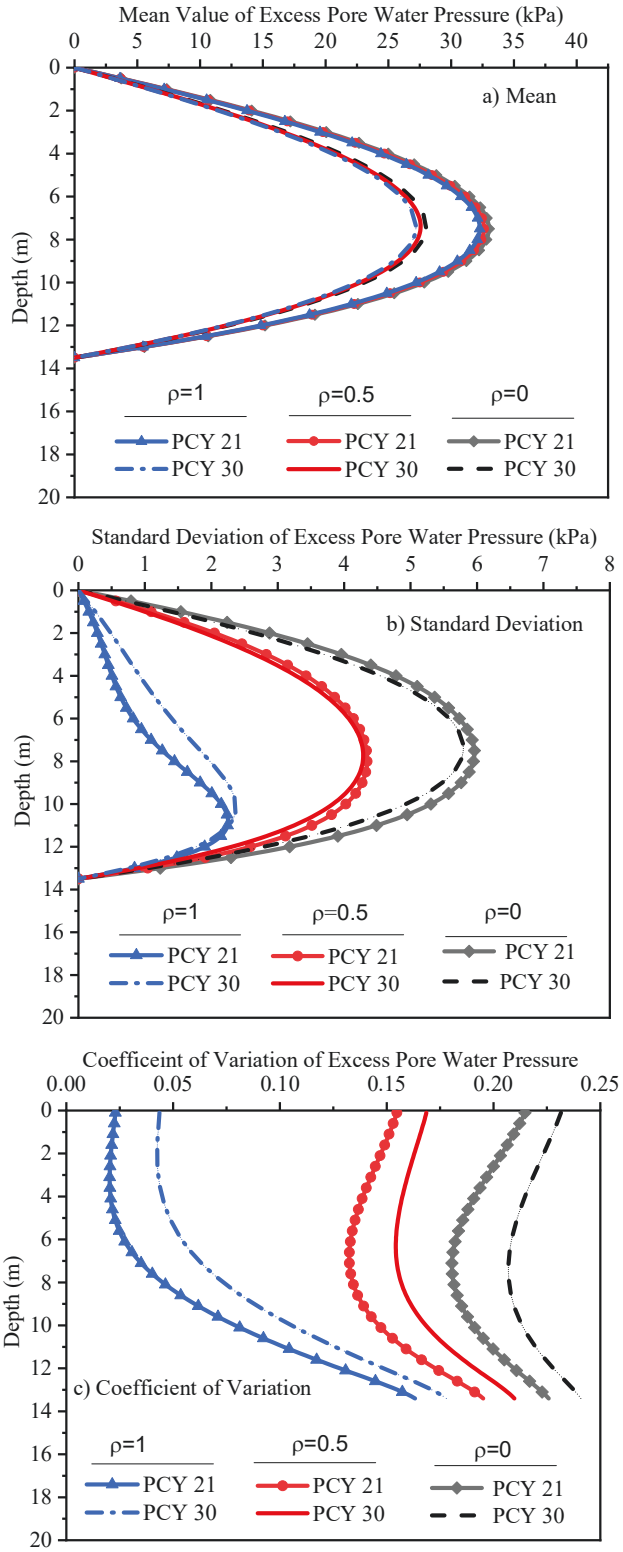

Figure 3.26 Statistical dispersions of excess pore water pressure with depth considering various cross correlation coefficients between the elastic-plastic parameter (λ/V) and the initial creep coefficient (ψ_0/V) (a) mean, (b) standard deviation and (c) coefficient of variation

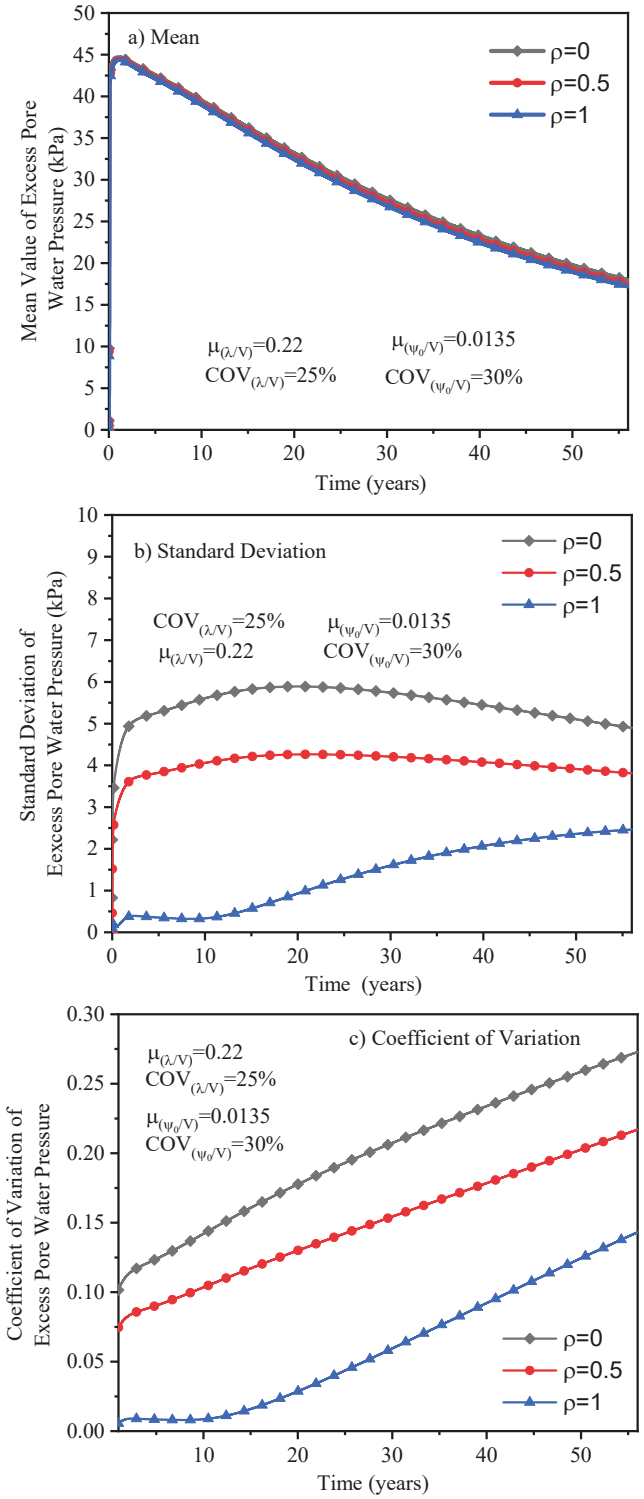

Figure 3.27 Statistical dispersions of excess pore water pressure with time considering various cross correlation coefficients between the elastic-plastic parameter (λ/V) and the initial creep coefficient (ψ_0/V) (a) mean, (b) standard deviation and (c) coefficient of variation

3.5 Summary

This chapter describes how a reliability-based analysis is used to evaluate the impact of uncertainties of the elastic-plastic model parameter (λ/V) and initial creep coefficient (ψ_0/V), and their cross correlation on the predicted settlement and excess pore water pressure of soft soils. A case study of the Väsby test fill embankment constructed on top of soft soil, with the results of more than 50 years of field monitoring, was used to verify the accuracy and application of the proposed method. For this purpose, a Monte-Carlo simulation is combined with the Gaussian copula analysis and finite difference numerical modelling capturing elastic visco-plastic behaviour of soft soil. The Crank-Nicolson method is adopted to solve the governing equations and a multivariate normal distribution is used to create the correlated random variables. The following conclusions could be drawn from this study:

- The elastic-plastic model parameter (λ/V) and the initial creep coefficient (ψ_0/V) are important factors in predicting the time-dependent settlement of soft soil considering uncertainties associated with determining these two parameters. When λ/V and ψ_0/V were used as random variables, the standard deviation of time-dependent settlement gradually increased with time as uncertainties accumulated.

- Different correlation coefficients were used to evaluate the effect of cross correlation coefficients between the random variables λ/V and ψ_0/V. When the predictions were compared to the measured data in the Vasby test fill, the settlements measured at different depths were between the upper and lower boundaries of predicted settlements with a 95% confidence interval

for all adopted cross correlation coefficients. However, by increasing the cross correlation coefficient, the standard deviation and also the coefficient of variation (COV) of the predicted settlements increased approximately 40%, resulting in more conservative design and predictions.

- The common methods used to evaluate errors were not efficient enough to quantify the most proper cross correlation coefficient between the elastic-plastic model parameter (λ/V) and the initial creep coefficient (ψ_0/V), so the settlement ratio was used to estimate the efficiency and suitability of selected cross correlation coefficients. Based on the obtained results, it is strongly recommended to consider λ/V and ψ_0/V as correlated random variables in probabilistic analysis. When random variables λ/V and ψ_0/V were considered fully correlated (i.e. $\rho = 1$), the settlement ratio was at most 10% more than the corresponding values for non-correlated random variables (i.e. $\rho = 0$). Although fully correlated random variables (i.e. $\rho = 1$) resulted in more conservative time-dependent settlement predictions, adopting the actual measured cross correlation coefficient (i.e. $\rho = 0.5$ in this study for Väsby clay) may result in a more realistic and cost effective design. Therefore, to optimise a design in terms of reliability and cost, the cross correlation coefficient between the elastic-plastic model parameter (λ/V) and the initial creep coefficient (ψ_0/V) based on the existing field and laboratory test results should be determined and applied in probabilistic analysis. However, in the absence of enough data to determine the exact value of cross correlation between λ/V and ψ_0/V, it is highly recommended to assume these two random variables fully-correlated (i.e. $\rho = 1$).

4 Random Field Reliability Analysis for Time-Dependent Behaviour of Soft Soils Considering Spatial Variability of Elastic Visco-Plastic Parameters in Low Embankments

4.1 Introduction

Low embankment strategy is one of the effective methods to control time-dependent settlement of soft soils in infrastructure construction projects. Spatial variability of soil characteristics is a crucial factor, affecting the reliability of predictions of the long-term settlement in soft soils. In this chapter, one-dimensional (1D) time-dependent behaviour of soft soils is analysed incorporating spatial variability of elastic visco-plastic model parameters. Standard Gaussian random fields for correlated elastic-plastic model parameter (λ/V) and the initial creep coefficient (ψ_0/V) are generated adopting Karhunen-Loeve expansion method based on the spectral decomposition of correlation function into eigenvalues and eigenfunctions. Then the generated random fields are incorporated in the proposed non-linear elastic visco-plastic (EVP) creep model. The impacts of spatially variable elastic visco-plastic model parameters (i.e. ψ_0/V and λ/V) on long-term settlement predictions are evaluated through random field analysis (RF) with different spatial correlation lengths, and results are then compared to a single random variable (SRV) analysis. Then, by adopting the field measurements of Skå–Edeby trial embankment and

determining the maximum probability of failure, the critical spatial correlation length is determined, which is required for a reliable design in the absence of sufficient data for model parameters.

4.2 Methodology

In order to conduct random field (RF) and single random variable (SRV) analyses, the finite difference solutions with two-way drainage boundary conditions are encoded in MATLAB to provide the predicted average vertical strains for RF and SRV analyses. An elastic visco-plastic model adopting the time line concept with non-linear creep function is adopted in this study to determine the time-dependent settlement of soft soil. Fundamental of adopted elastic-visco plastic model was outlined in Section 3.2 of Chapter 3. The adopted probabilistic analysis and computational procedure are explained in the following section.

4.2.1 Karhunen-Loeve Expansion Method

The Karhunen-Loeve (K-L) expansion of a random field is based on the spectral decomposition of correlation function $\rho(x_1, x_2)$, which can be expressed as:

$$\int \rho(x_1, x_2)\varphi_i(x_2)d\Omega_{x_2} = \Lambda_i\varphi_i(x_1) \tag{4.1}$$

where, x_1 and x_2 are spatial coordinates in space of Ω, φ_i and Λ_i are the eigenfunctions and eigenvalues of correlation function $\rho(x_1, x_2)$, respectively.

In principle, the eigenvalues and eigenfunctions reported in Equation (4.1) can be solved analytically or numerically. Referring to Van Trees (2004), when the

correlation function is exponential, the analytical solution for Equation (4.1) for a one-dimensional random field can be presented as:

$$\begin{cases} \varphi_i(x_2) = \dfrac{\cos(\omega_i x_2)}{\sqrt{a+\frac{\sin(2\omega_i x_2)}{2\omega_i}}} & \text{for even } i \\ \varphi_i(x_2) = \dfrac{\sin(\omega_i x_2)}{\sqrt{a-\frac{\sin(2\omega_i^* x_2)}{2\omega_i^*}}} & \text{for odd } i \end{cases} \tag{4.2}$$

$$\begin{cases} \Lambda_i = \dfrac{2c}{{\omega_i}^2+c^2} & \text{for even } i \\ \Lambda_i = \dfrac{2c}{{\omega_i^*}^2+c^2} & \text{for odd } i \end{cases} \tag{4.3}$$

$$\begin{array}{ll} c - \omega\tan(a\omega) = 0 & \text{for even } i \\ \omega^* + ctan(a\omega^*) = 0 & \text{for odd } i \end{array} \tag{4.4}$$

where, $a = H/2$, $c = 1/l_C$ and H is the dimension of the field, ω and ω^* are angular frequencies for even and odd counter numbers i, respectively. In this study, the closed form solution for Equation (4.1) as presented by Zhang and Lu (2004) is adopted, which can be written as follows:

$$\widehat{H}(x,\vartheta) = \mu + \sum_{i=1}^{M} \sigma\sqrt{\Lambda_i}\,\varphi_i(x)\xi_i(\vartheta), \qquad x \in \Omega \tag{4.5}$$

where, μ is the mean and σ is the standard deviation of the random field variables, $\xi_i(\vartheta)$ is a vector of uncorrelated standard normal variables, and M is number of truncated terms.

Generally, there are more than one random variable in soils such as elastic visco-plastic model parameters in this research ($\lambda/V, \psi_0/V$), while these model

parameters are frequently reported to be correlated in real practice (Mesri 2003; Mesri and Choi 1985; Mesri and Godlewski 1977b). In probabilistic analysis, the cross correlation coefficient (ρ) is available to capture the degree of dependency of generated random variables on each other. By applying cross correlated effects into Equation (4.5), Gaussian random field can be introduced as follows:

$$\widehat{H}_l(x,\vartheta) = \mu_l + \sum_{j=1}^{M} \sigma_l \sqrt{\Lambda_j}\, \varphi_j(x) \chi_{l,j}(\vartheta), \qquad x \in \Omega \quad (for\ l = \frac{\lambda}{V}, \frac{\psi_0}{V}) \tag{4.6}$$

where, $\chi_{l,j}$ is the correlated random vector whose k th column, χ^k, is given by:

$$\chi^k = \left[\chi^k_{\frac{\psi_0}{V}}, \chi^k_{\frac{\lambda}{V}}\right] = \left[\xi^k_{\frac{\psi_0}{V}}, \xi^k_{\frac{\lambda}{V}} \cdot \rho_{\frac{\psi_0}{V},\frac{\lambda}{V}} + \xi^k_{\frac{\lambda}{V}} \sqrt{1 - \left(\rho_{\frac{\psi_0}{V},\frac{\lambda}{V}}\right)^2}\right] \tag{4.7}$$

where, ξ_l ($l = \frac{\lambda}{V}, \frac{\psi_0}{V}$) is a vector of uncorrelated standard normal variables used to discretise the random fields, and $\rho_{\frac{\psi_0}{V},\frac{\lambda}{V}}$ is the cross correlation coefficient between λ/V and ψ_0/V. As the elastic visco-plastic parameters (i.e. $\lambda/V, \psi_0/V$) are always positive, the Gaussian (normal) random field is not applicable and thus λ/V and ψ_0/V were assumed to be log-normally distributed random variables in this study which can be obtained from Equation (4.8) below:

$$\widehat{H}_l(x,\vartheta) = exp\left(\mu_{lnl} + \sum_{j=1}^{M} \sigma_{lnl} \sqrt{\Lambda_j}\, \varphi_j(x) \chi_{l,j}(\vartheta)\right) \qquad (for\ l = \frac{\lambda}{V}, \frac{\psi_0}{V}) \tag{4.8}$$

where, μ_{lnl} and σ_{lnl} are the mean and standard deviation of the Gaussian random variables ln (l) , respectively which are defined as:

$$\mu_{lni} = ln\mu_l - \frac{\sigma_{lnl}^2}{2}, and\ \sigma_{\ln l} = \sqrt{ln(1 + (COV_l)^2)} \qquad (where\ l = \frac{\lambda}{V}, \frac{\psi_0}{V}) \tag{4.9}$$

where, COV_l is the coefficients of the variation of selected random variables indicating the mean and standard deviation in terms of a dimensionless parameter and $COV_l = \sigma_l/\mu_l$. It should be noted that low values of COV_l indicates the high confidence level in soil parameters and vice versa. The flowchart of adopted methodology is shown in Figure 4.1.

In order to evaluate the accuracy of generated random variables, it is suggested by Spanos and Ghanem (1989) to determine the relative error between the target correlation function and the generated correlation function, established via K-L expansion method which is adopted in this study, as follows:

$$Error\left(\rho(x_1, x_2).C_{\hat{H}\hat{H}(x_1,x_2)_{K-L}}\right) = 1 - \frac{C_{\hat{H}\hat{H}(x_1,x_2)_{K-L}}}{exp\left(-\frac{|x_1-x_2|}{l_C}\right)} \tag{4.10}$$

where $C_{\hat{H}\hat{H}(x_1,x_2)_{K-L}}$ is covariance function developed by K-L expansion method and can be expressed as:

$$C_{\hat{H}\hat{H}(x_1,x_2)_{K-L}} = \sum_{n=1}^{M} \Lambda_n\, \varphi_n(x_1)\varphi_n(x_2) \tag{4.11}$$

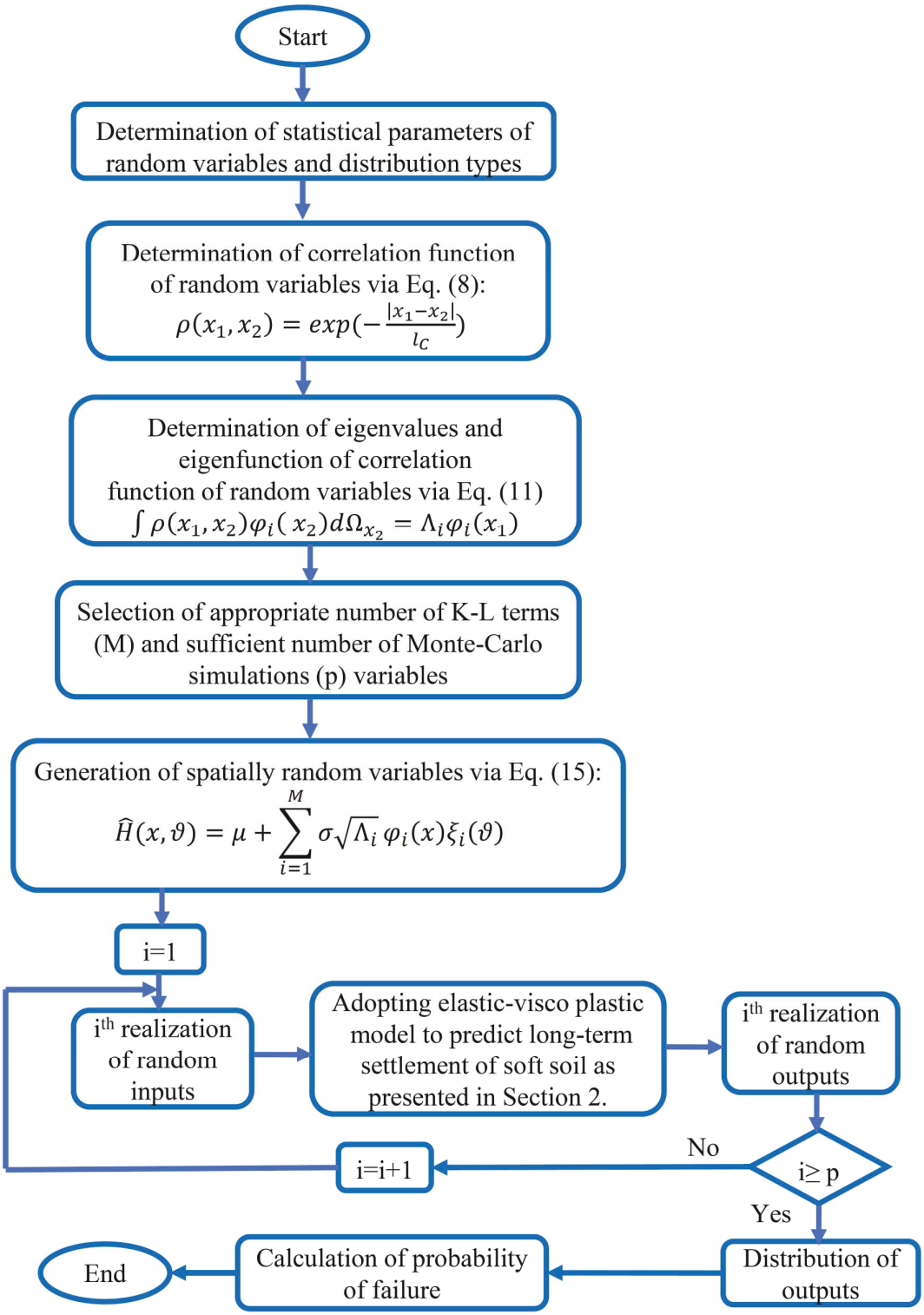

Figure 4.1 Flowchart of adopted random field methodology

4.3 Adopted Case Study

The Skå–Edeby test embankment is chosen as a case study to conduct the random field reliability analysis and verify the results. The Skå–Edeby area was located 25km west of Stockholm, which was considered a possible site for constructing an airfield. In order to evaluate the suitability of site and study the long-term behaviour of Swedish clays, three test fills with vertical drains and one without vertical drains were constructed on top of the Skå–Edeby soft soil (Larsson and Mattsson 2003). In this study, the test fill without vertical drain is used as a case study. The adopted test fill with 35 m diameter, a height of 1.5 m, the slope of 1(V): 1.5 (H), and gravel fill with an average unit weight of 17.56 kN/m3 was constructed over 70 days. As reported by Larsson and Mattsson (2003), the total applied load induced by test fill was estimated to be 27 kPa at the ground surface and the ground water table was approximately 1m below the ground surface with seasonal fluctuation of ±0.5 m. As shown in Figure 4.2, the subsoil profile at the Skå–Edeby site consisted of a 12 m recent, post glacial and glacial clays overlying a rock with a 0.5m crust at the top (Holtz and Lindskog 1972). Figure 4.3 illustrates the soil properties used for numerical simulation, including the soil unit weight, the soil permeability, the over consolidated ratio (OCR), and the void ratio which were determined based on laboratory test results (Hansbo 1960; Larsson and Mattsson 2003). Referring to Hansbo (1960), these properties were obtained by carrying out a series of laboratory tests. In order to determine the elastic visco-plastic model parameters including the initial creep coefficient (ψ_0/V) and the time independent elastic-plastic parameters (κ/V, σ'_{z_0}, and λ/V), the curve fitting method as reported in the literature (Le et al. 2015; Le et al. 2017; Yin 1999; Yin and Graham 1994; Yin et al. 2002) is used based

on three oedometer tests (samples A, B, and C) reported by Hansbo (1960) and presented in Figure 4.4. By comparing the properties of sample with the soil condition, it can be assumed that sample A was taken at depth 2 m, while samples B and C were obtained from deeper depth of 8 m and 9 m, respectively.

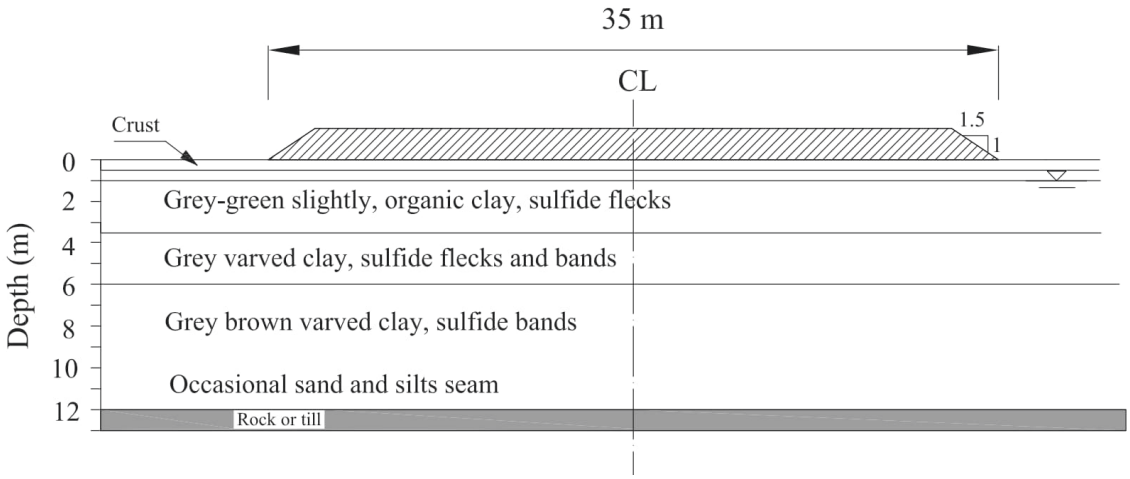

Figure 4.2 Subsoil layers for Skå–Edeby test fill (Data taken from Larsson and Mattson 2003)

4.3.1 Generating Statistical Parameters of Probabilistic Variables

In this study, the initial creep coefficient (ψ_0/V) and elastic-plastic parameter (λ/V) are considered as probabilistic variables due to the lack of long-term creep tests. A common curve fitting method proposed by Yin (1999) is used to obtain the initial creep coefficient (ψ_0/V).

By adopting existing oedometer test results and utilising the curve fitting approaches outlined in Section 3.2.2, a set of data for the elastic-plastic parameters (λ/V and σ'_{z_0}) are determined. It should be noted that λ/V and σ'_{z_0} are interdependent parameters, so it was essential to find a relationship between λ/V and σ'_{z_0} so that by generating random values for λ/V, the corresponding values for σ'_{z_0} could be generated simultaneously. For this purpose, the regression analysis is

adopted to find the best fit curve between λ/V and σ'_{z_0} . As shown in Table 4.1, the exponential regression could be considered as the best fitted curve for relationship between λ/V and σ'_{z_0}.

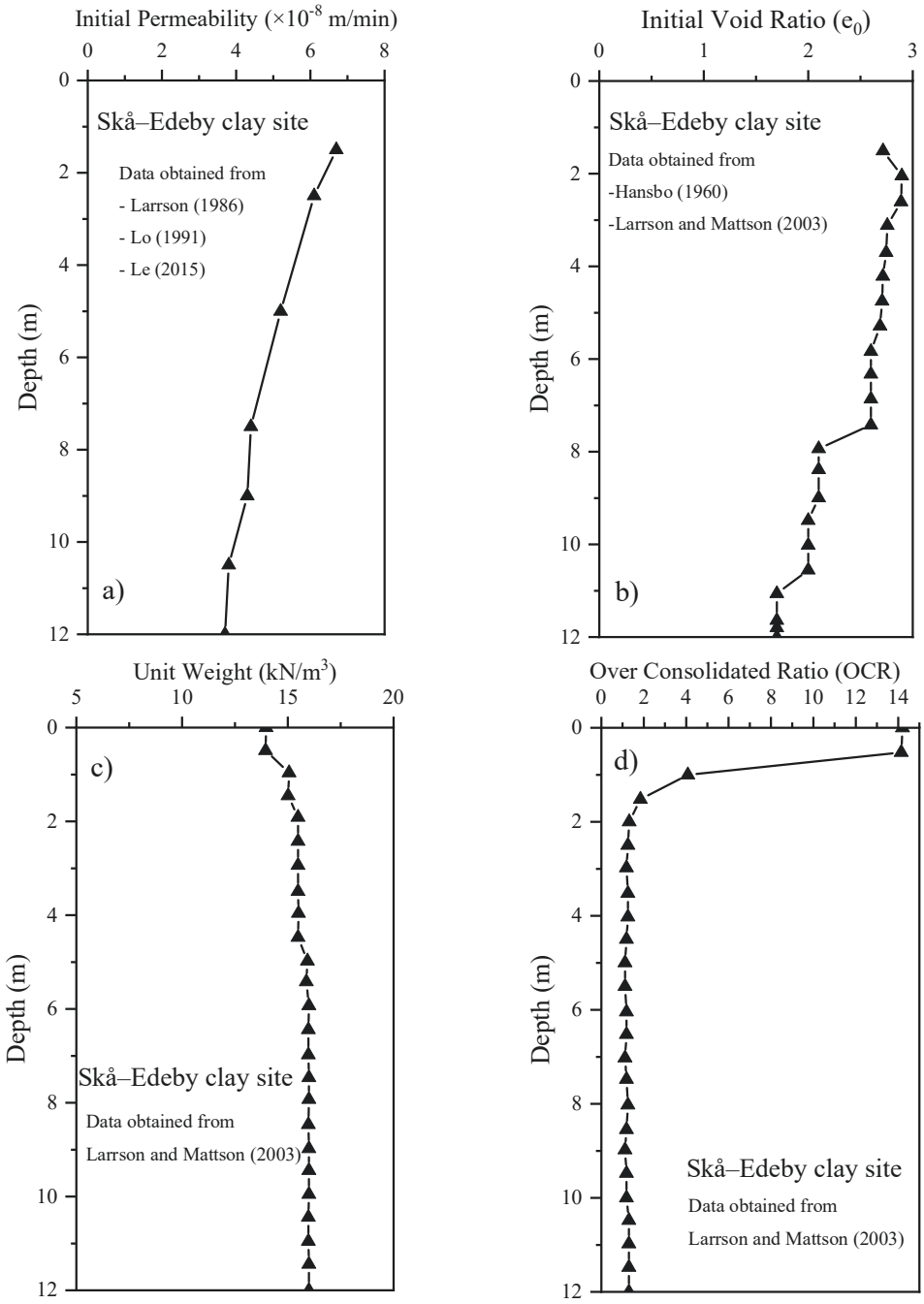

Figure 4.3 Adopted soil properties of Skå–Edeby test fill for numerical modelling (a) permeability (b) initial void ratio (c) total unit weight and (d) over-consolidated ratio

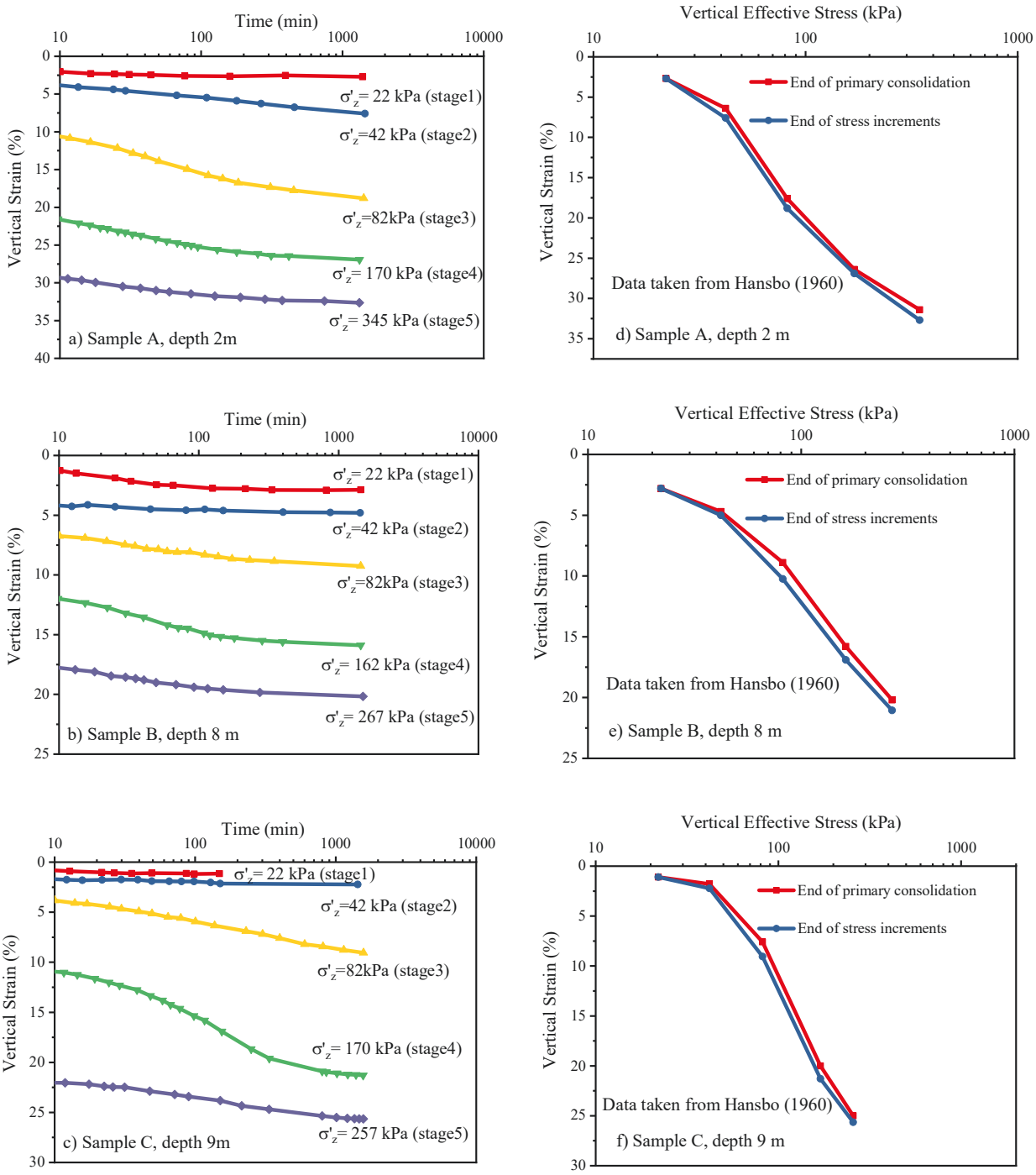

Figure 4.4 Oedometer test results of Skå–Edeby test fill (a), (b), (c) vertical strain versus time for samples A, B, and C, respectively (d), (e), (f) vertical strain versus vertical effective stress for samples A, B, and C, respectively

The generated random variables of the initial creep coefficient (ψ_0/V) and the elastic-plastic model parameters (λ/V) and their corresponding statistical properties based on existing oedometer test are shown graphically in Figure 4.5. The cross correlation coefficient between λ/V and ψ_0/V is calculated to be $\rho_{\lambda/V,\psi_0/V} = 0.6$ (Feng and Zhang 2021; Genz and Bretz 2002; Zhang et al. 2019). Moreover, Table 4.1 summarises the adopted probabilistic and deterministic model parameters adopted in this study to predict the long-term settlement of the Skå–Edeby test fill and compare to the field measurements.

Table 4.1 Adopted deterministic and probabilistic model parameters for Skå–Edeby test fill

Model parameter	Type	Mean (μ)	Coefficient of Variation (υ_X)	Distribution
λ/V	random	0.11	0.3	Lognormal
ψ_0/V	random	0.01	0.3	Lognormal
κ/V	deterministic	0.04	-	-
$t_0(min)$	deterministic	370	-	-

Note: $\sigma'_{z_0}(kPa) = 6e^{12\lambda/V}$

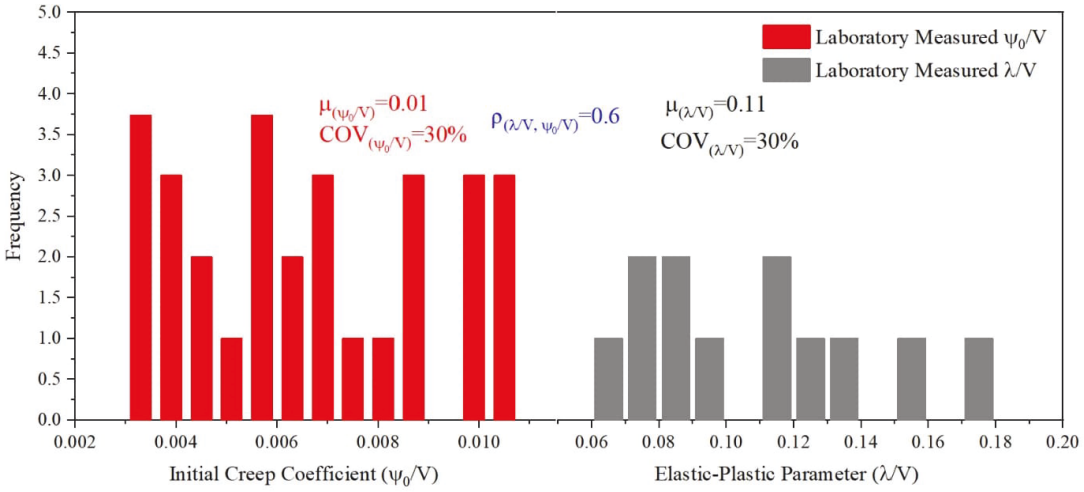

Figure 4.5 Generated random variables of the elastic-plastic parameter (λ/V) and the initial creep coefficient (ψ_0/V) based on existing oedometer test data

4.3.2 Implementation of K-L Expansion Method

In order to generate spatially correlated random variables for the elastic-plastic and the initial creep model parameters (λ/V , ψ_0/V), K-L expansion method, explained in the previous section, is adopted by considering statistical properties reported in Table 4.1. As shown in Equations (4.10) and (4.11), in order to generate random fields based on K-L expansion method, number of truncated terms (M) and spatial correlation length (l_C) are two key factors to evaluate the accuracy of generated random variables. It should be noted that for the sake of generality, the correlation length (l_C) is presented in dimensionless form as normalised spatial correlation length ($\theta = l_C/H_0$). Referring to Equation (4.6), the maximum number of truncated terms (M_{max}) in K-L expansion method must be equal to the maximum number of elements in finite difference code. Therefore, in this study, the maximum number of elements is considered equal to the number of finite difference nodes (n). In the developed finite difference code for the Skå–Edeby clay with 12 m depth and 0.1 m node interval, the maximum number of truncated terms is calculated to be $M_{max} = 121$. Moreover, Siripatana et al. (2020) introduced 90% of spatially averaged variability as a criterion to determine the minimum number of truncated terms (M_{min}). This criterion ensures that the reference eigenbasis encapsulates 90% of the information in assumed correlation function and the error obtained from Equation (4.10) is less than 10%. According to this requirement, M_{min} increases from $M_{min} = 1$ corresponding to $\theta = 0.01$ to $M_{min} = 90$ corresponding to $\theta = 100$ which means that the adopted $M_{max} = 121$ was suitable.

Figure 4.6 shows the variation of eigenvalues versus number of truncated terms for different normalised spatial correlation lengths. It is evident that the smaller

correlation length results in the reduced number of truncated terms needed for a given accuracy. Moreover, Figure 4.7 illustrates an example of the comparison between target and approximated correlation functions for the case of $\theta = 1, \text{and } M = 121$. It can be seen that the maximum error is 1%, which fulfills the criteria for the maximum acceptable error of 10%, recommended by Siripatana et al. (2020). Figure 4.8 shows samples of generated random field based on K-L expansion method for various normalised spatial correlation lengths. It can be seen that when $\theta > 1$, the generated random variables are more uniform along the model dimension.

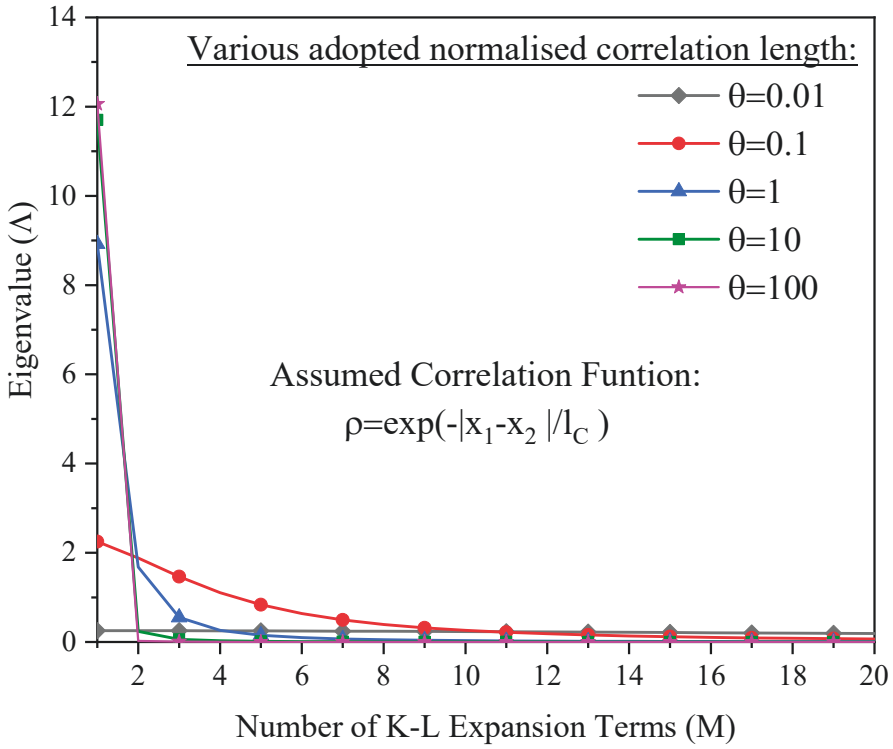

Figure 4.6 Variation of eigenvalues versus number of truncated terms for different normalised spatial correlation length

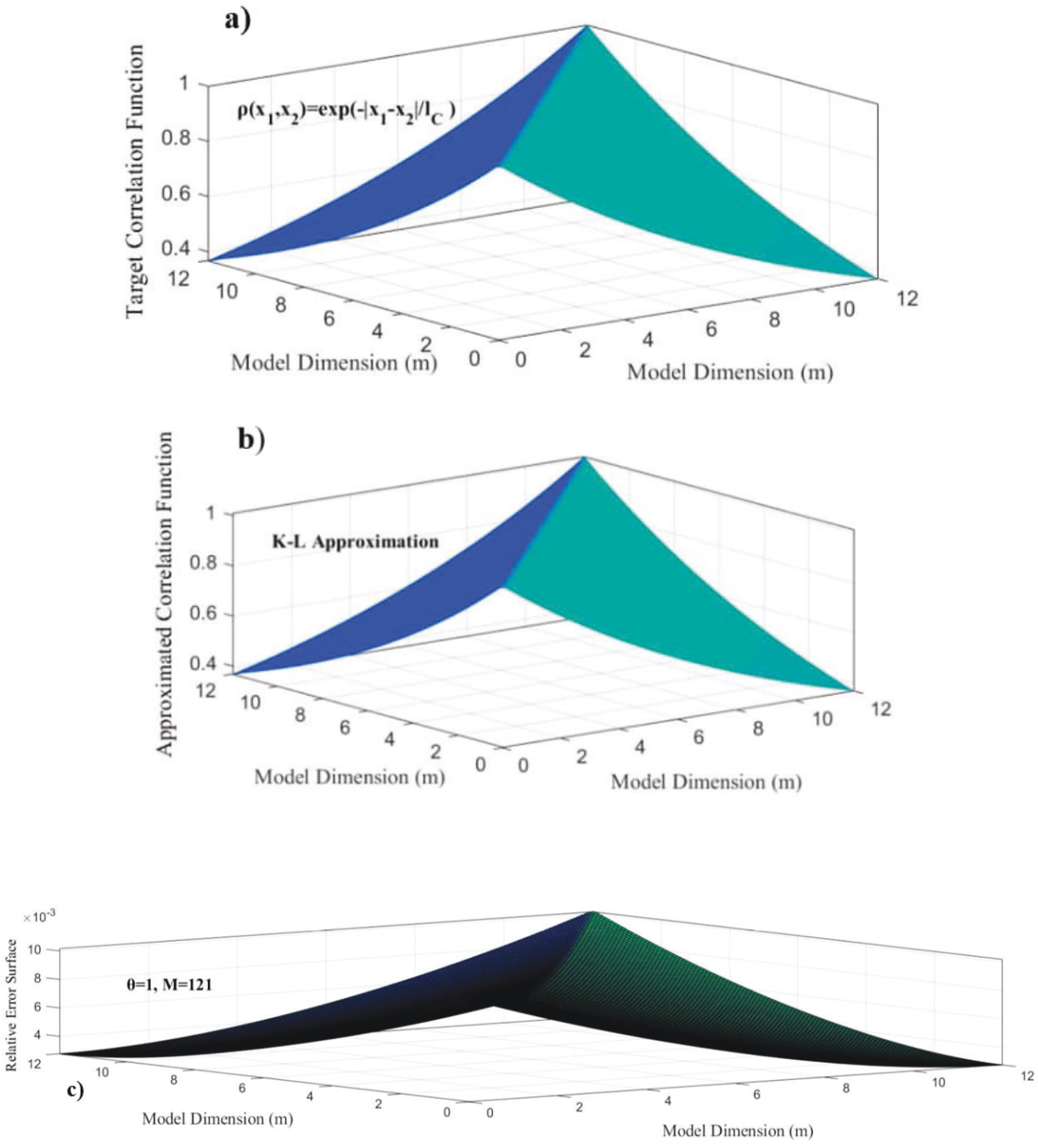

Figure 4.7 Comparison of target and approximated correlation function (a) target correlation function, (b) approximated correlation function, (c) relative error surface

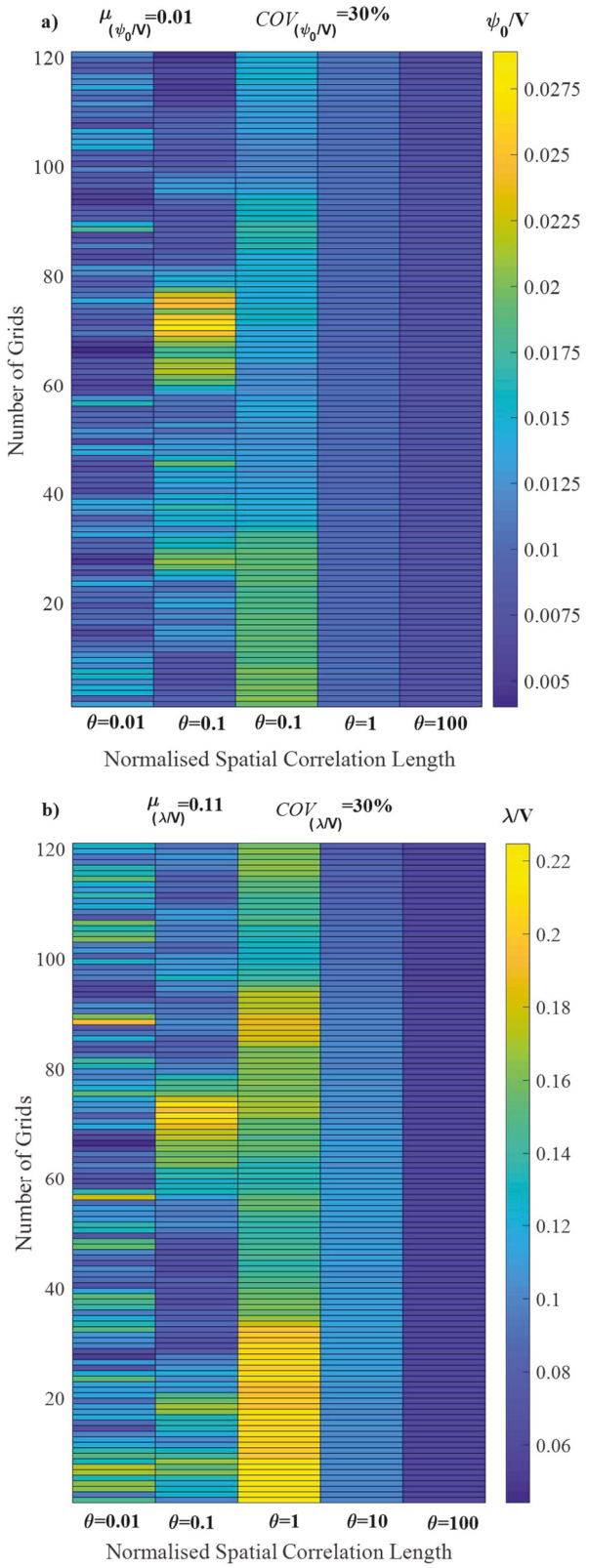

Figure 4.8 Generated random field for various normalised spatial correlation lengths (a) initial creep coefficient (ψ_0/V), (b) elastic-plastic model parameter (λ/V)

4.4 Results and Discussion

There are a variety of concerns contributing to risks and considerations associated with construction on top of soft soils. Predicting time-dependent behaviour of soft soils is a crucial element in reducing risks and instabilities. As a result, it is essential to evaluate the uncertainties related to model parameters in predicting time-dependent behaviour quantitatively. In this study, the effect of spatial correlation length is evaluated adopting the elastic visco-plastic model parameters (λ/V , ψ_0/V) as random variables to obtain a range of possible time-dependent settlement and excess pore water pressure (EPWP) distribution for the Skå–Edeby test fill. Then, in order to verify the undertaken probabilistic analysis, results are compared with the field measurements. In the last step, a parametric study is performed to identify the critical spatial correlation length (θ_w) with the maximum probability of failure to substantiate the importance of random field (RF) analysis in comparison with the single random variable (SRV) analysis.

4.4.1 Comparison between Random Field (RF) and Single Random Variable (SRV) Analyses for Prediction of Time-dependent Settlement and EPWP

A set of predicted ground surface settlement of the Skå–Edeby fill at different time stages are obtained from random field analysis (RF) for various spatial correlation lengths in addition to single random variable (SRV) analysis. As mentioned earlier, the elastic-plastic model parameter (λ/V) and the initial creep coefficient (ψ_0/V) are considered as random variables. In the first step, it is essential to ensure that the assumed number of Monte-Carlo simulations is efficient and reliable enough. For this purpose, the optimal number of Monte-Carlo simulations is considered to be the minimum number of simulations in which the standard deviation of the outputs

converged. Figure 4.9 illustrates the standard deviation of the surface settlement versus the number of Monte-Carlo simulations at various post construction times in years (PCY) while considering the normalised spatial correlation length to be equal to one (i.e. $\theta = 1$). It is concluded that the standard deviation of the ground surface settlement stayed almost constant when the number of Monte-Carlo simulations is more than 1000. Therefore, 2000 Monte-Carlo simulations are used in the follow up analyses to provide the required accuracy and efficiency.

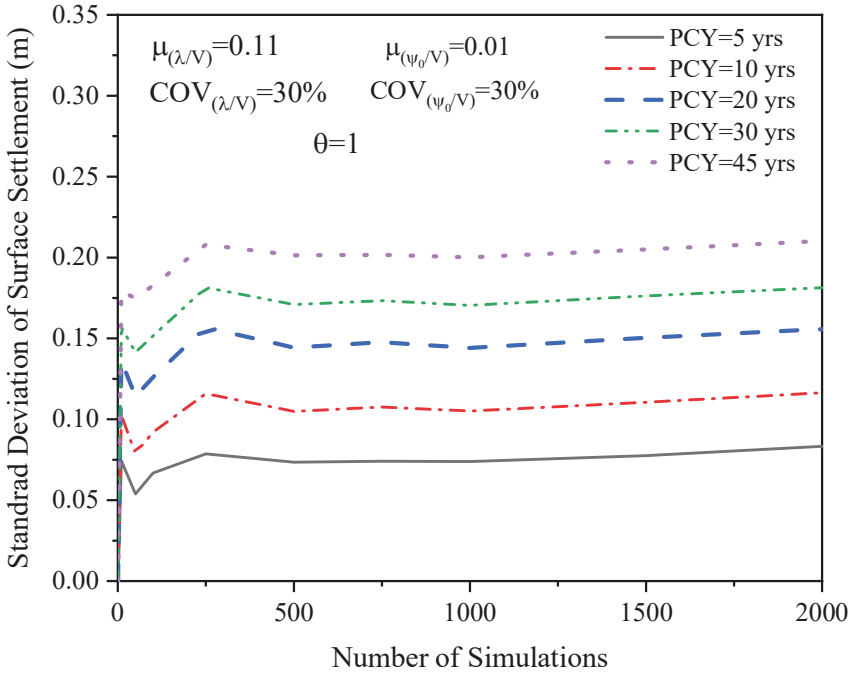

Figure 4.9 Convergence of the number of simulations for the surface settlement at different time stages

Figure 4.10 exhibits the probability density function of the ground surface settlement at different PCY for RF analysis with various spatial correlations length and SRV analysis adopting λ/V and ψ_0/V as random variables. It can be observed that when spatial correlation length increases in RF analysis, standard deviation and corresponding coefficient of variation (COV) increase resulting in lower levels of confidence in prediction of time-dependant settlement. Moreover, when normalised

spatial correlation length is more than 1 (i.e. $\theta > 1$), the results of RF analysis are close to those obtained by SRV analysis. Figure 4.11 compares statistical dispersions of the ground surface settlement obtained from RF analysis with different spatial correlation length and SRV analysis. As expected, the mean value of predicted ground surface settlement is almost constant for all adopted analysis with slight differences due to computational approximation in generating random numbers. Moreover, Figure 4.11b and Figure 4.11c show that in RF analysis, by increasing spatial correlation length, the standard deviation and coefficient of variation (COV) of the ground surface settlement increase. A Similar trend is observed by Wang et al. (2021), where standard deviation of creep deformation after 30 years increased from 0.045 to 0.13, when correlation length of creep coefficient increased from 4 m to 20 m, respectively. However, when normalised spatial correlation length is more than 1 (i.e. $\theta > 1$), standard deviation and coefficient of variation (COV) are higher than the corresponding values in SRV analysis. This observation indicates that by increasing correlation length, uncertainties in settlement predictions are higher than the corresponding predictions obtained from SRV analysis resulting in lower confidence level of predictions. Figure 4.11c also shows that for both RF and SRV analyses, the COV of the ground surface settlement becomes rather constant as time progresses, indicating that the uncertainties in settlement prediction are higher at early stages of construction on top of soft soils and then approach an asymptote over time.

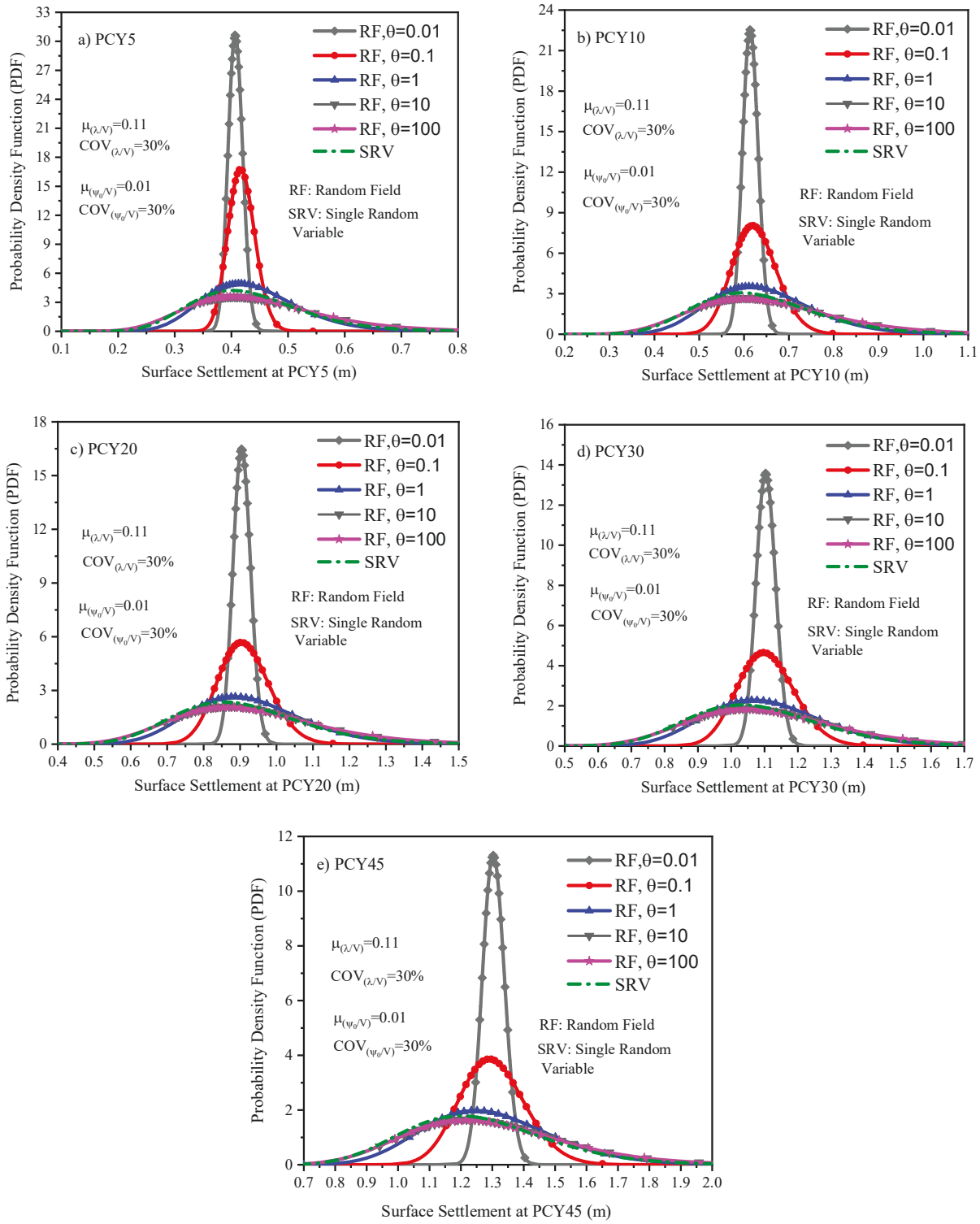

Figure 4.10 Influence of RF analysis with different normalised spatial correlation lengths and SRV analysis on the surface settlement of the Skå–Edeby test fill at various time stages (a) PCY5, (b) PCY10, (c) PCY20, (d) PCY30 and (e) PCY45

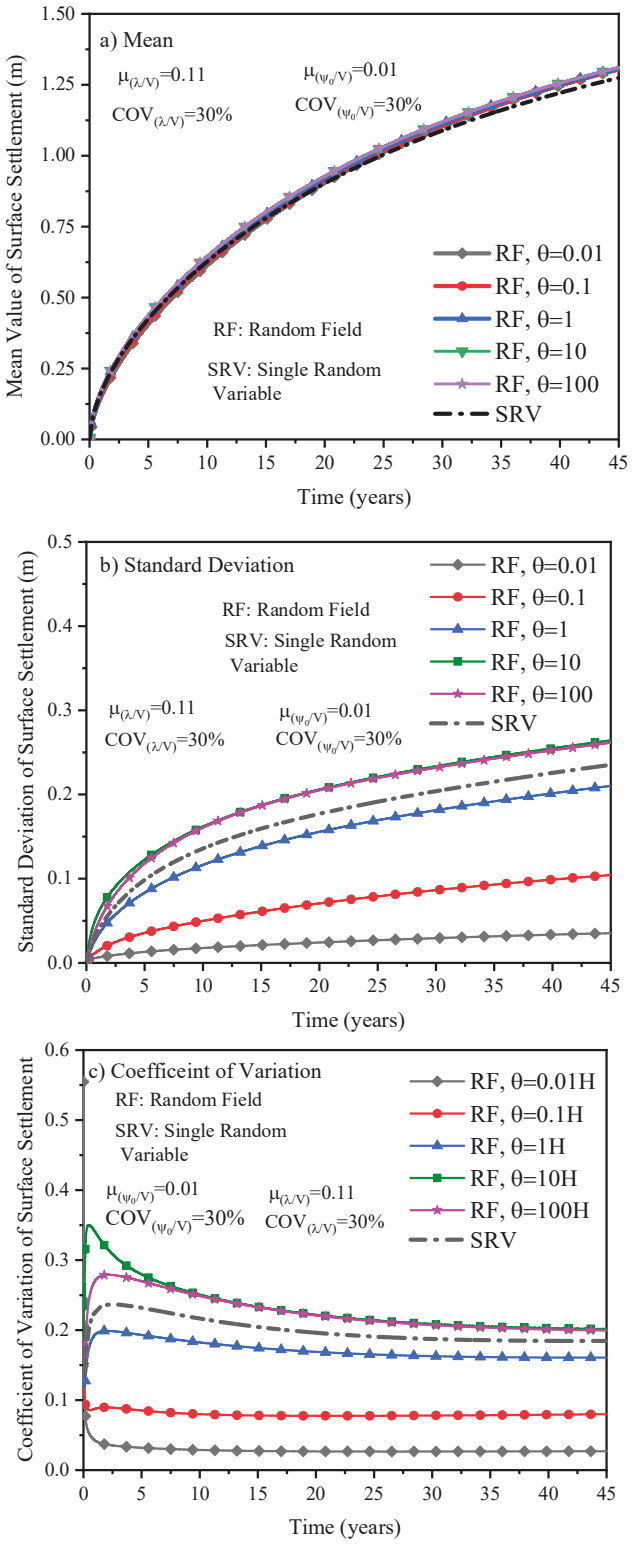

Figure 4.11 Statistical dispersions of ground surface settlement versus time adopting RF analysis with various normalised spatial correlation lengths and SRV analysis (a) mean, (b) standard deviation and (c) coefficient of variation

For further discussion, the variation of statistic dispersions of settlement with depth at PCY45 (i.e. 45 years post construction) are plotted in Figure 4.12. As expected, the mean value of soil settlement is approximately constant for all adopted analyses and increase from depth of 12 m to the surface. Figure 4.12b shows that the standard deviation of the predicted settlement decreases with depth and it is independent of the analysis type (i.e. RF or SRV analysis). This is due to the fact that the uncertainties of settlement prediction in the sub-layers are accumulated at the surface. Moreover, Figure 4.12c illustrates that when normalised spatial correlation length is less than unity in RF analysis (i.e. $\theta < 1$), the coefficient of variation (COV) increases sharply with depth, because the uncertainties in generated parameters is higher at lower depths. However, for SRV analysis and for RF analysis with normalised spatial correlation length more than unity (i.e. $\theta > 1$), COV of the settlement prediction changes slightly with depth indicating that uncertainties in settlement prediction does not change much with depth. Figure 4.12c also confirms that by increasing normalised spatial correlation length, the uncertainties in settlement prediction increases as presented earlier in Figure 4.11c, and when the normalised spatial correlation length is more than unity (i.e. $\theta > 1$), RF analysis is more conservative than SRV analysis.

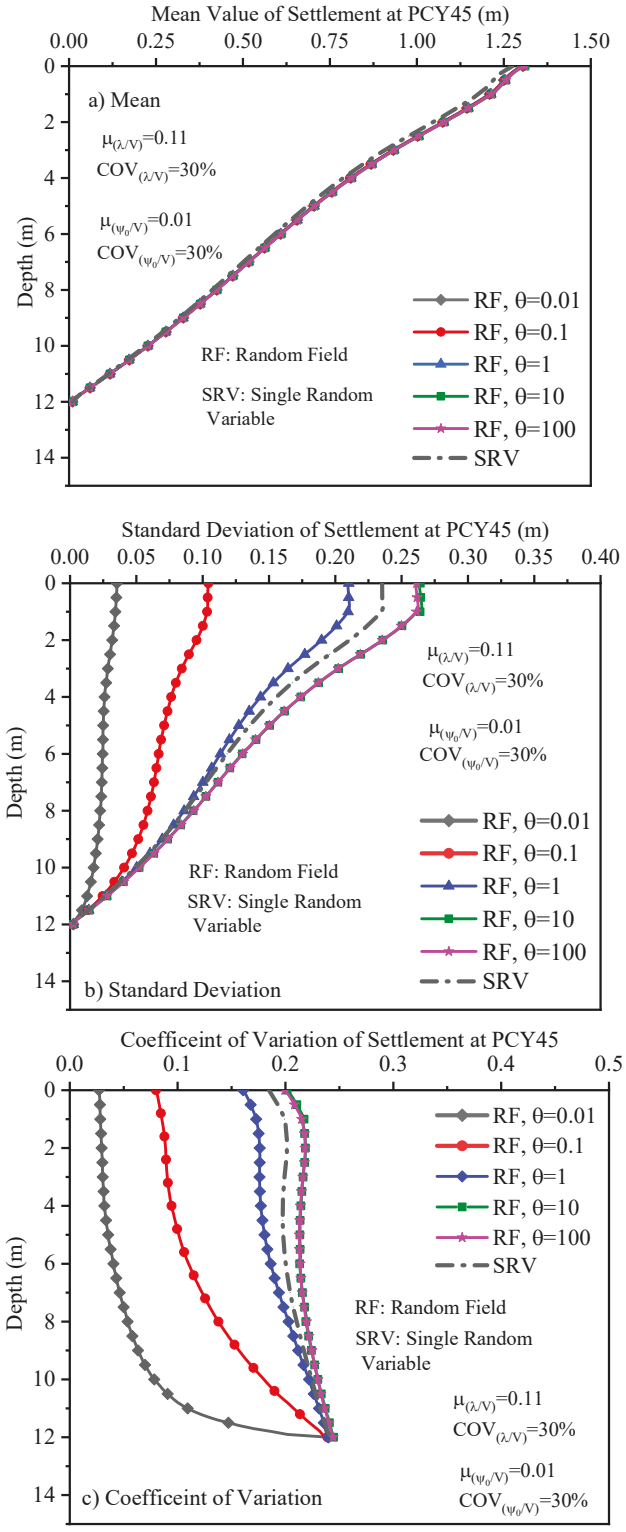

Figure 4.12 Statistical dispersions of settlement versus depth at PCY45 adopting RF analysis with various normalised spatial correlation lengths and SRV analysis (a) mean, (b) standard deviation and (c) coefficient of variation

In addition to evaluating soil settlement when evaluating the time-dependent behaviour of soft soils, investigating excess pore water pressure (EPWP) is also a key factor because it has an impact on the stress, stiffness, and shear strength of the soil. Therefore, in order to evaluate the variation of EPWP in RF and SRV analyses, the statistical dispersions of predicted excess pore water pressure over time are plotted in Figure 4.13. Since the horizontal axis captures the time from the beginning of construction, Figure 4.13a shows that the mean value of EPWP for all adopted analysis increases sharply during the first 70 days (i.e. during the embankment construction) and then gradually decreases over time. Similar to predicted settlement (Figure 4.11), Figure 4.13b and Figure 4.13c show that in RF analysis, the uncertainties in predicting EPWP increase as the normalised spatial correlation length increases, and when the normalised spatial correlation length is more than unity (i.e. $\theta > 1$), RF analysis indicates a lower confidence level in predicting EPWP compared to SRV analysis. Furthermore, Figure 4.14 shows the statistical properties of predicted excess pore water pressure at PCY45 for all adopted analyses. As evident in Figure 4.14a and Figure 4.14b, the maximum mean and standard deviation occurs at the mid-depth due to the fact that in two-way drainage system, the maximum EPWP occurs around the mid-depth of the soil deposit. Figure 4.14c illustrates that the coefficient of variation (COV) for the predicted EPWP increases gradually with depth and the maximum uncertainties occurred at lower depths since soil experienced higher rate of excess pore water pressure dissipation due to the larger strains and being in the vicinity of the drainage boundary. By referring to Figure 4.14c, it can be also concluded that the uncertainties in EPWP prediction increase as spatial correlation length increases, and SRV analysis is less uncertain in comparison to RF analysis with $\theta > 1$.

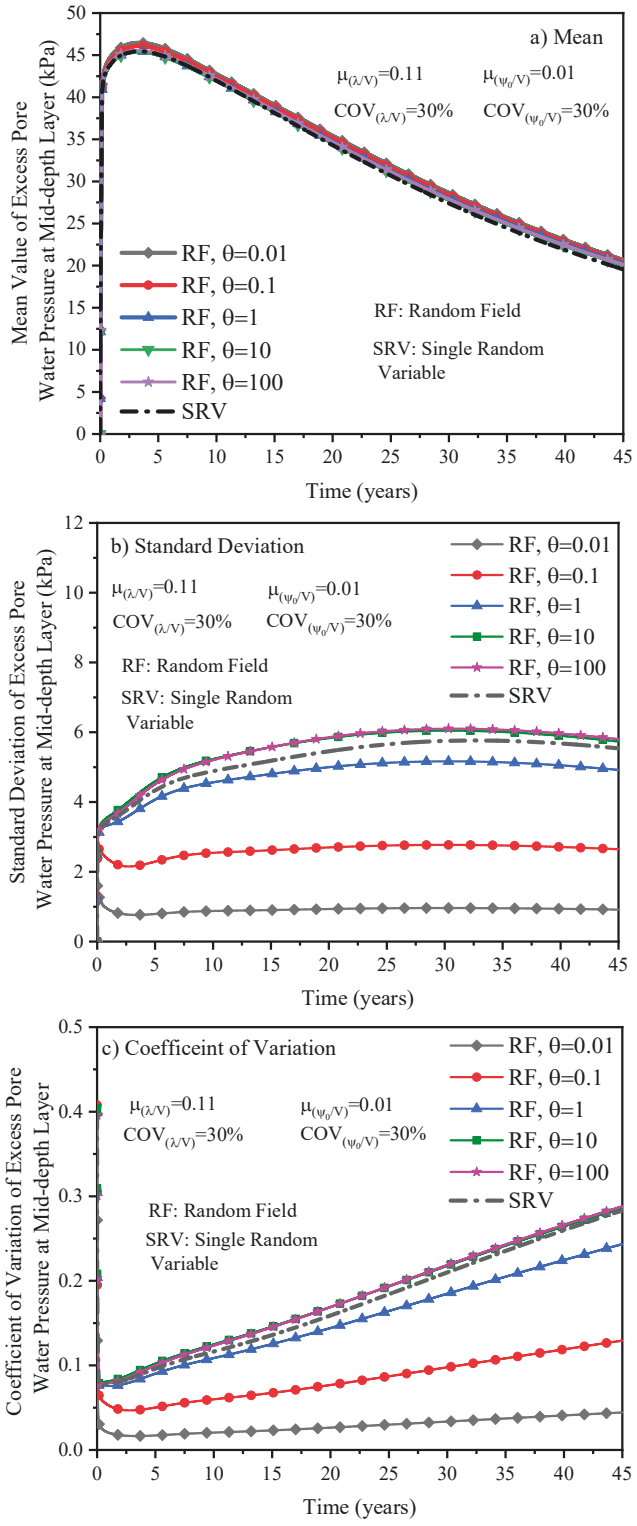

Figure 4.13 Statistical dispersions of excess pore water pressure at mid-depth layer with time adopting RF analysis with various normalised spatial correlation lengths and SRV analysis (a) mean, (b) standard deviation and (c) coefficient of variation (Note: time in horizontal axis is construction years (CY) plus post construction years (PCY)).

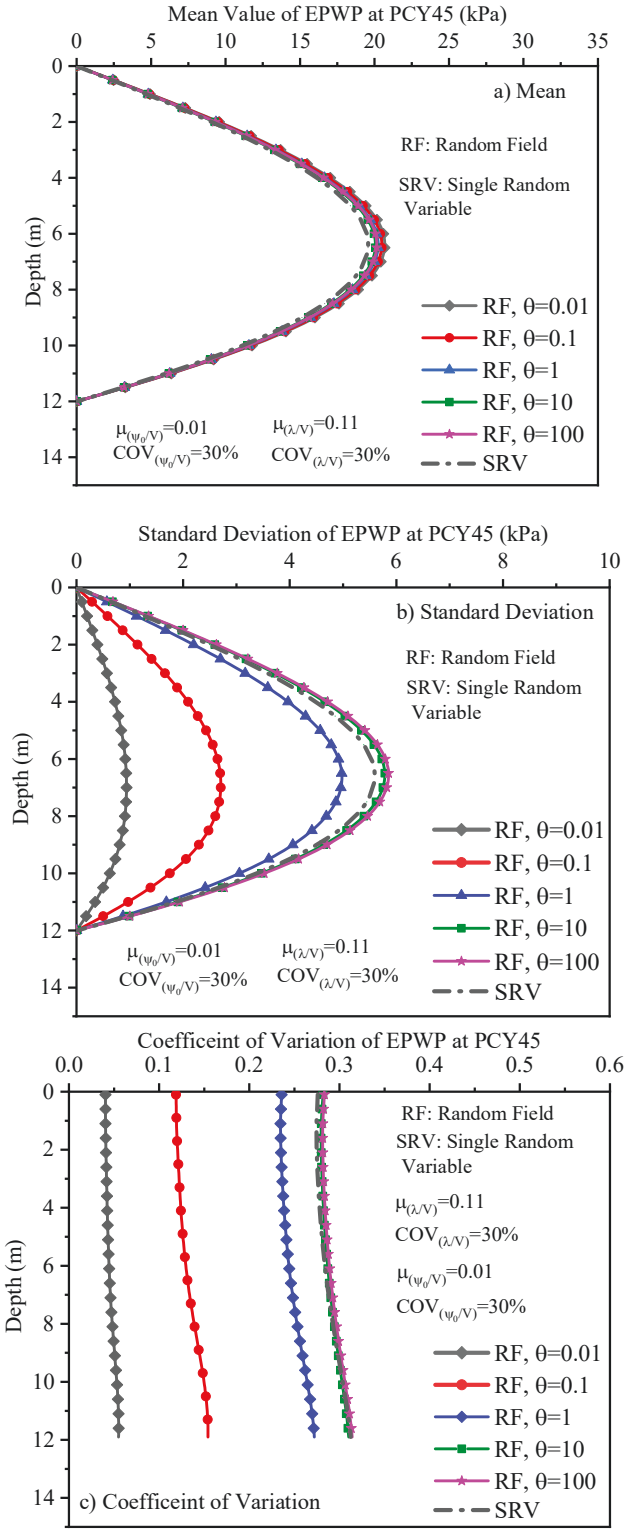

Figure 4.14 Statistical dispersions of excess pore water pressure with depth at PCY45 adopting RF analysis with various normalised spatial correlation lengths and SRV analysis (a) mean, (b) standard deviation and (c) coefficient of variation

4.4.2 Comparison with Field Measurements

Figure 4.15 to Figure 4.18 present a comparison between field settlement measurements at different depths reported by Larsson and Mattsson (2003) and the obtained results with 95% confidence interval (CI). As reported by Zhou, Tan, et al. (2018), $\mu_s \pm 1.96\sigma_s$ approximates the upper boundary (UB) and the lower boundary (LB) with 95% CI for lognormal distribution (where μ_s is the mean and σ_s is the standard deviation of predicted settlement, respectively). It should be noted that the most probable (MP) characteristic corresponds to the average of all obtained results at each time step. As can be seen in Figure 4.15 to Figure 3.19, by adopting RF analysis with $\theta > 1$ or SRV analysis, the field measurements at different depths are located between the upper and lower boundaries of predicted settlements with 95% CI. Figure 4.15 shows that at the surface, the measured settlements are close to the predicted mean values (MP) till PCY 20, whereas at later stages the measured data are located between the mean and lower bound values. As shown in Figure 4.18, at lower depths (e.g. depth of 7.5 m), the field measurements are close to LB of predicted settlement till PCY 10, and then gradually approach to the predicted mean values. Since the mean value of the predicted settlements can be used as an approximation for deterministic analysis predictions, it can be observed that the deterministic analysis could lead to underestimated or overestimated predictions of the actual behaviour. As a result, conducting a reliability analysis is essential to have a better understanding of predictions and risks involved. Moreover, among different adopted methods in this study (i.e. RF and SRV), it is necessary to make a quantitative comparison between field and predicted settlements to have a better insight about suitability of each method. For this purpose, two error indicators were

employed, namely the root mean square error ($RMSE$) and the mean absolute error (MAE). Table 4.2 summarises the calculated $RMSE$ and MAE for RF and SRV analyses. It can be seen that when spatial correlation length decreases in RF analysis, the predicted settlement has better agreement with field measurements. Moreover, the error indicators for SRV analysis are close to the corresponding values for RF analysis with $\theta > 1$. As expected, the error indicators at the surface are more than the errors at depths due to the fact that the settlement accumulates from the depth to the surface, which is also leading to the error accumulation.

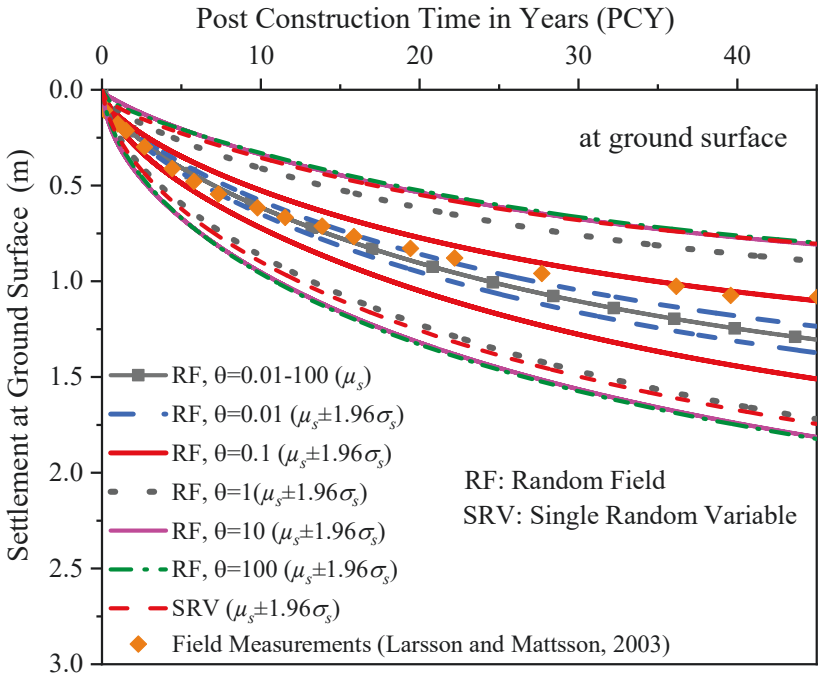

Figure 4.15 Comparison of measured and predicted settlement with 95% CI adopting RF analysis with various normalised spatial correlation lengths and SRV analysis at ground surface

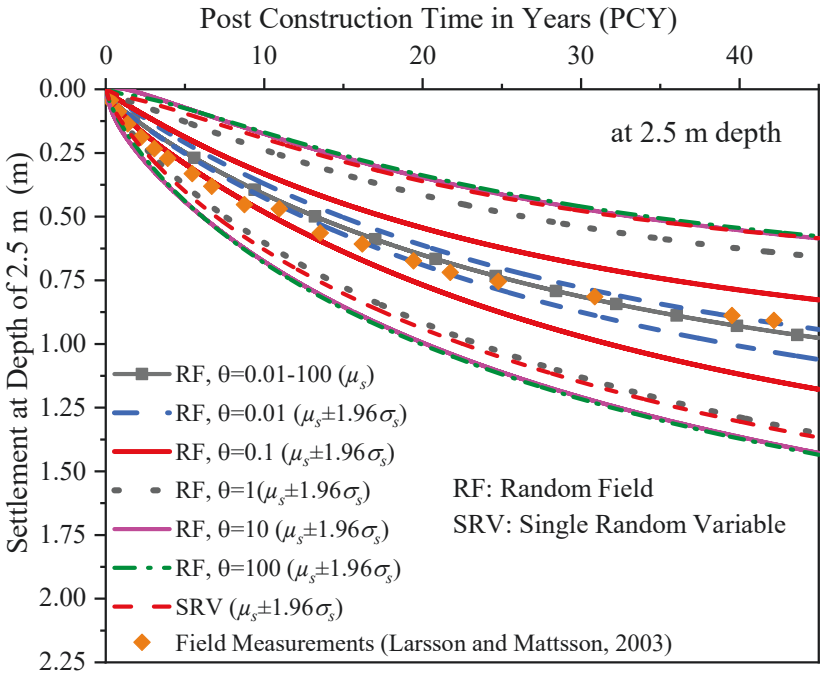

Figure 4.16 Comparison of measured and predicted settlement with 95% CI adopting RF analysis with various normalised spatial correlation lengths and SRV analysis at depth of 2.5m

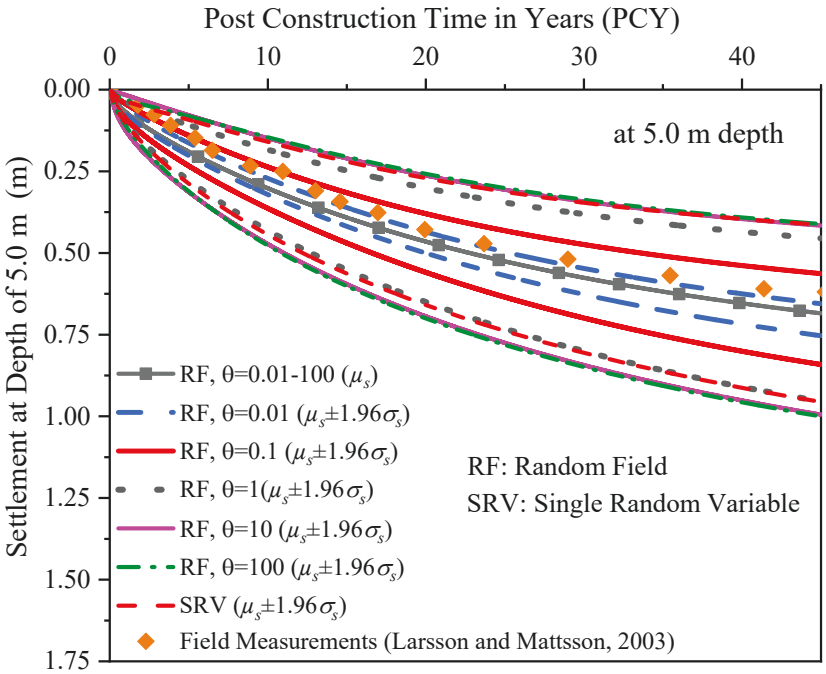

Figure 4.17 Comparison of measured and predicted settlement with 95% CI adopting RF analysis with various normalised spatial correlation lengths and SRV analysis at depth of 5.0m

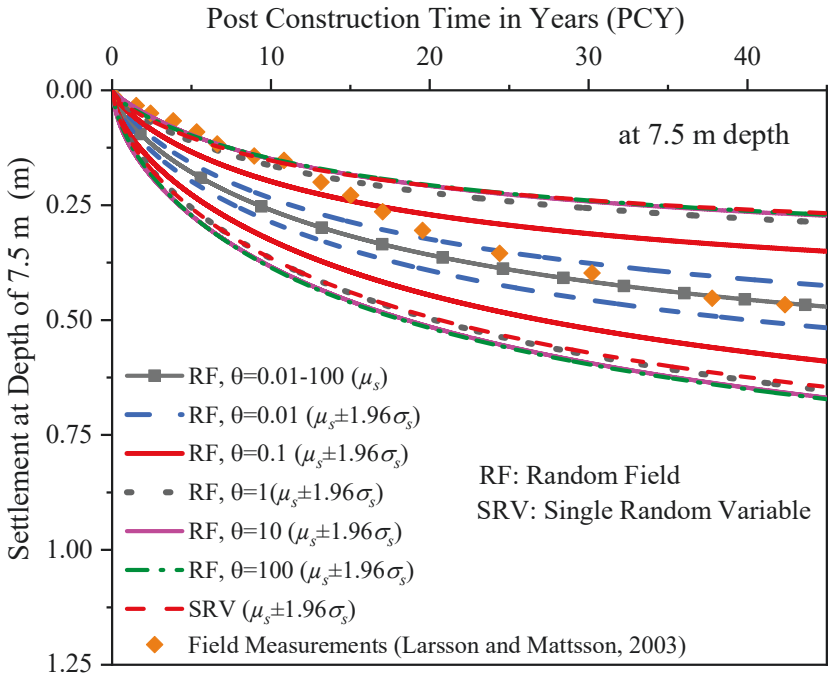

Figure 4.18 Comparison of measured and predicted settlement with 95% CI adopting RF analysis with various normalised spatial correlation lengths and SRV analysis at depth of 7.5m

Table 4.2 Settlement error indicators for all adopted analysis

	Method	RF					SRV
		$\boldsymbol{\theta = 0.01}$	$\boldsymbol{\theta = 0.1}$	$\boldsymbol{\theta = 1}$	$\boldsymbol{\theta = 10}$	$\boldsymbol{\theta = 100}$	
at Surface	*RMSE*	0.09	0.11	0.2	0.25	0.25	0.22
	MAE	0.06	0.09	0.17	0.22	0.22	0.19
at 2.5 m depth	*RMSE*	0.07	0.09	0.16	0.2	0.2	0.18
	MAE	0.06	0.09	0.15	0.19	0.19	0.17
at 5 m depth	*RMSE*	0.05	0.07	0.12	0.15	0.15	0.13
	MAE	0.05	0.07	0.11	0.14	0.14	0.12
at 7.5 m depth	*RMSE*	0.07	0.09	0.11	0.12	0.12	0.11
	MAE	0.07	0.08	0.1	0.11	0.11	0.1

Note: $RMSE$ and MAE denote the root mean square error and the mean absolute error, respectively.

Figure 4.19 and Figure 4.20 show the comparison between excess pore water pressure (EPWP) and the field measurements at PCY14 and PCY45, respectively. It is evident that all predicted values with 95% confidence interval (CI) overestimate the field measurements at PCY 14. As reported by Larsson and Mattsson (2003), the differences between measured and predicted EPWP could be due to many factors including the accuracy of the measurement devices, seasonal variations of the ground water and temperature. Figure 4.20 shows that at PCY 45, the agreement between the measured and the predicted EPWP is improved as the measured data are closer to the lower boundary of predicted EPWP, obtained from RF analysis with $\theta > 1$ and SRV analysis.

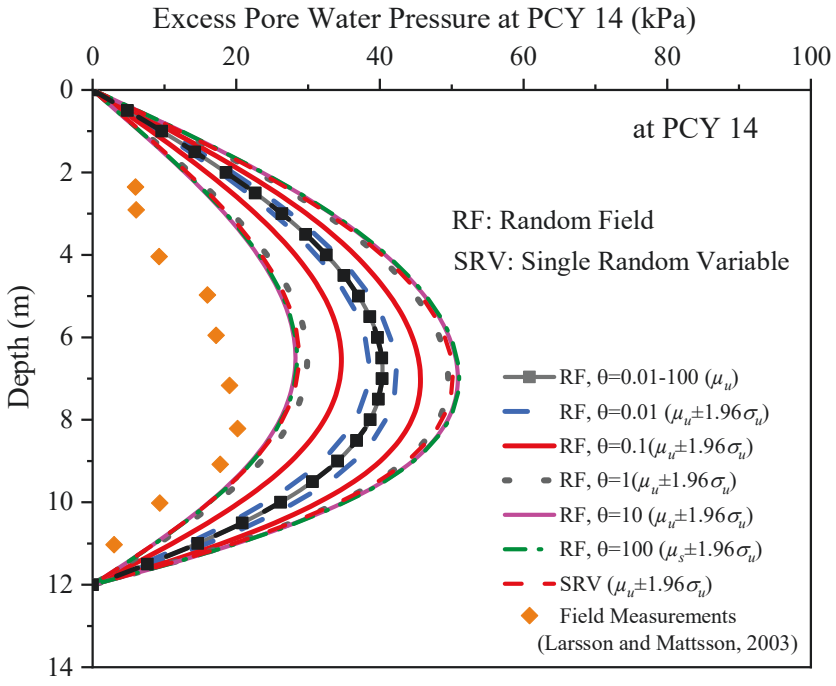

Figure 4.19 Comparison of measured and predicted excess pore water pressures with 95% CI adopting RF analysis with various normalised spatial correlation lengths and SRV analysis at CPY14

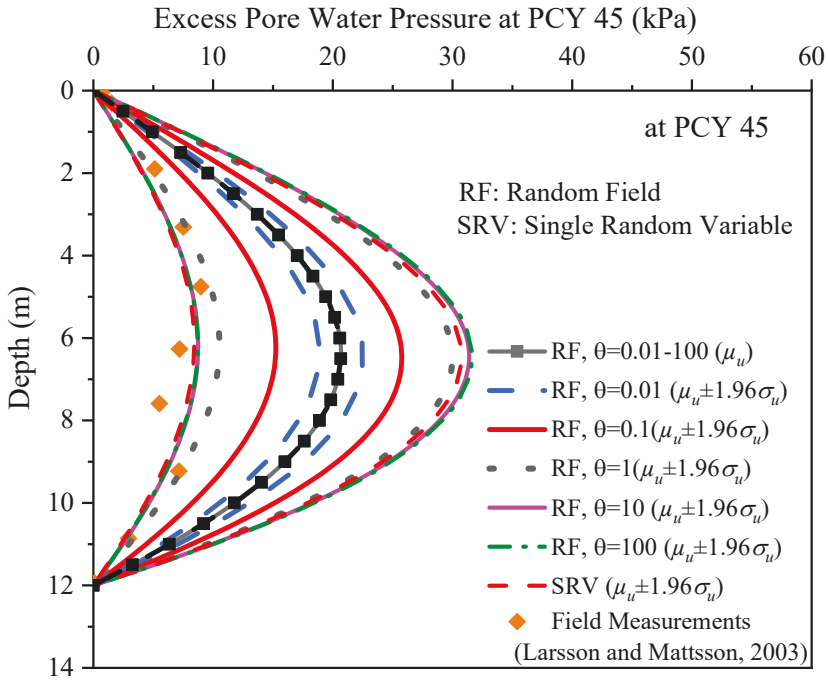

Figure 4.20 Comparison of measured and predicted excess pore water pressures with 95% CI adopting RF analysis with various normalised spatial correlation lengths and SRV analysis at CPY45

4.4.3 Probability of Exceedance/Failure

It should be noted that in the common system of error evaluation, the absolute distance between measured and predicted settlement is calculated, which does not identify whether the predicted settlement is underestimated or overestimated, and the minimum error does not mean that the predicted results are acceptable or reliable. For construction of road and railway embankments adopting low embankment strategy, it is essential to introduce a criterion called probability of exceedance/failure (PF) to fulfill the requirements for reliable prediction of long-term settlement. In this study, a probability of exceedance/failure (PF_{MC}) based on Monte-Carlo simulation results corresponds to the situation in which the predicted settlement (S_P) exceeds the allowable surface settlement (S_{all}):

$$PF_{MC} = P[S_P > S_{all}] \quad (4.12)$$

By considering the allowable design surface settlement at PCY5 equal to 500 mm ($S_{all-PCY5} = 500\,mm$) for a low embankment, the variations of PF_{MC} at different time steps for RF and SRV analyses are plotted in Figure 4.21. It is evident that the predicted probability of failure (PF_{MC}) significantly depends on the adopted value of the spatial correlation length. By increasing the spatial correlation length, PF_{MC} increases, and the maximum PF_{MC} occurs when $\theta \simeq 10$ and this normalised spatial correlation length is called the critical normalised spatial correlation length (calculated to be $\theta_w = 10$ in this study). The reported results in the literature also show that adopting SRV method can lead to underestimation of probability of failure (Allahverdizadeh et al. 2016; Griffiths et al. 2009; Jha and Ching 2013; Li et al. 2017). For example, referring to the slope stability analysis results, reported in the literature (Allahverdizadeh et al. 2016; Li et al. 2017), the critical spatial correlation length was determined to be 0.5H to 1H, where H is the height of slope. Moreover, in the other research studies reported in the literature, the critical spatial correlation length for the block compression problem was reported to be 0.1B to 2B, where B in the square block dimension (Allahverdizadeh et al. 2016), and for shallow foundation bearing capacity, the critical spatial correlation length was estimated to be between 2B and 10B, where B is the width of the strip footing (Allahverdizadeh Sheykhloo 2015). It can be observed that while critical spatial correlation lengths are observed, the values significantly depended on the geotechnical problem to be addressed, and thus this study attempt to give indication of the critical spatial correlation length for long term settlement prediction of clay deposits. It should be noted that in the absence

of adequate data to determine the applicable spatial correlation length, it is essential to determine the critical spatial correlation length via a proper parametric study.

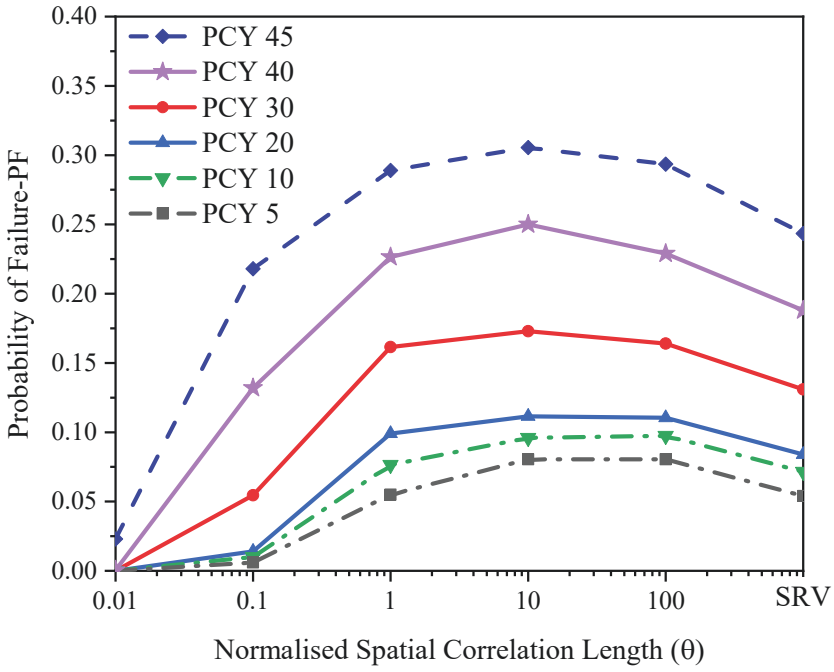

Figure 4.21 Variation of probability of failure with different spatial correlation lengths in RF analysis and comparison with SRV analysis at different time steps

There is another alternative to determine probability of failure (PF_β) recommended by several design and construction guidelines such as U.S. Army Corps of Engineers (1995), which correlates probability of failure to reliability index (β) as below:

$$PF_\beta = 1 - \Phi(\beta) \tag{4.13}$$

$$\beta = \frac{\ln(S_{all}) - \mu_{\ln(S_P)}}{\sigma_{\ln(S_P)}} \tag{4.14.a}$$

$$\Phi(\beta) = \int_{-\infty}^{\beta} \frac{1}{\sqrt{2\pi}} e^{-\frac{1}{2}x^2}\, dx \tag{4.14.b}$$

where Φ denotes standard normal cumulative density function of predicted settlements, $\mu_{\ln(S_P)}$ and $\sigma_{\ln(S_P)}$ denote mean and standard deviation of underlying normal distribution of log-normally distributed of predicted settlement, respectively. It should be noted that probability of failure (PF_β) determined from Equations (4.13) - (4.14) are based on the assumption that the log-normal distribution applies to the predicted settlements. The determined probability of failure based on Monte-Carlo simulation (PF_{MC}) and reliability index (PF_β) for different adopted analyses (i.e. RF and SRV) are summarised in Table 4.3. The results show considerable disparities between the probability of failure estimated based on the reliability index (PF_β) and corresponding value based on the Monte-Carlo simulation (PF_{MC}) which adopted the actual predictions without a need to assume a perfect log normal distribution for the predicted settlement. For critical normalised spatial correlation length ($\theta_w = 10$), the maximum difference between PF_{MC} and PF_β is 60% at PCY5 (PF_β is overestimated comparing to PF_{MC}). As a result, determining probability of failure estimated based on the reliability index (PF_β) can lead to overconservative and cost inefficient design. Therefore, for a reliable risk assessment, it is essential to adopt to actual Monte-Carlo simulation results to determine the probability of failure as a result of excessive settlement.

For large spatial correlation lengths (e.g. $\theta \approx 100$), the distribution of random parameters in each Monte-Carlo simulation is rather uniform, but different from other simulations. Therefore, the predictions for RF analysis with large correlation length is expected to be comparable to the results obtained from a simple Monte-Carlo simulation with a single random variable approach (i.e. SRV method). As mentioned earlier, it was reported in some studies that the SRV analysis is the more conservative

analysis than the RF analysis with large correlation length (Cho 2007; Javankhoshdel and Bathurst 2014) while Figure 4.21 and Table 4.3 clearly illustrate that PF obtained from SRV method is not the safest for the design. In other words, SRV method can lead to underestimation of probability of the failure and thus provide incorrect evaluation of PF. In order to quantify the difference between predictions from SRV and RF analysis methods, the percentage of error in predicted PF (i.e. $E_{PF(SRV-RF)}$) is introduced as below:

$$E_{PF(SRV-RF)} = \frac{PF_{RF}-PF_{SRV}}{PF_{SRV}} \times 100 \tag{4.15}$$

where PF_{RF} and PF_{SRV} are the probability of failure (i.e. predicted settlement exceeding the allowable design settlement) obtained from RF and SRV analyses, respectively. The positive value of the error indicates that the SRV underpredicts the probability of failure/exceedance in comparison to RF approach. Figure 4.22 shows the calculated $E_{PF(SRV-RF)}$ for a range of spatial correlation lengths in RF analysis and at different time steps (PCY5, PCY10, PCY20, PCY30, PCY40, and PCY45). As shown in Figure 4.22, at PCY5, SRV analysis is more conservative than RF analysis with $\theta < 1$, while at PCY45, the corresponding feature for correlation length decreases to $\theta < 0.1$. In contrast, by increasing spatial correlation length beyond the above-mentioned ones (i.e., $\theta < 1$ at PCY5 and $\theta < 0.1$ at PCY45), the RF predictions are more conservative compared to SRV predictions. The calculated values of $E_{PF(SRV-RF)}$ are summarised in Table 4.4. According to Table 4.4, the maximum error in PF is 49% obtained from RF analysis with $\theta \approx 10,100$ at PCY5, which indicates a significant difference in reliability of predicted settlement obtained

from RF and SRV analyses. Thus, it is evident that conducting RF analysis is essential to reduce risk and increase reliability when designing low embankments for transport infrastructure.

Table 4.3 Probability of failure determined from Monte-Carlo simulation and reliability index

	Method		PCY5	PCY10	PCY20	PCY30	PYC40	PCY45
Probability of Failure based on Monte-Carlo Simulation, PF_{MC}	RF	$\theta = 0.01$	0.00	0.00	0.00	0.00	0.00	0.02
		$\theta = 0.1$	0.01	0.01	0.01	0.05	0.13	0.22
		$\theta = 1$	0.06	0.08	0.10	0.16	0.23	0.29
		$\theta = 10$	0.08	0.10	0.11	0.17	0.25	0.31
		$\theta = 100$	0.08	0.10	0.11	0.16	0.23	0.29
	SRV		0.05	0.07	0.08	0.13	0.19	0.24
Probability of Failure based on Reliability Index, PF_{β}	RF	$\theta = 0.01$	0.00	0.00	0.00	0.00	0.00	0.02
		$\theta = 0.1$	0.00	0.00	0.00	0.04	0.13	0.23
		$\theta = 1$	0.10	0.12	0.13	0.19	0.27	0.32
		$\theta = 10$	0.19	0.19	0.18	0.23	0.29	0.33
		$\theta = 100$	0.18	0.20	0.19	0.24	0.28	0.32
	SRV		0.12	0.14	0.13	0.19	0.23	0.28

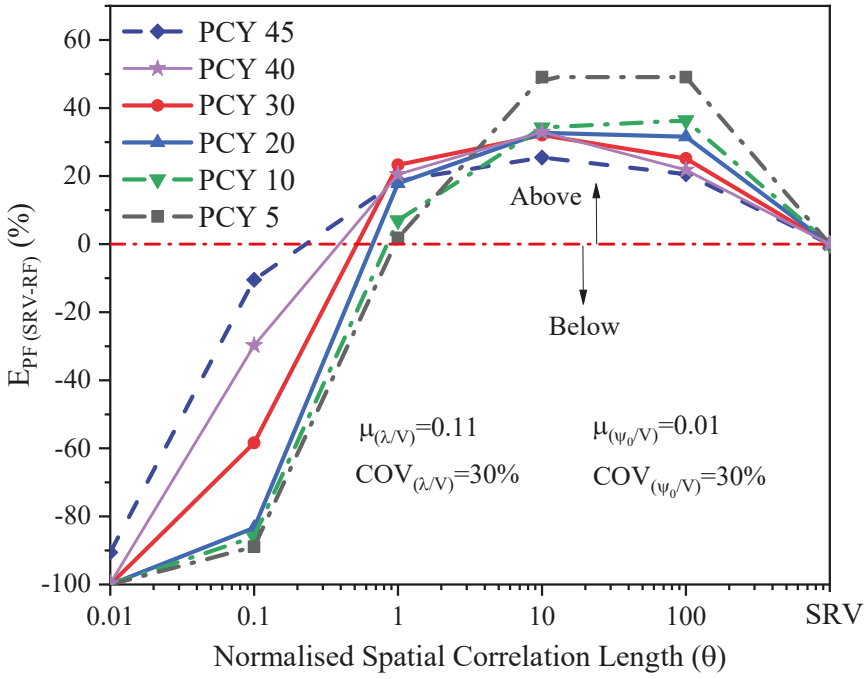

Figure 4.22 Error estimation of probability of failure for adopted RF and SRV analysis

Table 4.4 Calculated difference between predicted probability of failure predictions from SRV and RF analysis methods for different adopted normalised spatial correlation lengths at various time steps (note: positive error percentage means $PF_{RF} > PF_{SRV}$ and vice versa)

	Normalised Spatial Correlation length	PCY5	PCY10	PCY20	PCY30	PYC40	PCY45
$E_{PF(SRV-RF)}$ (%)	$\theta = 0.01$	-100	-100	-100	-100	-100	-91
	$\theta = 0.1$	-89	-86	-83	-58	-30	-10
	$\theta = 1$	2	7	18	23	20	19
	$\theta = 10$	49	34	33	32	33	25
	$\theta = 100$	49	36	32	25	22	21

The critical and acceptable value of probability of failure in low embankment strategy is associated with the risk taken by clients or owners of the infrastructure. Indeed, the risk is related to the periodic maintenance cost as a part of the design.

Figure 4.23 shows the risk associated with the assessment of post-construction settlement, while considering λ/V and ψ_0/V as spatially random variables. The risk is assessed by determining the probability that the predicted settlement exceeds the allowable values. For the sake of simple representation of risk in this study, the maintenance cost is considered to be \$10M. As can be concluded from Figure 4-23, for critical normalised spatial correlation length ($\theta_w = 10$), the risk of settlement prediction is the highest at all post-construction times, resulting in the most expensive and critical maintenance program.

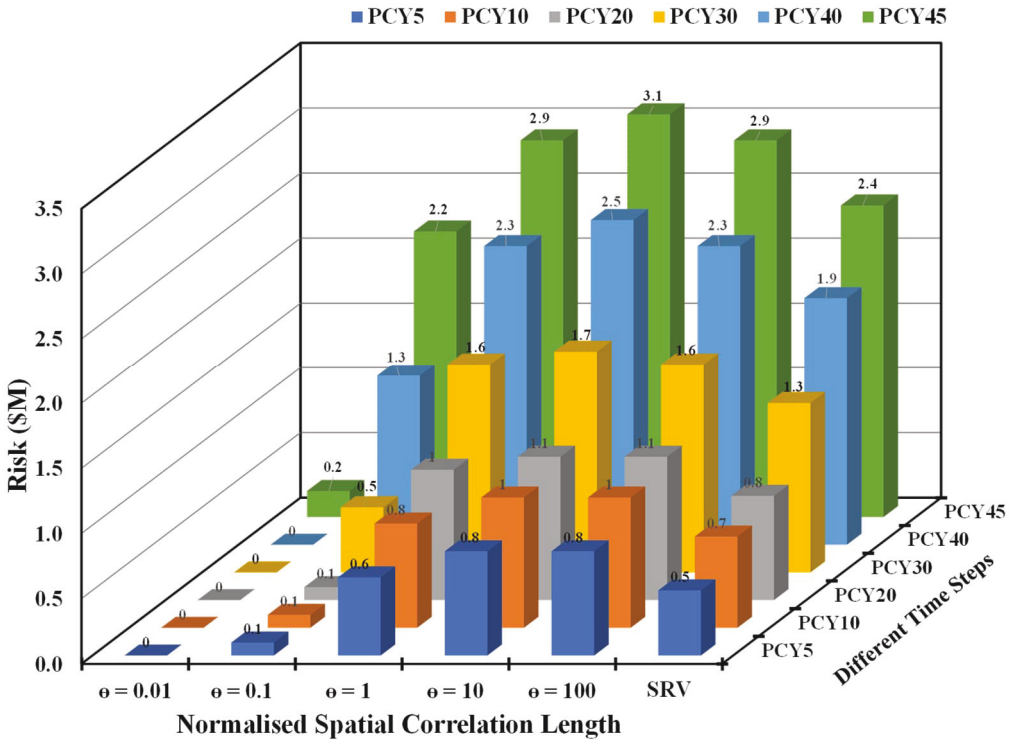

Figure 4.23 Risk associated with assessment of post-construction settlement for adopted RF and SRV analysis

4.5 Summary

This chapter has presented the effect of spatially variable elastic visco-plastic model parameters, including the elastic-plastic model parameter (λ/V) and the initial creep coefficient (ψ_0/V), on the long-term behaviour of low embankments constructed on top of soft soils incorporating random field (RF) and single random variable (SRV) analyses. For SRV method, a simple Monte-Carlo simulation is combined with Crank-Nicolson finite difference numerical model developed based on nonlinear elastic visco-plastic (EVP) model. However, for RF analysis, the Karhunen-Loeve (K-L) expansion method expressed by spectral decomposition of correlation function into eigenvalues and eigenfunctions is adopted to generate random field with different spatial correlation lengths. The generated random variables are then combined with developed finite difference numerical code to predict settlement and excess pore water pressure and the associated reliability indices. Field measurements of the Skå–Edeby test fill for about 45 years are used to assess and verify the accuracy of the proposed methods. Moreover, the effect of spatial correlation length is evaluated in order to determine the critical spatial correlation length. The key findings of this study are summarised below:

- Normalised spatial correlation length (θ) plays an important role in predicting the time-dependent settlement of soft soils considering the elastic visco-plastic parameters (λ/V and ψ_0/V) as spatial random variables. By increasing the normalised spatial correlation length in RF analysis, the probability density function (PDF) becomes wider indicating more uncertainties in post construction settlement prediction. Moreover, when normalised spatial correlation length exceeds unity (i.e. $\theta > 1$), the RF

settlement prediction converges with those obtained from rather simple SRV analysis. The coefficient of variation (COV) of settlement increases at early stages of loading for all adopted analyses and then approaches an asymptote after about 5 years post construction (i.e. PCY5) indicating that the uncertainties in settlement prediction are higher at early stages of loading. Furthermore, the uncertainties in settlement prediction increases significantly with depth when $\theta < 1$, while COV of settlement predictions are almost constant in RF analysis with normalised spatial correlation length exceeding unity (i.e. $\theta > 1$) as well as SRV analysis.

- Comparing the predicted settlement with the field measurements in the Skå–Edeby test fill, it is evident that the measured settlements at different depths are in good agreement with the predicted settlement with 95% confidence interval, obtained from RF analysis with $\theta > 1$ and SRV analysis.

- The effect of the spatial correlation length on the probability of failure/exceedance (PF) is investigated and results are compared with SRV analysis predictions. The results indicate that a critical spatial correlation length existed for predicting time-dependent settlement of soft soils resulting in the maximum PF while adopting random field reliability analysis. In this study, the critical spatial correlation length is determined to be in the order of $10H$, where H is the soft soil thickness. As a result, in the absence of adequate data to determine exact spatial correlation length, conducting SRV analysis is deemed unsafe/unreliable. Thus, it is deemed necessary to perform random field reliability analysis considering the critical spatial correlation length following a parametric study to determine

this critical value. Indeed, since comprehensive, time consuming and costly laboratory test are required to estimate the soil spatial variability and correlation length, findings of this study can be used as guidelines by practicing engineers, designing structures on soft soils, particularly when adopting low embankment strategy for design of transport infrastructure.

5 Back Analysis of Long-term Settlement of Low Embankment on Soft Soils using Bayesian Updating

5.1 Introduction

Chapter 4 has provided a method to manage the risks in low embankment strategy by adopting random field reliability analysis and introducing critical spatial correlation length. Predicting time-dependent settlement of low embankment is commonly the most critical design and construction aspect affecting the maintenance plan and cost, pavement design and drainage requirements, public awareness about periodic maintenance, and instrumentation and monitoring programs. Periodic monitoring data can be used for updating the elastic visco-plastic model parameters to predict a more realistic long-term settlement. Therefore, Chapter 5 provides two case studies of Väsby and Skå-Edeby test fills to confirm how model updating can reduce the risks of one-dimensional (1D) long-term settlement predictions. In this chapter, the elastic-plastic model parameter (λ/V) and the initial creep coefficient (ψ_0/V) are updated by adopting the Bayesian updating method and transitional Markov Chain Monte Carlo (TMCMC) algorithm. Then, the long-term settlement predictions obtained from updated parameters based on field data are compared with the predictions obtained from updated parmeters based on oedometer test results. This chapter focuses on how applying field monitoring results can reduce risks in predicting the long-term settlement of low embankments constructed on soft soils.

5.2 Bayesian Theory

In the Bayesian framework, the uncertainties of model parameters are quantified based on measurement data. The relationship between the predicted settlement (S_P) and measured data (S_m) is:

$$S_m = S_P + S_e \tag{5.1}$$

where, S_e is the settlement prediction error.

Field monitoring data and oedometer test results can be used to find the most optimised model parameters. In this study, the elastic-plastic model parameters are assumed as uncertain model parameters denoted as $x = \left[\frac{\lambda}{V}, \frac{\psi_0}{V}\right]$. Observations are used to update the prior probability density function (PDF) of model parameters, $f(x)$. The prior PDF of model parameters represents the user's adjustment before observing measured data. Based on Bayesian theory (Yuen 2010), the posterior PDF of $x = \left[\frac{\lambda}{V}, \frac{\psi_0}{V}\right]$, $f(x|S_m)$, can be obtained:

$$f(x|S_m) = \frac{f(x).f(S_m|x)}{f(S_m)} \tag{5.2}$$

where, $f(S_m)$ is the evidence of measured settlement, and $f(S_m|x)$ is the likelihood function representing the probability of observing measured settlement (S_m) given a set of model parameters ($x = \left[\frac{\lambda}{V}, \frac{\psi_0}{V}\right]$), which is given as:

$$f(S_m|x) = (2\pi\sigma_e)^{-\frac{N_d}{2}} exp\left[-\frac{\sum_{j=1}^{N}(S_m - S_P)^2}{2{\sigma_e}^2}\right] \quad (5.3)$$

where, σ_e is the standard deviation of the error between predicted and measured settlement, and N_d is the number of measured data. The posterior PDF, $f(x|S_m)$, represents the updated model parameters after observing measured data. The optimal model parameter vector $x = \left[\frac{\lambda}{V}, \frac{\psi_0}{V}\right]$, are calculated by maximising the posterior PDF, $f(x|S_m)$, or equivalently $f(x).f(S_m|x)$. Considering the non-linearity of the numerical model for long-term settlement of soft soils based on the elastic visco-plastic (EVP) model (Yin 1999), there is not any analytical form of $f(x|S_m)$. As a result, the transitional Markov Chain Monte Carlo (TMCMC) (Ching and Chen 2007) method is applied to quantify uncertainties of the visco-plastic model parameters.

5.3 Transitional Markov Chain Monte Carlo Algorithm

The TMCMC method is based on the idea proposed by Beck and Au (2002) which includes constructing a series of intermediate PDFs. One of the advantages of the TMCMC method is that it is not required to perform Kernel density estimation. Moreover, the intermediate PDFs can be selected automatically. Since the TMCMC algorithm is based on a series of resampling stages which is more robust to x dimension, it can be used for higher-dimensional problems. In addition, the TMCMC method can update the parameters without solving any integral problem (Zhou et al. 2018).

The constructed series of intermediate PDFs will converge to the target PDF, $f(S_m|x)$, from the prior PDF, $f(x)$, as defined by Ching and Chen (2007):

$$f_j(x) \propto f(S_m|x)^{\xi_j} f(x)$$
$$(for\ j = 0, \dots, N_j\ and\ 0 = \xi_0 < \xi_1 < \cdots < \xi_{N_j} = 1) \tag{5.4}$$

where, the index j denotes the stage number and N_j is the total number of stages. At the initial stage with $\xi_0 = 0$, the intermediate PDF is proportional to the prior PDF (i.e. $f_0(x) = f(x)$) and ends with the posterior PDF (i.e. $f_{N_j}(x) = f(x|S_m)$). Since the geometry change from $f_0(x)$ to $f(x|S_m)$ is significantly large, it can cause difficulties in parameter updating. But the change between two adjacent intermediate PDFs is small and can enable a good means of transitioning and efficiently obtaining samples from $f_{j+1}(x)$ based on $f_j(x)$. The following steps can be applied for parameter updating based on TMCMC algorithm (Zhou et al. 2018):

1. At the initial stage ($j = 0$), obtain samples $\{x_{0,k}: k = 1, 2, \dots, N_j\}$ from the prior PDF $f_0(x)$;

2. Define a prescribed threshold, and select ξ_{j+1} so that the Coefficient of Variation (COV) of $\left\{f\left(S_m|x_{j,k}\right)^{\xi_{j+1}-\xi_j}: k = 1, 2, \dots, N_j\right\}$ equals to the prescribed threshold.

3. Calculate the plausibility weight according to the following equation:

$$w(x_{j,k}) = f(S_m|x_{j,k})^{\xi_{j+1}-\xi_j} \qquad (for\ k = 1, 2, \dots, N_j)$$

$$S_j = \sum_{k=1}^{N_s} w(x_{j,k})/N_j \tag{5.5}$$

where, S_j is a factor to compute the evidence $f(S_m)$, and $x_{j,k}$ denotes the k_{th} sample belonging to level j.

4. Generate the samples $\{x_{0,k}: k = 1, 2, \dots, N_j\}$ from $f_{j=1}(x)$ by applying Metropolice-Hastings (MH) algorithm (Beck and Au 2002). The probability of selecting the l_{th} initial sample $x_{j,l}$ is equal to $w(x_{j,l})/\sum_{l=1}^{N_j} w(x_{j,l})$. The Marco chain sample in the k_{th} chain with $x_{j,k}$ as the leader is generated from a Gaussian proposal PDF. Σ_s is the covariance matrix of the Gaussian proposal PDF to the scaled version of the estimated covariance matrix of $f_{j+1}(x)$ and can be estimated based on the following equation:

$$\Sigma_s = \varsigma^2 \sum_{k=1}^{N_j} w(x_{j,k}) \left\{ x_{j,k} - \left[\sum_{l=1}^{N_j} w(x_{j,k}) x_{j,k} \Big/ \sum_{l=1}^{N_j} w(x_{j,l}) \right] \right\} \times \left\{ x_{j,k} - \left[\sum_{l=1}^{N_j} w(x_{j,k}) x_{j,k} \Big/ \sum_{l=1}^{N_j} w(x_{j,l}) \right] \right\}^T \tag{5.6}$$

where, ς is the prescribed scaling factor and should be selected to avoid the rejection rate and large MCMC jumps, simultaneously. It is suggested by Ching and Chen (2007) that $\varsigma = 0.2$ is the reasonable choice.

5. Generate the candidate sample x^c of j_{th} sample from $N(x_{j,l}, \Sigma_s)$ and set $x_{j+1,k} = x^c$ and $x_{j,l} = x^c$ with probability equals to $f_{j+1}(x^c)/f_{j+1}(x_{j,l})$, otherwise $x_{j+1,k} = x^c$.

6. Repeat steps (2) to (5) till $\xi_{N_j} = 1$. At the end of the algorithm, samples $\{x_{N_j,k}: k = 1, 2, \dots, N_{N_j}\}$ are asymptotically distributed as $f(x|S_m)$, and $j = \prod_{j=1}^{N_j-1} j_j$ is asymptotically unbiased estimation of the evidence $f(S_m)$.

The flowchart in Figure 5.1 summarizes the TMCMC algorithm incorporating the Bayesian updating method.

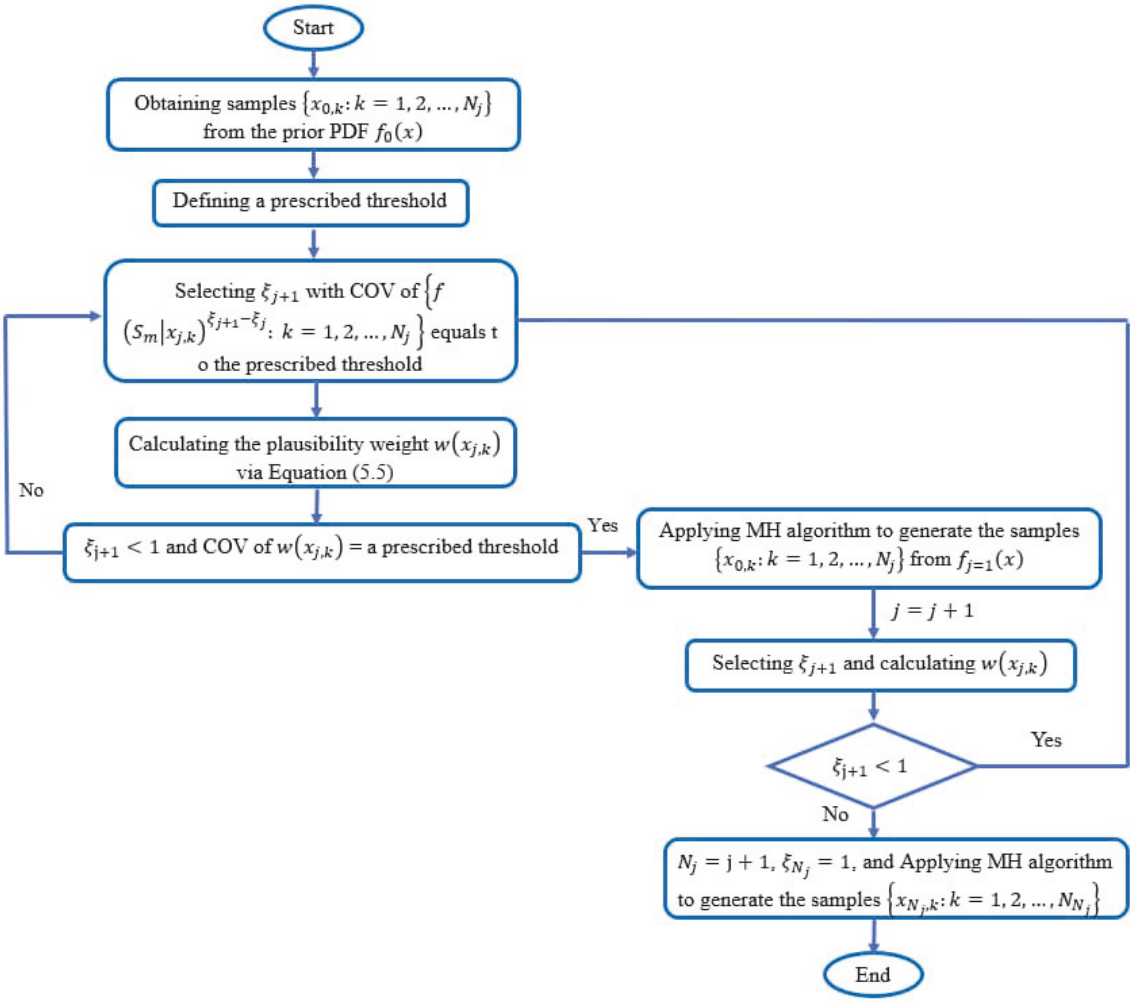

Figure 5.1 Flowchart for Transitional Markov Chain Monte Carlo (TMCMC) algorithm (Ching and Chen 2007)

5.4 Case Study

Two case studies of Väsby and the Skå-Edeby test fills are selected for back analysis of long-term settlement using Bayesian updating method. To predict long-term behavior of soft soils, the non-linear elastic visco-plastic (EVP) creep model proposed by Yin (1999) is adopted. Methodology for developing the numerical code to predict long-term behaviour of soft soils was described in Section 3.2. Bayesian updating method is respectively performed using the oedometer test data and field data.

5.4.1 Väsby Test Fill

In this study, 2.5m high test fill without any vertical drain located near upland Väsby village in Sweden is selected. Subsoil profile, soil and embankment properties, and stress applied at the ground surface due to the fill weight were presented in Section 3.3.2. Oedometer test results (Figure 3.6) were used to determine elastic visco-palstic model parameters as shown in Table 3.2.

5.4.1.1 Settlement prediction using observation of oedometer test results for Väsby soft soil

Black clay sample with the dimension of 0.02 m height and 0.05 mm diameter was taken at 5 m depth below ground level. As reported by Le (2015), soil permeability for the sample was calculated from the coefficient of consolidation (c_v) and coefficient of volume change (m_v) and it is equal to $k_0 = 1.9 \times 10^{-7}\ m/min$. Initial void ratio ($e_0$) and coefficient of permeability change index (c_k) are equal to 3.04 and 0.543, respectively (Le 2015). As shown in Figure 3.6, the last four stages within the normally consolidated range are used to determine elastic visco-palstic model parameters based on Bayesian updating method. Table 5.1 shows the initial stress-strain data employed for Bayesian updating method based on oedometer test results for Väsby soft soil.

Bayesian updating method is applied to update elastic visco-plastic model parameters ($\frac{\lambda}{V}, \frac{\psi_0}{V}$) by adopting initial stress-strain data (Table 5.1) and the soil permeability properties. Prior and posterior statistics of elastic visco-plastic model parameters are presented in 0. Figure 5.2 shows the comparison between predicted strain adopting updated model parameters and oedometer test results.

Table 5.1 Initial stress-strain data employed for Bayesian updating method based on oedometer test results for Väsby soft soil

Loading Stage (kPa)	Initial Thickness (m)	Initial Stress (kPa)	Final Stress (kPa)	Initial Strain (%)	Time (min)
30-45	0.02	30	45	3.8	1440
45-67.5	0.02	45	67.5	8.8	1440
67.5-105	0.02	67.5	105	17.8	1440
105-160	0.02	105	160	26.0	1440

Table 5.2 Prior and posterior statistics of elastic visco-plastic model parameters ($\lambda/V, \psi_0/V$) based on oedometer test results applying Bayesian updating method for Väsby soft soil

Model Parameter				Mean (μ)	Coefficient of Variation (COV_X)
λ/V	Prior			0.22	0.25
	Posterior	Loading Stage	30-45 kPa	0.24	0.02
			45-67.5 kPa	0.18	0.002
			67.5-105 kPa	0.17	0.05
			105- 160 kPa	0.2	0.04
ψ_0/V	Prior			0.0135	0.3
	Posterior	Loading Stage	30-45 kPa	0.029	0.08
			45-67.5 kPa	0.022	0.006
			67.5-105 kPa	0.029	0.04
			105- 160 kPa	0.023	0.03

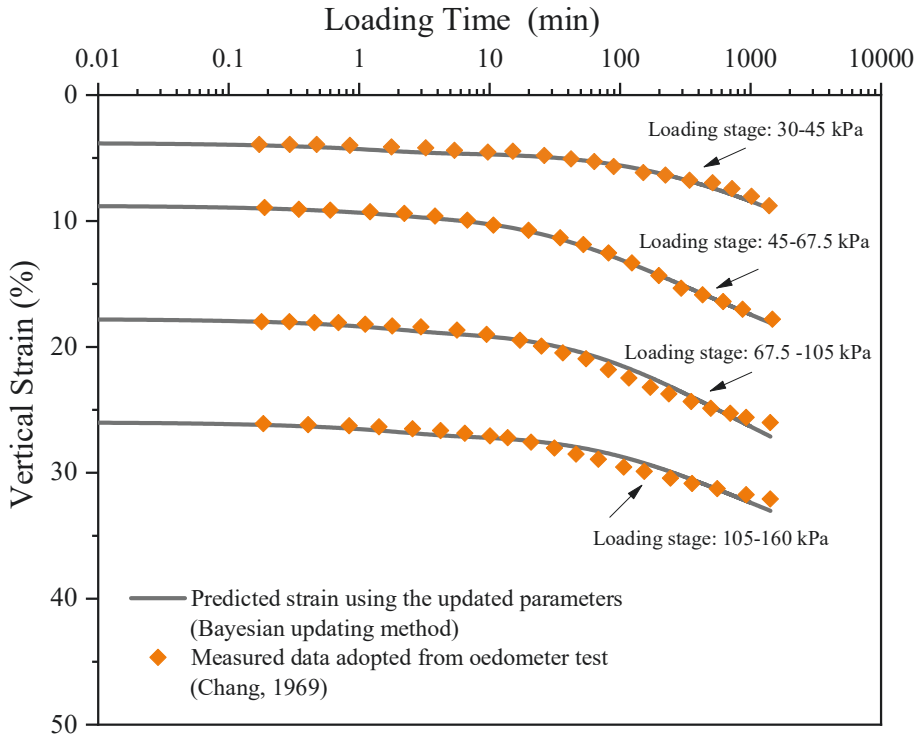

Figure 5.2 Predicted strain adopting Bayesian updating method comparing with oedometer test results for Väsby soft soil

To evaluate discrepancy between predicted strains prior and after updating parameters, three indicators namely the root mean square error ($RMSE$) index, the mean absolute error (MAE), and the coefficient of determination (R^2) are calculated and presented in Table 5.3. In order to quantify the difference between predictions based on prior and posterior (updated) model parameters, the error in indicators RMSE and MAE is introduced as below:

$$E_{x(prior-posterior)} = \frac{x_{posterior} - x_{prior}}{x_{prior}} \times 100 \quad (x = RMSE, and\ MAE) \tag{5.7}$$

As can be observed in Table 5.3, the difference between predicted strain and measured strain can be reduced by 90% when Bayesian updating method is applied. The quantitative comparison shown in Table 5.3 indicates a significant improve in

predicting strains when elastic visco-plastic model parameters are updated by adopting Bayesian updating method.

Table 5.3 Summary of strain indicators for all adopted loading stages of oedometer test by using prior and posterior elastic visco-plastic model parameters ($\lambda/V, \psi_0/V$) for Väsby soft soil

Loading Stage (kPa)		$RMSE$	MAE	R^2	$E_{RMSE\ (prior\text{-}posterior)}$ (%)	$E_{MAE\ (prior\text{-}posterior)}$ (%)
30-45	Prior	0.0044	0.003	0.99	45	30
	Posterior	0.0025	0.002	0.99		
45-67.5	Prior	0.0208	0.015	0.99	90	90
	Posterior	0.0013	0.015	0.97		
67.5-105	Prior	0.0224	0.016	0.99	80	80
	Posterior	0.0042	0.003	0.98		
105-160	Prior	0.0101	0.007	0.99	60	60
	Posterior	0.0041	0.003	0.99		

5.4.1.2 Prediction using observation of field measurements for Väsby test fill

Based on the mean values of the posterior distribution of elastic visco-plastic model parameters obtained from oedometer test results (0), settlement of embankment at different depths are calculated adopting the numerical model based on Yin's elastic viso-plastic model (Yin 1999) (Note: the details of all soil and embankment properties were presented in Chapter 3, Section 3.3).

Figure 5.3 shows the comparison between field measurement and predicted settlement based on updated parameters from oedometer test results. It can be seen from Figure 5.3, when the elastic visco-plastic model parameters are updated based on oedometer test results, the predicted settlement deviates a lot from the field

(observed) measurements. Since the surface settlement is an accumulation of settlement of all the sub-layers below, the disparities between predicted and measured settlement are higher at the ground surface (Note: the measured data at depth of 7.5m is not available at the first 20 PCY).

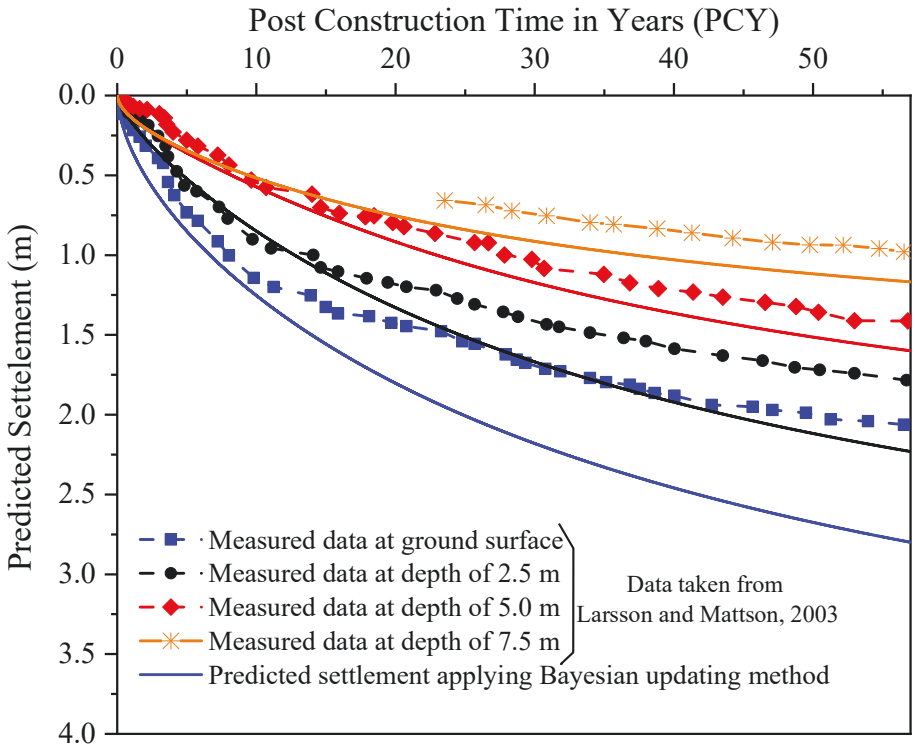

Figure 5.3 Comparison of measured and predicted settlement using updated parameters based on oedometer test results for Väsby test fill

One of the main design and construction considerations in low embankment strategy is implementing a detailed instrumentation and monitoring program. Therefore, an observational approach can be adopted to review and modify the design if required. In this study, Bayesian updating approach is applied on monitoring data to predict post-construction settlement so that the maintenance program and whole-of-life costing can be planned. Since the surface settlement is the influential factor for periodic maintenance cost and plan, monitoring data at ground surface are used to update elastic visco-plastic model parameters. Using the observed ground

settlement from MD10 to MD100 and the Bayesian updating method, the TMCMC samples are generated (Note: MDxx indicates xx% of the total design life are monitored and the data are used to update parameters). Posterior statistics of elastic visco-plastic model parameters (i.e. $\lambda/V, \psi_0/V$) updated based on various MDxx (monitored data) are presented in Table 5.4. As shown in Figure 5.4, the settlements at the ground surface are calculated based on the mean values of the posterior samples and are compared with predicted settlement obtained from updated parameters based on oedometer test results. The comparison shows that by using 20% of design life monitored data, disparities between predicted and measured ground surface settlements decrease considerably in comparison with using updated parameters based on oedometer test results. To evaluate the performance of using monitored data for back calculating settlement, a quantitative comparison is made between the prediction and field measurements using monitored data and oedometer test results. Table 5.5 summarises error indicators to compare predicted with measured data using updated parameters based on various monitored data and oedometer test results. Moreover, to evaluate the efficiency of using monitored data comparing to oedometer test data in predicting more realistic long-term settlements, the error in determining indicators RMSE and MAE is calculated as below:

$$E_{x(oed-MD)} = \frac{x_{MD}-x_{oed}}{x_{oed}} \times 100 \quad (x = RMSE, and\ MAE) \tag{5.8}$$

As can be seen in Table 5.5, when 10% of total design life is monitored and parameters are updated by the use of these monitored data (i.e. MD10), the error between predicted and measured settlement decreased about 45% comparing to using updated parameters based on oedometer test results. The corresponding value is

approximately 77% when 20% of total design life is monitored and the elastic visco-plastic model parameters are updated using MD20 which substantiates significance of using monitored data to predict long-term settlement of low embankment compared to just applying oedometer test data.

Table 5.4 Posterior statistics of elastic visco-plastic model parameters ($\lambda/V, \psi_0/V$) updated based on monitored data applying Bayesian updating method for Väsby soft soil

Model Parameter	Monitored Data	Mean (μ)	Coefficient of Variation (COV_X)
λ/V	MD10	0.18	0.10
	MD20	0.16	0.08
	MD40	0.15	0.06
	MD60	0.16	0.05
	MD80	0.18	0.04
	MD100	0.21	0.02
ψ_0/V	MD10	0.02	0.14
	MD20	0.016	0.10
	MD40	0.017	0.06
	MD60	0.015	0.04
	MD80	0.013	0.04
	MD100	0.011	0.03

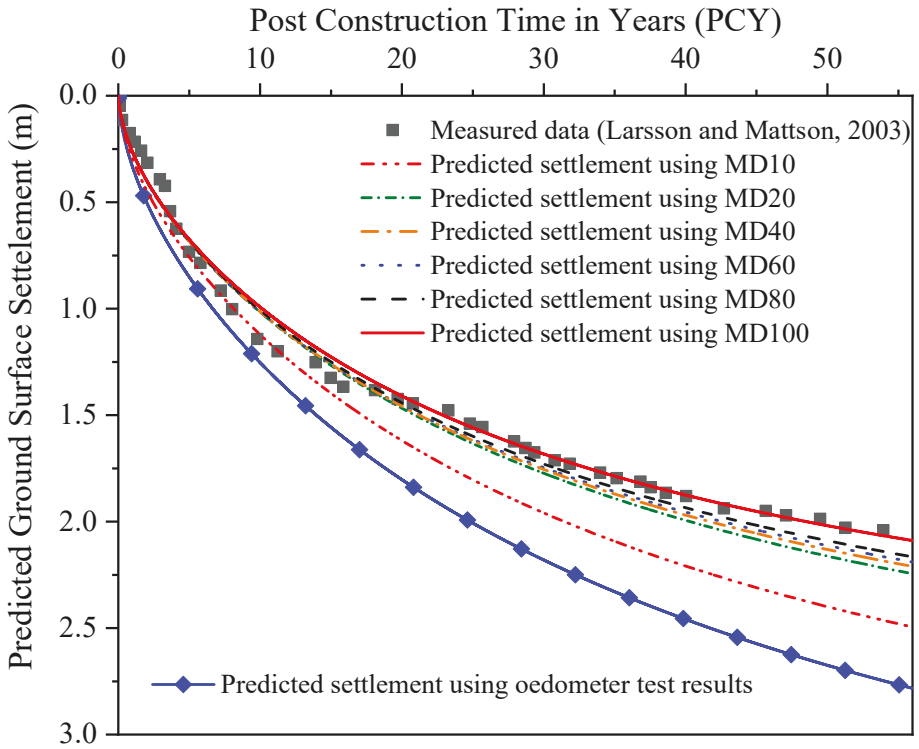

Figure 5.4 Comparison of measured and predicted settlement using updated parameters based on monitored data (MD) and oedometer test results for Väsby test fill

Table 5.5 Summary of surface settlement error indicators using updated model parameters $(\lambda/V, \psi_0/V)$ based on monitored data at different time stages and oedometer test results for Väsby soft soil

Monitored Data (%)	***RMSE***	***MAE***	R^2	$E_{RMSE\ (Oed\text{-}MD)}$ (%)	$E_{MAE\ (Oed\text{-}MD)}$ (%)
MD10	0.24	0.20	0.971	43	45
MD20	0.10	0.09	0.995	77	76
MD40	0.09	0.08	0.996	80	79
MD60	0.09	0.08	0.996	80	79
MD80	0.07	0.06	0.997	83	83
MD100	0.06	0.04	0.998	85	88
Oedometer Test Results	0.42	0.37	0.911	-	-

5.4.1.3 Risk analysis for Väsby test fill

In low embankment strategy, the risk taken by the client is not related to the failure of the low embankment and safety. The risk is mostly associated with the periodic maintenance cost and program. If the predicted settlements are more than the field measurements, settlement prediction is unsatisfactory which overestimates planning the maintenance cost and program. Therefore, the risk can be evaluated by calculating the prediction bias or settlement bias, which is defined as the ratio of predicted settlements (S_P) to field measurements (S_m) as presented in Equation (3.27). In this risk assessment, the maintenance cost is assumed to be \$10M. Figure 5.5 shows the risk associated with over-predicted settlement which can cause an expensive and long-term maintenance program and increases the risk related to the prediction of reasonable and realistic periodic maintenance cost and program.

As can be observed in Figure 5.5, when updated parameters based on oedometer test results are used to predict post-construction settlement, the risk related to overpredicted maintenance cost is considerably high and equals to \$13.5M. When 10% of total design life is monitored (i.e.MD10) and settlements are back analysed using updated parameters based on MD10, the risk decreases around 15% and is equal to \$12.0M. By using 20% of total design life monitored data (i.e. MD20), the corresponding risk decreases to \$11.0M which is 25% less than the risk assessment by using updated parameters based on oedometer test data. It can be concluded that, adopting monitored data has significant effect in predicting more realistic post-construction settlements and managing risk associated with maintenance cost and time.

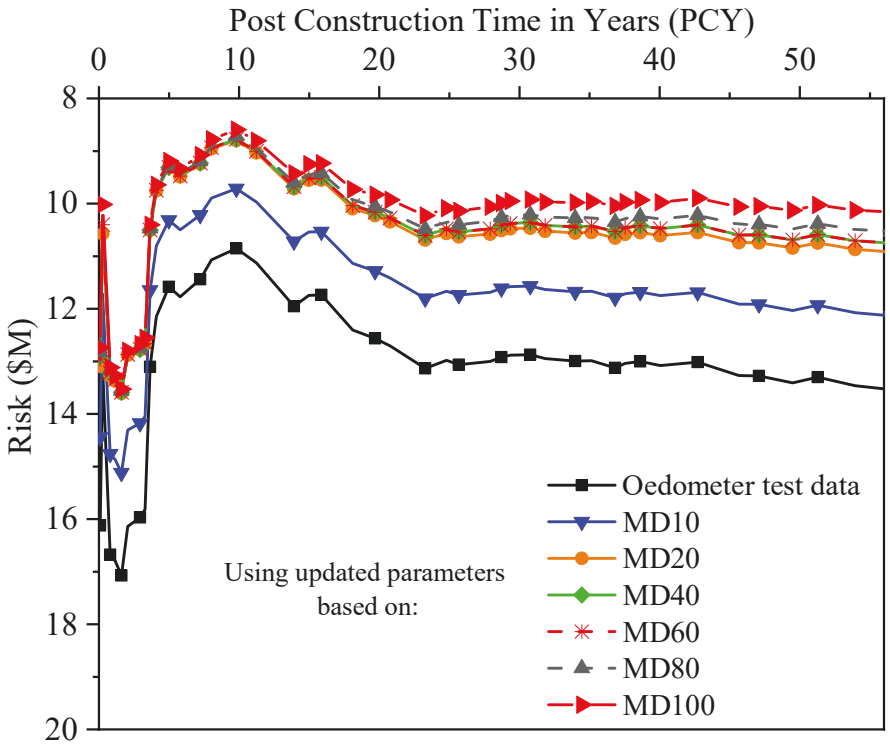

Figure 5.5 Risk associated with overpredicted post-construction settlement using updated elastic visco-elastic parameters ($\lambda/V, \psi_0/V$) based on oedometer test results and monitored data (MD) for Väsby test fill

5.4.2 Skå-Edeby Test Fill

Skå-Edeby test embankment without vertical drain is adopted as the second case study. The height of Skå-Edeby embankment was 1.5m and was located 25m west Stockholm. Subsoil profile, soil and embankment properties, and stress applied at the ground surface due to the fill weight were presented in Section 4.3. As presented in Figure 4.4, oedometer test results of the samples taken at depth 2 m, 8 m, and 9 m depths were used to determine elastic visco-palstic model parameters. Adopted model parameters for Skå-Edeby test were presented in Table 4.1.

5.4.2.1 Settlement prediction using observation of oedometer test results for Skå-Edeby soft soil

Oedometer test results of sample A and B taken at 2 m and 8 m depth, respectively are adopted to update the elastic visco-plastic model parameters ($\lambda/V, \psi_0/V$). For

sample A, the height of sample is 0.015m and the drainage condition is one way drainage from the top surface. As reported by Le (2015), the soil permeability for the sample was selected based on optimised model parameters and it is equal to $k_0 = 1.7 \times 10^{-7}\ m/min$. Initial void ratio ($e_0$) and coefficient of permeability change index (c_k) are equal to 2.68 and 0.737, respectively (Le 2015). As shown in Figure 4.4.a, the last three stages within the normally consolidated range are used to determine elastic visco-palstic model parameters for Bayesian updating method. The height of sample B is 0.0125m and the drainage condition is one way drainage from the bottom surface. For sample B, Le (2015) reported the optimised permeability (k_0) equals to $2.9 \times 10^{-8}\ m/min$, and corresponding value of e_0 and c_k are equal to 2.02 and 1.32, respectively. Table 5.6 shows the initial stress-strain data employed for Bayesian updating method based on oedometer test results for samples A and B.

Elastic-plastic model parameter (λ/V) and the initial creep coefficient (ψ_0/V) are updated by applying Bayesian method and adopting initial stress-strain data (Table 5.6) and the soil permeability properties. Table 5.7 shows prior and posterior statistics of elastic visco-plastic model parameters. Figure 5.6 illustrates the comparison between predicted strain adopting updated elastic visco-plastic model parameter based on Bayesian updating method with oedometer test results. To evaluate discrepancy between predicted strains prior and after updating parameters, three indicators, including $RMSE$ index, MAE, and R^2 are calculated and presented in Table 5.8. The difference between predicted strain based on prior and posterior (updated) model parameters is evaluated quantitatively by determining the error in indicators as presented in Equation (5.7).

As can be seen in Table 5.8, by applying Bayesian updating method, the difference between predicted and measured strains can be reduced by 80%. The quantitative comparison shown in Table 5.8 indicates a significant improve in predicting strains when elastic visco-plastic model parameters are updated by adopting Bayesian updating method.

Table 5.6 Initial stress-strain data employed for Bayesian updating method based on oedometer test results for Skå-Edeby soft soil

Sample	Loading Stage (kPa)	Initial Thickness (m)	Initial Stress (kPa)	Final Stress (kPa)	Initial Strain (%)	Time (min)
A	42-82	0.015	42	82	7.7	1440
	82-170	0.015	82	170	18.8	1440
	170-345	0.015	170	345	26.8	1440
B	42-82	0.0125	42	82	5.7	1440
	82-162	0.0125	82	162	10.0	1440
	162-267	0.0125	162	267	16.6	1440

Table 5.7 Prior and posterior statistics of elastic visco-plastic model parameters ($\lambda/V, \psi_0/V$) based on oedometer test results applying Bayesian updating method for Skå-Edeby soft soil

Model Parameter				Mean (μ)	Coefficient of Variation (COV_X)
λ/V	Prior			0.11	0.3
	Posterior	Sample A	42-82 kPa	0.17	0.05
			82-170 kPa	0.14	0.04
			170-345 kPa	0.13	0.003
		Sample B	42-82 kPa	0.15	0.04
			82-162 kPa	0.13	0.04
			162-267 kPa	0.18	0.005
ψ_0/V	Prior			0.01	0.3
	Posterior	Sample A	42-82 kPa	0.009	0.04
			82-170 kPa	0.013	0.04
			170-345 kPa	0.018	0.005
		Sample B	42-82 kPa	0.012	0.03
			82-162 kPa	0.009	0.04
			162-267 kPa	0.015	0.03

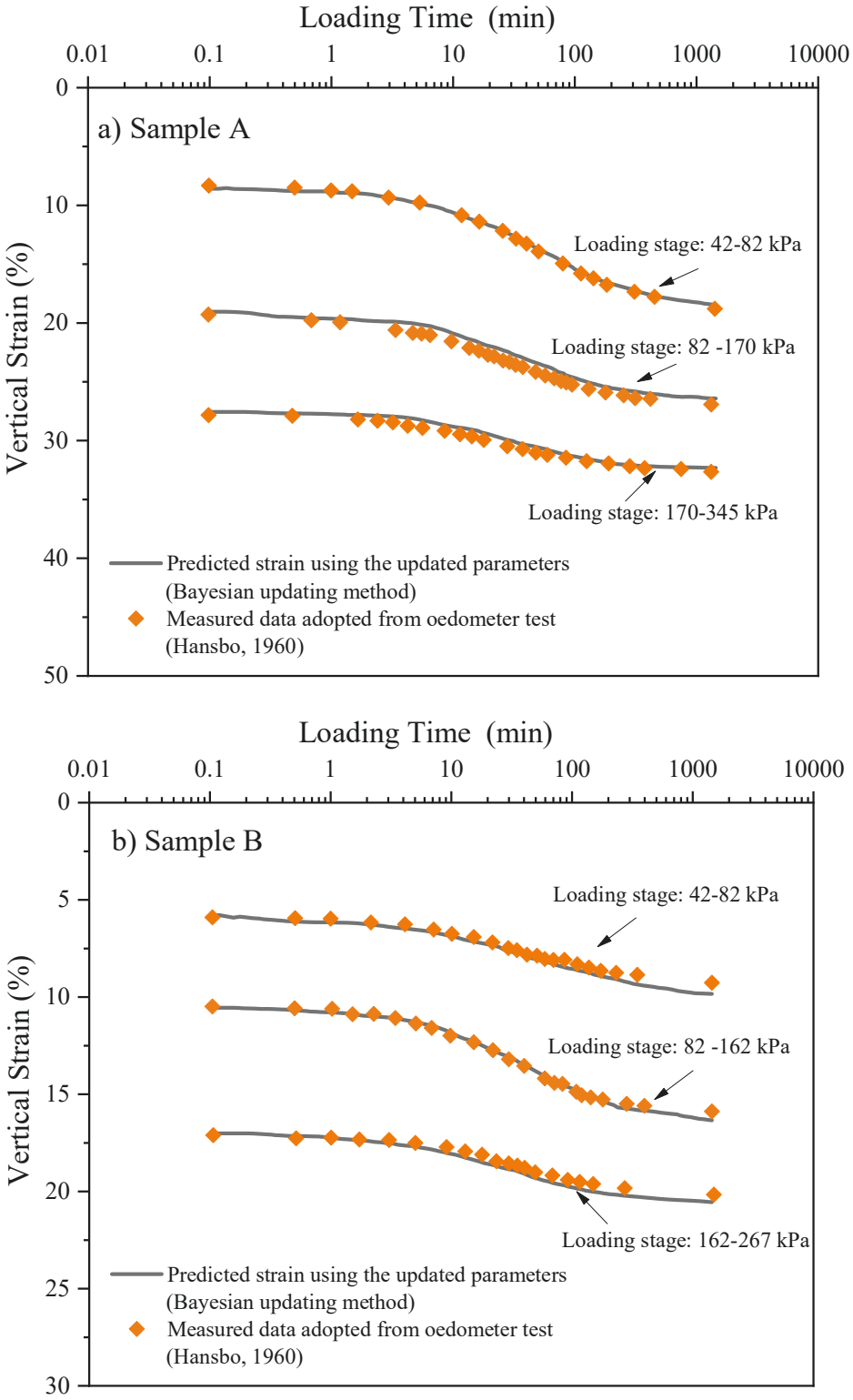

Figure 5.6 Predicted strain adopting updated elastic visco-plastic model parameters $(\lambda/V, \psi_0/V)$ comparing with oedometer test results for Skå-Edeby soft soil (a) Sample A, (b) Sample B

Table 5.8 Summary of strain indicators for all adopted loading stages of oedometer test by using prior and posterior elastic visco-plastic model parameters ($\lambda/V, \psi_0/V$) for Skå-Edeby soft soil

Sample	Loading Stage (kPa)		***RMSE***	***MAE***	R^2	$E_{RMSE\ (prior\text{-}posterior)}$ (%)	$E_{MAE\ (prior\text{-}posterior)}$ (%)
A	42-82	Prior	0.0119	0.012	0.99	80	80
		Posterior	0.0023	0.002	0.99		
	82-170	Prior	0.0179	0.018	0.99	60	60
		Posterior	0.0072	0.007	0.99		
	170-345	Prior	0.0081	0.008	0.99	45	50
		Posterior	0.0046	0.004	0.98		
B	42-82	Prior	0.006	0.006	0.99	60	65
		Posterior	0.0023	0.002	0.99		
	82-162	Prior	0.0061	0.005	0.99	75	75
		Posterior	0.0016	0.001	0.99		
	162-267	Prior	0.0062	0.006	0.99	55	60
		Posterior	0.0027	0.0025	0.99		

5.4.2.2 Prediction using observation of field measurements for Skå-Edeby test fill

Settlement of Skå-Edeby test fill at different depths are calculated using the mean values of the posterior distribution of elastic visco-plastic model parameters obtained from oedometer test results as presented in Table 5.7 (Note: the details of all soil and embankment properties were presented in Chapter 4, Section 4.3).

Figure 5.7 compares field measurement and predicted settlement based on updated parameters from oedometer test results. As shown in Figure 5.7, there is a considerable difference between field (observed) measurements and predicted settlement when the elastic visco-plastic model parameters are updated based on the

oedometer test results. The deviation between observed and calculated settlement is higher at the ground surface due to the fact that strain at the surface is an accumulation of all sub-layer's strains.

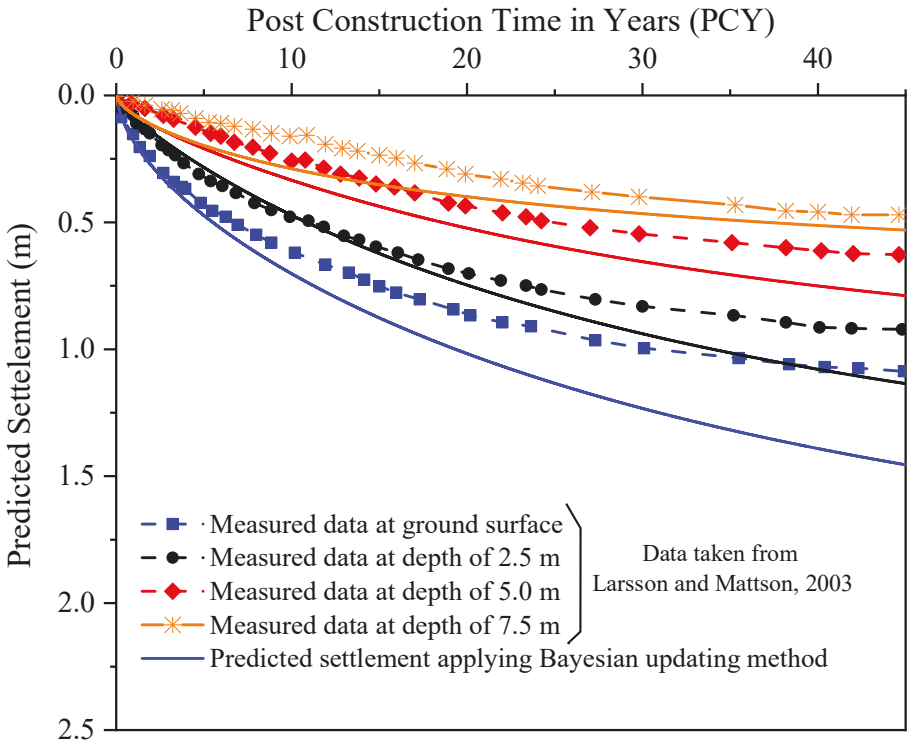

Figure 5.7 Comparison of measured and predicted settlement using updated parameters based on oedometer test results for Skå-Edeby test fill

As can be seen in Figure 5.7, adopting elastic visco-plastic model parameters $(\lambda/V, \psi_0/V)$ updated based on oedometer test data can lead to over predicted settlement which can affect periodic maintenance cost and program in projects with low embankment strategy. In order to have more realistic settlement predictions in low embankments, periodic monitoring data can be used to update parameters. Similar to Väsby test fill case study, measured settlement at ground surface are used to update elastic visco-plastic model parameters. Table 5.9 summarizes posterior statistics of elastic visco-plastic model parameters updated based on different MDxx (MD10 to MD100). Thereafter, post-construction ground surface settlements in Skå-

Edeby embankment are calculated adopting the mean values of the posterior samples. Figure 5.8 compares settlements at ground surface with measured data when elastic visco-plastic model parameters are updated based on oedometer test data and monitored data. The comparison shows a significant decrease in disparities between predicted and measured ground surface settlements when 20% of design life monitored data are used to update the parameters in comparison with applying the updated parameters obtained based on oedometer test results.

Table 5.9 Posterior statistics of elastic visco-plastic model parameters ($\lambda/V, \psi_0/V$) updated based on monitored data applying Bayesian updating method for Skå-Edeby soft soil

Model Parameter	Monitored Data	Mean (μ)	Coefficient of Variation (COV_X)
λ/V	MD10	0.14	0.01
	MD20	0.16	0.003
	MD40	0.17	0.004
	MD60	0.06	0.002
	MD80	0.06	0.002
	MD100	0.05	0.01
ψ_0/V	MD10	0.010	0.02
	MD20	0.007	0.01
	MD40	0.005	0.02
	MD60	0.007	0.001
	MD80	0.007	0.001
	MD100	0.007	0.005

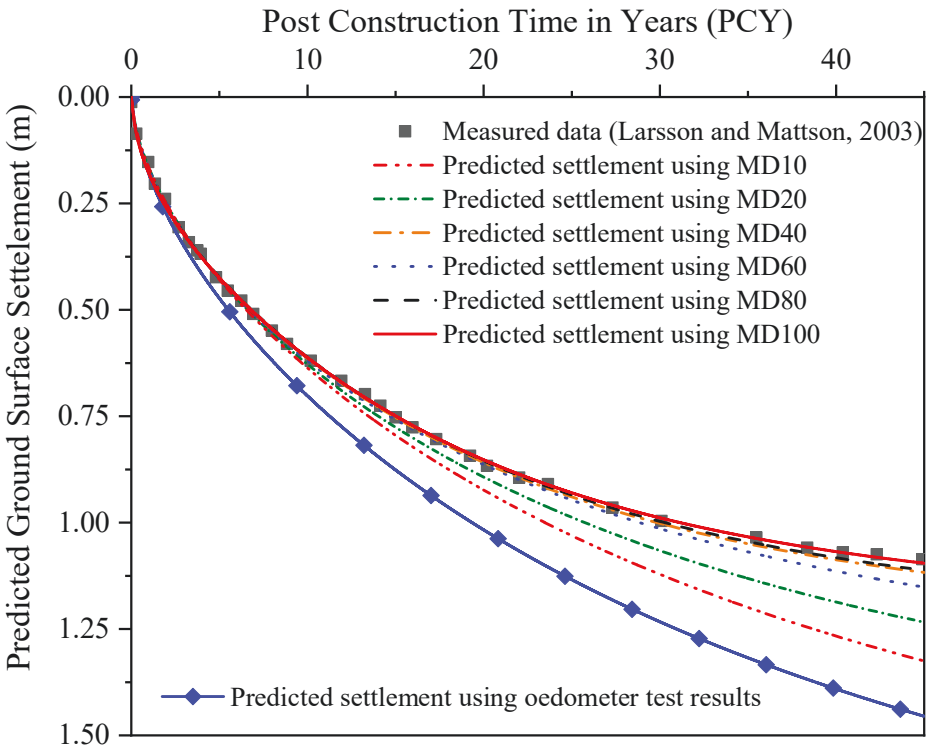

Figure 5.8 Comparison of measured and predicted settlement using updated parameters based on monitored data (MD) and oedometer test results for Skå-Edeby test fill

To quantify the effect and significance of using monitored data for back calculating settlement, a comparison is made between the prediction and field measurements using monitored data and oedometer test results. Table 5.10 presents error indicators to make a comparison between predicted settlement using updated parameters and field measurements. The error in determining indicators RMSE and MAE is calculated according to Equation (5.8). Table 5.10 shows using 10% of total monitored data (i.e. MD10) decrease the error between predicted and measured settlement about 35% to 55% comparing to using updated parameters based on oedometer test results. The corresponding value is approximately 60% to 70% when model parameters are updated based on 20% of total design life monitored data (i.e. MD20). These results confirm the effectiveness and efficiency of using monitored data to predict long-term settlement of low embankment compared to just applying oedometer test data.

Table 5.10 Summary of surface settlement error indicators using updated model parameters $(\lambda/V, \psi_0/V)$ based on monitored data at different time stages and oedometer test results for Skå-Edeby soft soil

Monitored Data (%)	$RMSE$	MAE	R^2	$E_{RMSE\ (Oed\text{-}MD)}$ (%)	$E_{MAE\ (Oed\text{-}MD)}$ (%)
MD10	0.091	0.059	0.983	35	55
MD20	0.054	0.035	0.995	60	72
MD40	0.011	0.008	0.996	92	94
MD60	0.011	0.008	0.996	92	94
MD80	0.010	0.007	0.997	93	94
MD100	0.007	0.006	0.998	95	95
Oedometer Test Results	0.144	0.126	0.911	-	-

5.4.2.3 Risk analysis for Skå-Edeby test fill

The risk is calculated based on the prediction bias or settlement bias, which is defined as the ratio of predicted settlements (S_P) to field measurements (S_m) as presented in Equation (3-27). In this risk assessment, the maintenance cost is assumed to be \$10M. Figure 5.9 presents the risk associated with over-predicted settlement which can affect the periodic maintenance cost and program. Higher risk is related to prediction of expensive and long-term maintenance program.

Figure 5.9 shows that when updated parameters based on oedometer test results are used to predict post-construction settlement, the risk related to overpredicted maintenance cost is significantly high and equals to \$13.4M. When settlements are back analysed using updated parameters based on MD10, the risk decreases to \$12.0M which is 15% less than the risk assessed using oedometer test data. By using

MD20, the corresponding risk decreases around 20% and is equal to \$11.0M. To summarize, Figure 5.9 illustrates that adopting monitored data has considerable effect in predicting more realistic post-construction settlements and managing risk associated with maintenance cost and time.

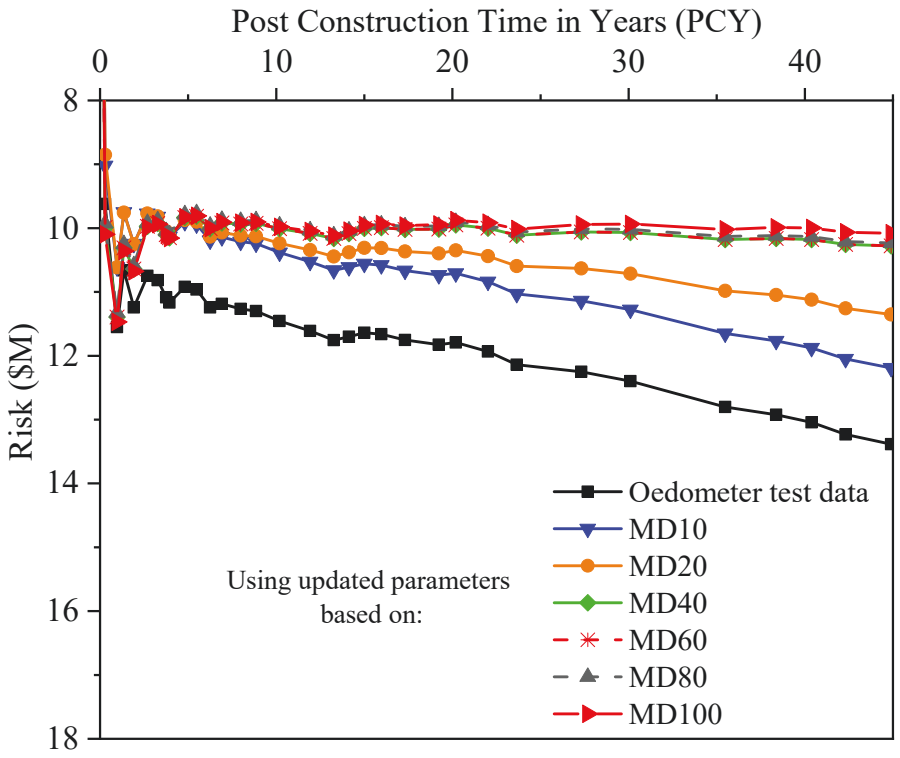

Figure 5.9 Risk associated with overpredicted pos-construction settlement using updated vico-elastic parameters based on oedometer test results and monitored data (MD) for Skå-Edeby test fill

5.5 Summary

In this chapter, Bayesian updating method of identifying the model parameters has been used to predict the long-term settlement of low embankments constructed on soft soils. The numerical solution for the coupled Yin's elastic visco-plastic (EVP) model and consolidation theory is applied to predict the long-term behavior of soft soils. In this study, the elastic-plastic model parameter (λ/V) and the initial creep coefficient (ψ_0/V) have been updated using field and oedometer test data by applying

the TMCMC method. Two in-situ case studies of test fills at Väsby and Skå-Edeby in Sweden have been selected to verify the effectiveness of Bayesian updating method to update the model parameters. In both case studies, when the elastic visco-plastic model parameters are updated based on oedometer test data, long-term settlements are over-predicted. The predictions by using 10% of monitored data results in a considerable decrease in discrepancies between predicted and measured settlements. Moreover, when 20% of total design life is used to update elastic visco-plastic model parameters, the prediction is in good agreement with field measurements and the difference between predicted and measured settlements decreases significantly.

The risk assessment has been undertaken by determining the prediction bias or settlement bias. Since in low embankment strategy, the risk is mostly associated with the periodic maintenance cost and schedule, adopting at least 20% of total monitored data for updating model parameters has a considerable impact in predicting more realistic post-construction settlements and consequently more reasonable and economical maintenance cost and time. It should be noted that the findings of this chapter are based on two case studies of Väsby and Skå-Edeby test fill. To generalize the findings, more case studies are required, which is suggested for further studies.

6 Conclusions and Recommendations

6.1 Summary

Chapters 1 and 2 have provided an introduction and a comprehensive literature review about various probabilistic methods and several existing methods to predict time-dependent stress-strain behaviour of soft soils. Chapter 2 has also presented several probabilistic methods and reliability analysis in geotechnical engineering, particularly in long-term settlement of soft soils.

In Chapter 3, the influence of the elastic-plastic and creep parameter uncertainties and contribution of each random variable on the time-dependent deformation of soft soils has been presented. Since the elastic-visco plastic materials are interdependent parameters, the effect of cross correlation coefficients between two random variables, namely the elastic-plastic (λ/V) and initial creep (ψ_0/V) model parameters on the system response has been investigated. Väsby trial embankment data was adopted to obtain the deterministic and probabilistic parameters and validate the proposed model. A suitable cross correlation coefficient between selected random variables has been recommended by evaluating the proposed probabilistic analysis against field measurements.

Chapter 4 has investigated the influence of spatial variability of the elastic visco-plastic model parameters affecting the time-dependent behaviour of soft soils. To generate the random field, Karhunen-Loeve (K-L) expansion method has been adopted and then combined with the developed finite difference-based model. To determine the critical spatial correlation length, the maximum probability of failure has been calculated by adopting the field measurements of Skå–Edeby trial embankment.

Chapter 5 has provided monitoring measurements of two case studies of Väsby and Skå-Edeby test fills to investigate how applying field monitoring results can reduce risks in predicting the long-term settlement of low embankments constructed on soft soils. The elastic visco-plastic model parameters have been updated by adopting the Bayesian updating method and transitional Markov Chain Monte Carlo (TMCMC) algorithm. Then, the results were compared with updated parameters obtained from oedometer test results.

6.2 Conclusions

Due to the rapid development of civil infrastructure and scarcity of land in urban areas, there is a growing demand to construct on top of weak ground with soft soil. The challenge then for geotechnical engineers is to predict the time-dependent behaviour of soft soil that has low strength and stiffness. Elastic visco-plastic model (EVP) developed by Yin (1999) is an effective model to predict time-dependent behaviour of soft soils. It is neither practical nor cost-effective to carry out very long-term creep tests to determine elastic visco-plastic model parameters and creep limit values, introducing uncertainties in design. Moreover, at each site the properties of

soil and rock vary depending on the lithological heterogeneity of the soil and its inherent spatial variability introducing another source of uncertainties in design. As a result, this research investigated the influence of the elastic-plastic and creep parameter uncertainties in predicting long-term behaviour of soft soils.

It is concluded that the elastic-plastic model parameter (λ/V) and the initial creep coefficient (ψ_0/V) are important factors in predicting the time-dependent settlement of soft soil considering uncertainties associated with determining these two parameters. The standard deviation of time-dependent settlement gradually increased with time as uncertainties accumulated. Moreover, the effect of cross correlation coefficients between the random variables λ/V and ψ_0/V was evaluated by comparing the predictions with the measured data in the Väsby test fill. It was concluded that by increasing the cross correlation coefficient, the standard deviation and also the coefficient of variation (COV) of the predicted settlements increased approximately 40%, resulting in more conservative design and predictions.

Furthermore, the settlement ratio is more accurate and reliable method to estimate the efficiency and suitability of selected cross correlation coefficients as the common methods used to evaluate errors were not efficient enough to quantify the most proper cross correlation coefficient between the elastic-plastic model parameter (λ/V) and the initial creep coefficient (ψ_0/V). It was concluded that to optimise a design in terms of reliability and cost, the cross correlation coefficient between the elastic-plastic model parameter (λ/V) and the initial creep coefficient (ψ_0/V) based on the existing field and laboratory test results should be determined and applied in probabilistic analysis. However, in the absence of enough data to determine the exact

value of cross correlation between λ/V and ψ_0/V, it is highly recommended to assume these two random variables fully-correlated (i.e. $\rho = 1$).

Moreover, the effect of spatially variable elastic visco-plastic model parameters on the long-term behaviour of low embankments constructed on top of soft soils was investigated incorporating random field (RF) and single random variable (SRV) analyses. The key findings of this study showed that normalised spatial correlation length (θ) plays an important role in predicting the time-dependent settlement of soft soils considering the elastic visco-plastic parameters (λ/V and ψ_0/V) as spatial random variables. By increasing the normalised spatial correlation length in RF analysis, the probability density function (PDF) becomes wider indicating more uncertainties in post construction settlement prediction. In addition to, when normalised spatial correlation length exceeds unity (i.e. $\theta > 1$), the RF settlement prediction converges with those obtained from rather simple SRV analysis.

On the other hand, it is concluded that a critical spatial correlation length existed for predicting time-dependent settlement of soft soils resulting in the maximum PF while adopting random field reliability analysis. In this study, the critical spatial correlation length is determined to be in the order of $10H$, where H is the soft soil thickness. As a result, in the absence of adequate data to determine exact spatial correlation length, conducting SRV analysis is deemed unsafe/unreliable. It can be noted that comprehensive, time consuming and costly laboratory tests are required to estimate the soil spatial variability and correlation length. Therefore, the findings of this study can be used as guidelines by practicing engineers, designing

structures on soft soils, particularly when adopting low embankment strategy for design of transport infrastructure.

In this study, the elastic-plastic model parameter (λ/V) and the initial creep coefficient (ψ_0/V) were updated using field and oedometer test data by applying the TMCMC method. Two in-situ case studies of test fills at Väsby and Skå-Edeby in Sweden were selected to verify the effectiveness of Bayesian updating method to update the model parameters. In both case studies, when the elastic visco-plastic model parameters are updated based on oedometer test data, long-term settlements are over-predicted. The predictions by using 10% of monitored data results in a considerable decrease in discrepancies between predicted and measured settlements. Moreover, when 20% of total design life is used to update elastic visco-plastic model parameters, the prediction is in good agreement with field measurements.

This study can be employed by design engineers while adopting reliability-based design approach to predict long-term settlement of soft soils. The main findings of this study provide a practical insight into selecting the most suitable cross correlation coefficient between elastic visco-plastic model parameters and the critical spatial correlation length for safe design in the absence of adequate data. It is also recommended that even adopting 20% of total monitored data for updating model parameters has a considerable impact in predicting more realistic post-construction settlements and consequently reducing the risks associated with unsatisfactory settlement prediction.

6.3 Recommendations for Future Research

This research may be extended by conducting the following directions and ideas:

- In this study, the reliability analysis and probabilistic method has been applied for predicting soft soils one dimensional settlement without vertical drains. It is more popular to improve soft soil performance employing the pre-loading system combined with the installation of vertical drains. Accordingly, the proposed reliability analysis and probabilistic method can be extended based to the case studies with vertical drains in 2D and 3D consolidation conditions.

- One of the applications of constructing embankment without vertical drains are ground improvement of landfills. It is recommended to evaluate the application of proposed reliability analysis combined with non-linear elastic visco-plastic model to predict long-term settlement of landfills by adopting settlement measurements of a landfill case study.

- More case studies can be analysed to validate the critical spatial correlation length proposed in this research to predict time dependent settlement of soft soils in RF analysis.

- In this study, findings of updating elastic visco-plastic model parameters adopting Bayesian updating method and field monitoring data are based on two case studies of Väsby and Skå-Edeby test fill. As a result, to generalize the findings, it is suggested to analysis more case studies.

- Bayesian updating method and transitional Markov Chain Monte Carlo (TMCMC) algorithm can be extended to incorporate spatial variability of elastic visco-plastic model parameters. Therefore, the model will be more versatile to address uncertainties due to the model parameters determination methods and spatial variability of parameters.

- In this study, the reliability analysis and probabilistic method has been applied for predicting soft soils settlement incorporating uncertainties and spatial variability of elastic visco-plastic model parameters. It is suggested to extend the study considering uncertainties and spatial variability associated with more than two probabilistic parameters such as permeability.

References

Aboshi, H. 1973, 'An experimental investigation on the similitude in the one-dimensional consolidation of a soft clay including the secondary creep settlement', *Proc. 8th ICSMFE, 1973*, vol. 4, p. 88.

Ahmed, A. & Soubra, A.-H. 2012, 'Probabilistic analysis of strip footings resting on a spatially random soil using subset simulation approach', *Georisk: Assessment and Management of Risk for Engineered Systems and Geohazards*, vol. 6, no. 3, pp. 188-201.

Allahverdizadeh, P., Griffiths, D. & Fenton, G. 2015, 'The Random Finite Element Method (RFEM) in probabilistic slope stability analysis with consideration of spatial variability of soil properties', *IFCEE 2015*, pp. 1946-55.

Allahverdizadeh, P., Griffiths, D. & Fenton, G.A. 2016, 'Influence of soil shear strength spatial variability on the compressive strength of a block', *Georisk: Assessment and Management of Risk for Engineered Systems and Geohazards*, vol. 10, no. 1, pp. 2-10.

Allahverdizadeh Sheykhloo, P. 2015, 'Risk assessment and spatial variability in geotechnical stability problems', Colorado School of Mines.

Army, U. 1995, 'Introduction to probability and reliability methods for use in geotechnical engineering', *Eng. Tech. Letter*, no. 1110-2, p. 547.

Azari, B. 2015, 'Behaviour of soft soil improved with vertical drain accelerated preloading incorporating visco-plastic deformation'.

Baecher, G.B. & Christian, J.T. 2005, *Reliability and statistics in geotechnical engineering*, John Wiley & Sons.

Barden, L. 1965, 'Consolidation of clay with non-linear viscosity', *Geotechnique*, vol. 15, no. 4, pp. 345-62.

Bari, M.W. & Shahin, M.A. 2014, 'Probabilistic design of ground improvement by vertical drains for soil of spatially variable coefficient of consolidation', *Geotextiles and Geomembranes*, vol. 42, no. 1, pp. 1-14.

Bari, M.W. & Shahin, M.A. 2015, 'Three-dimensional finite element analysis of spatially variable PVD improved ground', *GeoRisk: Assessment and Management of Risk for Engineered Systems and Geohazards*, vol. 9, no. 1, pp. 37-48.

Bari, M.W., Shahin, M.A. & Nikraz, H.R. 2013, 'Probabilistic analysis of soil consolidation via prefabricated vertical drains', *International Journal of Geomechanics*, vol. 13, no. 6, pp. 877-81.

Bari, M.W., Shahin, M.A. & Soubra, A.H. 2016, 'Probabilistic analyses of soil consolidation by prefabricated vertical drains for single-drain and multi-drain systems', *International Journal for Numerical and Analytical Methods in Geomechanics*, vol. 40, no. 17, pp. 2398-420.

Beck, J.L. & Au, S.-K. 2002, 'Bayesian updating of structural models and reliability using Markov chain Monte Carlo simulation', *Journal of engineering mechanics*, vol. 128, no. 4, pp. 380-91.

Betz, W., Papaioannou, I. & Straub, D. 2014, 'Numerical methods for the discretization of random fields by means of the Karhunen–Loève expansion', *Computer Methods in Applied Mechanics and Engineering*, vol. 271, pp. 109-29.

Biot, M.A. 1941, 'General theory of three-dimensional consolidation', *Journal of applied physics*, vol. 12, no. 2, pp. 155-64.

Bjerrum, L. 1967, 'Engineering geology of Norwegian normally-consolidated marine clays as related to settlements of buildings', *Geotechnique*, vol. 17, no. 2, pp. 83-118.

Bong, T., Son, Y., Noh, S. & Park, J. 2014, 'Probabilistic analysis of consolidation that considers spatial variability using the stochastic response surface method', *Soils and Foundations*, vol. 54, no. 5, pp. 917-26.

Buisman, C. 1936, 'Verslag Van De Onderzoekingen Over De Iepenziekte, Verricht In Het Phytopathologisch Laboratorium Willie Commelin Scholten Te Baarn Gedurende 1935', *Tijdschrift Over Plantenziekten*, vol. 42, no. 10, pp. 21-44.

Bungenstab, F.C. & Bicalho, K.V. 2016, 'Settlement predictions of footings on sands using probabilistic analysis', *Journal of Rock Mechanics and Geotechnical Engineering*, vol. 8, no. 2, pp. 198-203.

Cassidy, M.J., Uzielli, M. & Tian, Y. 2013, 'Probabilistic combined loading failure envelopes of a strip footing on spatially variable soil', *Computers and Geotechnics*, vol. 49, pp. 191-205.

Chang, Y.-C.E. 1981a, 'Long-term consolidation beneath the test fills at Väsby', *Swedish Geotechnical Institute, Linkoping, Sweden. Report*, vol. 13.

Chang, Y.C.E. 1981b, *Long term consolidation beneath the test fills at Väsby, Sweden*.

Ching, J. & Chen, Y.-C. 2007, 'Transitional Markov chain Monte Carlo method for Bayesian model updating, model class selection, and model averaging', *Journal of engineering mechanics*, vol. 133, no. 7, pp. 816-32.

Ching, J., Li, K.-H., Phoon, K.-K. & Weng, M.-C. 2018, 'Generic transformation models for some intact rock properties', *Canadian Geotechnical Journal*, vol. 55, no. 12, pp. 1702-41.

Ching, J. & Phoon, K.-K. 2020a, 'Constructing a site-specific multivariate probability distribution using sparse, incomplete, and spatially variable (MUSIC-X) data', *Journal of Engineering Mechanics*, vol. 146, no. 7, p. 04020061.

Ching, J. & Phoon, K.-K. 2020b, 'Measuring similarity between site-specific data and records from other sites', *ASCE-ASME Journal of Risk and Uncertainty in Engineering Systems, Part A: Civil Engineering*, vol. 6, no. 2, p. 04020011.

Cho, S.E. 2007, 'Effects of spatial variability of soil properties on slope stability', *Engineering Geology*, vol. 92, no. 3-4, pp. 97-109.

Christian, J.T. 2004, 'Geotechnical engineering reliability: How well do we know what we are doing?', *Journal of geotechnical and geoenvironmental engineering*, vol. 130, no. 10, pp. 985-1003.

Christian, J.T., Ladd, C.C. & Baecher, G.B. 1994, 'Reliability applied to slope stability analysis', *Journal of Geotechnical Engineering*, vol. 120, no. 12, pp. 2180-207.

Coccon, M.N., Song, J., Ok, S.-Y. & Galvanetto, U. 2017, 'A new approach to system reliability analysis of offshore structures using dominant failure modes identified by selective searching technique', *KSCE Journal of Civil Engineering*, vol. 21, no. 6, pp. 2360-72.

Cornell, C.A. 1969, 'A probability-based structural code', *Journal Proceedings*, vol. 66, pp. 974-85.

Crank, J. & Nicolson, P. 1947, 'A practical method for numerical evaluation of solutions of partial differential equations of the heat-conduction type', *Mathematical Proceedings of the Cambridge Philosophical Society*, vol. 43, Cambridge University Press, pp. 50-67.

De Jong, G.d.J. & Verruijt, A. 1965, 'Primary and secondary consolidation of a spherical clay sample', *Proceeding of the 6th international conference soil mechanic and foundation engineering, Montreal*, pp. 254-8.

Duncan, J.M. 2000, 'Factors of safety and reliability in geotechnical engineering', *Journal of Geotechnical and Geoenvironmental Engineering*, vol. 126, no. 4, pp. 307-16.

El-Ramly, H., Morgenstern, N. & Cruden, D. 2002, 'Probabilistic slope stability analysis for practice', *Canadian Geotechnical Journal*, vol. 39, no. 3, pp. 665-83.

Elkateb, T., Chalaturnyk, R. & Robertson, P.K. 2003, 'An overview of soil heterogeneity: quantification and implications on geotechnical field problems', *Canadian Geotechnical Journal*, vol. 40, no. 1, pp. 1-15.

Feng, L. & Zhang, L. 2020, 'Reliability Assessment of Tunnel Face Support Pressure Subjected to An Adjacent Tunnel', *Reliability Engineering & System Safety*, p. 107228.

Feng, L. & Zhang, L. 2021, 'Assessment of tunnel face stability subjected to an adjacent tunnel', *Reliability Engineering & System Safety*, vol. 205, p. 107228.

Fenton, G.A. & Griffiths, D. 2002, 'Probabilistic foundation settlement on spatially random soil', *Journal of Geotechnical and Geoenvironmental Engineering*, vol. 128, no. 5, pp. 381-90.

Fenton, G.A. & Griffiths, D. 2005, 'Three-dimensional probabilistic foundation settlement', *Journal of Geotechnical and Geoenvironmental Engineering*, vol. 131, no. 2, pp. 232-9.

Fenton, G.A., Griffiths, D. & Zhang, X. 2008, 'Load and resistance factor design of shallow foundations against bearing failure', *Canadian Geotechnical Journal*, vol. 45, no. 11, pp. 1556-71.

Fenton, G.A. & Griffiths, V.D. 2008, *Risk assessment in geotechnical engineering*, John Wiley & Sons.

Garlanger, J.E. 1972, 'The consolidation of soils exhibiting creep under constant effective stress', *Geotechnique*, vol. 22, no. 1, pp. 71-8.

Genz, A. & Bretz, F. 2002, 'Comparison of methods for the computation of multivariate t probabilities', *Journal of Computational and Graphical Statistics*, vol. 11, no. 4, pp. 950-71.

Gibson, R. 1961, 'A theory consolidation for soils exhibiting secondary compression', *Report*, vol. 41.

Gibson, R. & Lo, K. 1961, 'A Theory of Consolidation for Soils Exhibiting Secondary Compression. Norwegian Geotechnical Institute Publication No. 41', *also Acta Polytechnica Scandinavica*, vol. 296, p. 191.

Goh, A.T., Zhang, W. & Wong, K. 2019, 'Deterministic and reliability analysis of basal heave stability for excavation in spatial variable soils', *Computers and Geotechnics*, vol. 108, pp. 152-60.

Griffiths, D. & Fenton, G. 2000, 'Bearing capacity of heterogeneous soils by finite elements."', *Memorias Del V Congreso Internacional De Métodos Numéricos En Ingeniería Y Ciencias Aplicadas*, Puerto La Cruz, Venezuela, CI27–CI37.

Griffiths, D. & Fenton, G.A. 1994, *Observations on two-and three-dimensional seepage through a spatially random soil*, Geomechanics Research Center, Colorado School of Mines.

Griffiths, D., Huang, J. & Fenton, G.A. 2009, 'Influence of spatial variability on slope reliability using 2-D random fields', *Journal of geotechnical and geoenvironmental engineering*, vol. 135, no. 10, pp. 1367-78.

Hansbo, S. 1960, 'Consolidation of clay, with special reference to influence of vertical sand drains', *Swedish Geotechnical Institute Proc*, vol. 18.

Holtz, R.D. & Lindskog, G. 1972, 'Soil movements below a test embankment', *Performance of Earth and Earth-Supported Structures*, ASCE, p. 273.

Houmadi, Y., Ahmed, A. & Soubra, A.-H. 2012, 'Probabilistic analysis of a one-dimensional soil consolidation problem', *Georisk: Assessment and Management of Risk for Engineered Systems and Geohazards*, vol. 6, no. 1, pp. 36-49.

Huang, J., Griffiths, D. & Fenton, G.A. 2010, 'Probabilistic analysis of coupled soil consolidation', *Journal of Geotechnical and Geoenvironmental Engineering*, vol. 136, no. 3, pp. 417-30.

Huang, J., Kelly, R., Li, D., Zhou, C. & Sloan, S. 2016, 'Updating reliability of single piles and pile groups by load tests', *Computers and Geotechnics*, vol. 73, pp. 221-30.

Jamiolkowski, M., Ladd, C., Germaine, J. & Jamiolkowski, R. 1985, 'New developments in field and laboratory testing of soils', *11th International Conference on Soil Mechanics and Foundation Engineering*, vol. 1, San Francisco, pp. 57-153.

Javankhoshdel, S. & Bathurst, R.J. 2014, 'Simplified probabilistic slope stability design charts for cohesive and cohesive-frictional (c-ϕ) soils', *Canadian Geotechnical Journal*, vol. 51, no. 9, pp. 1033-45.

Jha, S.K. & Ching, J. 2013, 'Simplified reliability method for spatially variable undrained engineered slopes', *Soils and foundations*, vol. 53, no. 5, pp. 708-19.

Jiang, S.-H., Huang, J., Huang, F., Yang, J., Yao, C. & Zhou, C.-B. 2018, 'Modelling of spatial variability of soil undrained shear strength by conditional random fields for slope reliability analysis', *Applied Mathematical Modelling*, vol. 63, pp. 374-89.

Jung, B.-C., Biscontin, G. & Gardoni, P. 2009, 'Bayesian updating of a unified soil compression model', *Georisk*, vol. 3, no. 2, pp. 87-96.

Kabbaj, M. 1985, 'Aspects rhéologiques des argiles naturelles en consolidation', *Ph. D thesis, Laval Univ.*

Kasama, K. & Whittle, A.J. 2016, 'Effect of spatial variability on the slope stability using random field numerical limit analyses', *Georisk: Assessment and Management of Risk for Engineered Systems and Geohazards*, vol. 10, no. 1, pp. 42-54.

Kim, J. & Song, J. 2019, 'A comprehensive probabilistic model of traffic loads based on weigh-in-motion data for applications to bridge structures', *KSCE Journal of Civil Engineering*, vol. 23, no. 8, pp. 3628-43.

Kuhn, M.R. & Mitchell, J.K. 1993, 'New perspectives on soil creep', *Journal of Geotechnical Engineering*, vol. 119, no. 3, pp. 507-24.

Ladd, C.C., Foott, R., Ishihara, K., Scholosser, F. & Poulos, H.G. 1977, 'Stress deformation and strength characteristics', paper presented to the *The 9th international conference on soil mechanics and foundation engineering*, Tokyo, Japan.

Larsson, R. & Mattsson, H. 2003, *Settlements and shear strength increase below embankments-long-term observations and measurement of shear strength increase by seismic cross-hole tomography*, Report No.63, Swedish Geotechnical Institute.

Le, T.M. 2015, 'Analysing consolidation data to optimise elastic visco-plastic model parameters for soft clay'.

Le, T.M., Fatahi, B. & Khabbaz, H. 2015, 'Numerical optimisation to obtain elastic viscoplastic model parameters for soft clay', *International Journal of Plasticity*, vol. 65, pp. 1-21.

Le, T.M., Fatahi, B., Khabbaz, H. & Sun, W. 2017, 'Numerical optimization applying trust-region reflective least squares algorithm with constraints to optimize the non-linear creep parameters of soft soil', *Applied Mathematical Modelling*, vol. 41, pp. 236-56.

Le, T.M., Fatahi, B. & Owen, D. 2016, 'Trust-region reflective optimisation to obtain soil visco-plastic properties', *Engineering Computations*.

Leroueil, S. 1996, 'Compressibility of clays: fundamental and practical aspects', *Journal of geotechnical engineering*, vol. 122, no. 7, pp. 534-43.

Leroueil, S., Kabbaj, M., Tavenas, F. & Bouchard, R. 1985, 'Stress–strain–strain rate relation for the compressibility of sensitive natural clays', *Géotechnique*, vol. 35, no. 2, pp. 159-80.

Li, C.-C. & Der Kiureghian, A. 1993, 'Optimal discretization of random fields', *Journal of engineering mechanics*, vol. 119, no. 6, pp. 1136-54.

Li, J., Cassidy, M.J., Huang, J., Zhang, L. & Kelly, R. 2016, 'Probabilistic identification of soil stratification', *Géotechnique*, vol. 66, no. 1, pp. 16-26.

Li, X.-Y., Zhang, L.-M., Gao, L. & Zhu, H. 2017, 'Simplified slope reliability analysis considering spatial soil variability', *Engineering Geology*, vol. 216, pp. 90-7.

Liingaard, M., Augustesen, A. & Lade, P.V. 2004, 'Characterization of models for time-dependent behavior of soils', *International Journal of Geomechanics*, vol. 4, no. 3, pp. 157-77.

Liu, Z., Choi, J.C., Lacasse, S. & Nadim, F. 2018, 'Uncertainty analyses of time-dependent behaviour of Ballina test embankment', *Computers and Geotechnics*, vol. 93, pp. 133-49.

Lo, M.K. & Leung, Y. 2019, 'Bayesian updating of subsurface spatial variability for improved prediction of braced excavation response', *Canadian Geotechnical Journal*, vol. 56, no. 8, pp. 1169-83.

Malhotra, M., Srivastava, A. & Jawaid, S. 2020, 'Reliability analysis of shallow foundation in the vicinity of the existing buried conduit', *Geomechanics and Geoengineering*, vol. 15, no. 2, pp. 149-58.

Mesri, G. 1973, 'One-dimensional consolidation of a clay layer with impeded drainage boundaries', *Water Resources Research*, vol. 9, no. 4, pp. 1090-3.

Mesri, G. 2003, 'Primary compression and secondary compression', *Soil behavior and soft ground construction*, pp. 122-66.

Mesri, G. & Choi, Y. 1985, 'Settlement analysis of embankments on soft clays', *Journal of Geotechnical Engineering*, vol. 111, no. 4, pp. 441-64.

Mesri, G. & Godlewski, P.M. 1977a, 'Time-and stress-compressibility interrelationship', *Journal of Geotechnical and Geoenvironmental Engineering*, vol. 103, no. ASCE 12910.

Mesri, G. & Godlewski, P.M. 1977b, 'Time and stress-compressibility interrelationship', *ASCE J Geotech Eng Div*, vol. 103, no. 5, pp. 417-30.

Mesri, G., Lo, D.O.K. & Feng, T.W. 1994, 'Settlement of embankments on soft clays', *Proceedings of the Conference on Vertical and Horizontal Deformations of Foundations and Embankments. Part 2 (of 2)*, Publ by ASCE, pp. 8-56.

Mitchell, J.K., Campanella, R.G. & Singh, A. 1968, 'Soil creep as a rate process', *Journal of Soil Mechanics & Foundations Div*.

Morgenstern, N. 1995, 'Managing risk in geotechnical engineering', *10th Pan American Conference on Soil Mechanics and Foundation Engineering*.

Muhammed, J.J., Jayawickrama, P.W. & Ekwaro-Osire, S. 2020, 'Uncertainty Analysis in Prediction of Settlements for Spatial Prefabricated Vertical Drains Improved Soft Soil Sites', *Geosciences*, vol. 10, no. 2, p. 42.

Nelsen, R.B. 2007, *An introduction to copulas*, Springer Science & Business Media.

Ni, P., Li, J., Hao, H., Yan, W., Du, X. & Zhou, H. 2020, 'Reliability analysis and design optimization of nonlinear structures', *Reliability Engineering & System Safety*, vol. 198, p. 106860.

Olszak, W. & Perzyna, P. 1966a, ''On elastic-viscoplastic soils, rheology and soil mechanics', *International Union of Theoretical and Applied Mechanics Symposium, Grenoble*.

Olszak, W. & Perzyna, P. 1966b, 'On elastic/visco-plastic soils', *Rheology and Soil Mechanics/Rhéologie et Mécanique des Sols*, Springer, pp. 47-57.

Perrone, V.J. 1998, 'One dimensional computer analysis of simultaneous consolidation and creep of clay', Virginia Tech.

Perzyna, P. 1963, 'The constitutive equation for work-hardening and rate sensitive plastic materials', *Proc. Vibrational Problems*, vol. 4, pp. 281-90.

Pramanik, R., Baidya, D.K. & Dhang, N. 2020, 'Reliability analysis for bearing capacity of surface strip footing using fuzzy finite element method', *Geomechanics and Geoengineering*, vol. 15, no. 1, pp. 29-41.

Rajot, J. 1993, 'A theory for the time-dependent yielding and creep of clay'.

Siripatana, A., Le Maitre, O., Knio, O., Dawson, C. & Hoteit, I. 2020, 'Bayesian inference of spatially varying Manning'sn coefficients in an idealized coastal ocean model using a generalized Karhunen-Loève expansion and polynomial chaos', *Ocean Dynamics*, vol. 70, no. 8, pp. 1103-27.

Spanos, P.D. & Ghanem, R. 1989, 'Stochastic finite element expansion for random media', *Journal of engineering mechanics*, vol. 115, no. 5, pp. 1035-53.

Sudret, B. & Der Kiureghian, A. 2000, *Stochastic finite element methods and reliability: a state-of-the-art report*, Department of Civil and Environmental Engineering, University of California ….

Suklje, L. 1957, 'The analysis of the consolidation process by the isotaches method', *Proceedings of the 4th International Conference on Soil Mechanics and Foundation Engineering, London*, vol. 1, pp. 200-6.

Taylor, D.W. 1942, *Research on consolidation of clays*, vol. 82, Massachusetts Institute of Technology.

Taylor, D.W. & Merchant, W. 1940, 'A theory of clay consolidation accounting for secondary compression', *Journal of Mathematics and Physics*, vol. 19, no. 1-4, pp. 167-85.

Terzaghi, K. 1941, 'Undisturbed clay samples and undisturbed clays', *Journal of the Boston Society of Civil Engineers*, vol. 28, no. 3, pp. 45-65.

Tosoni, E., Salo, A., Govaerts, J. & Zio, E. 2019, 'Comprehensiveness of scenarios in the safety assessment of nuclear waste repositories', *Reliability Engineering & System Safety*, vol. 188, pp. 561-73.

Van der Have, R. 2015, 'Random fields for non-linear finite element analysis of reinforced concrete. MSc thesis', Delft University of Technology.

Van Trees, H.L. 2004, *Detection, estimation, and modulation theory, part I: detection, estimation, and linear modulation theory*, John Wiley & Sons.

Vanmarcke, E. 2010, *Random fields: analysis and synthesis*, World Scientific.

Wahls, H.E. 1962, 'Analysis of primary and secondary consolidation', *Journal of the Soil Mechanics and Foundations Division*, vol. 88, no. 6, pp. 207-34.

Wang, F., Huang, H., Yin, Z. & Huang, Q. 2021, 'Probabilistic characteristics analysis for the time-dependent deformation of clay soils due to spatial variability', *European Journal of Environmental and Civil Engineering*, pp. 1-19.

Wang, H. 2020, 'Finding patterns in subsurface using Bayesian machine learning approach', *Underground Space*, vol. 5, no. 1, pp. 84-92.

Wang, J. 2016, 'Site characterization with multiple measurement profiles from different tests: A Bayesian approach', *Soils and foundations*, vol. 56, no. 4, pp. 712-8.

Wang, M.-Y., Liu, Y., Ding, Y.-N. & Yi, B.-L. 2020, 'Probabilistic stability analyses of multi-stage soil slopes by bivariate random fields and finite element methods', *Computers and Geotechnics*, vol. 122, p. 103529.

Wang, Y., Cao, Z. & Li, D. 2016, 'Bayesian perspective on geotechnical variability and site characterization', *Engineering Geology*, vol. 203, pp. 117-25.

Wang, Z., Broccardo, M. & Song, J. 2019, 'Hamiltonian Monte Carlo methods for Subset Simulation in reliability analysis', *Structural Safety*, vol. 76, pp. 51-67.

Yin, J.-H. 1990, 'Constitutive modelling of time-dependent stress-strain behaviour of soils'.

Yin, J.-H. 1999, 'Non-linear creep of soils in oedometer tests', *Geotechnique*, vol. 49, no. 5, pp. 699-707.

Yin, J.-H. & Graham, J. 1989, 'Viscous–elastic–plastic modelling of one-dimensional time-dependent behaviour of clays', *Canadian Geotechnical Journal*, vol. 26, no. 2, pp. 199-209.

Yin, J.-H. & Graham, J. 1994, 'Equivalent times and one-dimensional elastic viscoplastic modelling of time-dependent stress–strain behaviour of clays', *Canadian Geotechnical Journal*, vol. 31, no. 1, pp. 42-52.

Yin, J.-H. & Graham, J. 1996, 'Elastic visco-plastic modelling of one-dimensional consolidation', *Geotechnique*, vol. 46, no. 3, pp. 515-27.

Yin, J.-H., Zhu, J.-G. & Graham, J. 2002, 'A new elastic viscoplastic model for time-dependent behaviour of normally and overconsolidated clays: theory and verification', *Canadian Geotechnical Journal*, vol. 39, no. 1, pp. 157-73.

Yin, J. 2003, 'Calculation of settlements of foundation soils considering creep', *soft ground engineering in coastal areas: proceedings of The Nakase memorial symposium*, pp. 205-11.

Yin, Z.-Y., Jin, Y.-F., Shen, S.-L. & Huang, H.-W. 2017, 'An efficient optimization method for identifying parameters of soft structured clay by an enhanced genetic algorithm and elastic–viscoplastic model', *Acta Geotechnica*, vol. 12, no. 4, pp. 849-67.

Yuen, K.-V. 2010, *Bayesian methods for structural dynamics and civil engineering*, John Wiley & Sons.

Zhang, D. & Lu, Z. 2004, 'An efficient, high-order perturbation approach for flow in random porous media via Karhunen–Loeve and polynomial expansions', *Journal of Computational Physics*, vol. 194, no. 2, pp. 773-94.

Zhang, Y., Gomes, A.T., Beer, M., Neumann, I., Nackenhorst, U. & Kim, C.-W. 2019, 'Reliability analysis with consideration of asymmetrically dependent variables: discussion and application to geotechnical examples', *Reliability Engineering & System Safety*, vol. 185, pp. 261-77.

Zhao, J. & Deng, Y. 2019, 'Performer Selection in Human Reliability Analysis: D numbers Approach', *International Journal of Computers, Communications & Control*, vol. 14, no. 3.

Zheng, X. & Deng, Y. 2018, 'Dependence assessment in human reliability analysis based on evidence credibility decay model and IOWA operator', *Annals of Nuclear Energy*, vol. 112, pp. 673-84.

Zhou, W.-H., Tan, F. & Yuen, K.-V. 2018, 'Model updating and uncertainty analysis for creep behavior of soft soil', *Computers and Geotechnics*, vol. 100, pp. 135-43.

Zhou, Y., Li, C., Zhou, C. & Luo, H. 2018, 'Using Bayesian network for safety risk analysis of diaphragm wall deflection based on field data', *Reliability Engineering & System Safety*, vol. 180, pp. 152-67.